



Lawrence Berkeley Laboratory

UNIVERSITY OF CALIFORNIA

ENERGY & ENVIRONMENT DIVISION

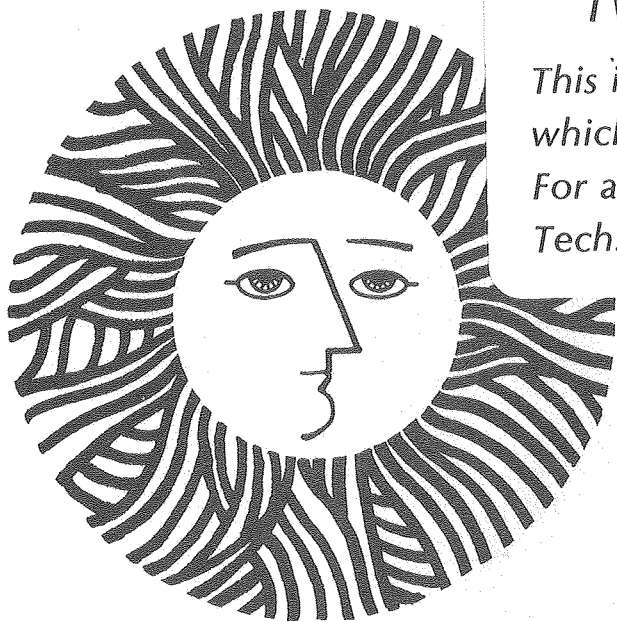
STUDIES OF WALL FLAME QUENCHING AND HYDROCARBON
EMISSIONS IN A MODEL SPARK IGNITION ENGINE

Nobuhiko Ishikawa
(Ph.D. thesis)

August 1978

TWO-WEEK LOAN COPY

*This is a Library Circulating Copy
which may be borrowed for two weeks.
For a personal retention copy, call
Tech. Info. Division, Ext. 6782.*



LBL-8819 c.2

DISCLAIMER

This document was prepared as an account of work sponsored by the United States Government. While this document is believed to contain correct information, neither the United States Government nor any agency thereof, nor the Regents of the University of California, nor any of their employees, makes any warranty, express or implied, or assumes any legal responsibility for the accuracy, completeness, or usefulness of any information, apparatus, product, or process disclosed, or represents that its use would not infringe privately owned rights. Reference herein to any specific commercial product, process, or service by its trade name, trademark, manufacturer, or otherwise, does not necessarily constitute or imply its endorsement, recommendation, or favoring by the United States Government or any agency thereof, or the Regents of the University of California. The views and opinions of authors expressed herein do not necessarily state or reflect those of the United States Government or any agency thereof or the Regents of the University of California.

STUDIES OF WALL FLAME QUENCHING AND HYDROCARBON EMISSIONS
IN A MODEL SPARK IGNITION ENGINE

By

Nobuhiko Ishikawa
(Ph.D. thesis)

Lawrence Berkeley Laboratory
University of California, Berkeley
Berkeley, California 94720

This work was supported by the Office of Energy Technology
of the U. S. Department of Energy under Contract No. W-7405-ENG-48.

Studies of Wall Flame Quenching and Hydrocarbon Emissions in a
Model Spark Ignition Engine

by Nobuhiko Ishikawa

ABSTRACT

The imposition of stringent motor vehicle emission standards combined with the recent demand for increased fuel economy have lead to renewed interest in operating automobile engines with very lean mixtures. But, the potential for reduction of pollutants by lean combustion is lessened by increased hydrocarbon emissions. The study of wall flame quenching is thus of great interest. The study, however, has been hampered by the difficulties in which flow characteristics with complicated engine geometries and wall flame quenching mechanisms under the effects of fluid dynamics have not been well developed.

In the present work, unburned hydrocarbon formation due to wall flame quenching was studied. The objectives of this study were to observe the wall flame quenching process, combustion processes, and flow characteristics in an engine under various conditions to obtain qualitative information for clarifying wall flame quenching mechanisms and then contribute to better design of engines to reduce hydrocarbon emissions. Effects of geometry, equivalence ratio, and ignition timing on the unburned hydrocarbon formation were examined.

The experiments were conducted using a model spark ignition engine. The engine has a square cross-sectional cylinder with two parallel quartz windows which allows a side view of the combustion chamber enabling direct observation of the flow patterns and combustion processes. The pneumatically driven model engine can be operated for a single

compression or expansion stroke, a compression-expansion combination, or three consecutive strokes. Methane was used as the fuel. Initial conditions were at atmospheric pressure and at room temperature for all cases. Five pistons with different geometries were used in an attempt to examine the flow variations. The visualizations were made by schlieren cine photographic technique. Hydrocarbon concentrations were measured by means of a conventional gas chromatography.

The major results are summarized as follows:

- 1) quench layer is observed along the cylinder walls and its thickness is of the same order of magnitude as that of local thermal boundary layer
- 2) piston geometry and the intake process can drastically modify the flow characteristics in an engine
- 3) the rolled-up vortex plays an important role in generating wall turbulence and the process of exhausting unburned hydrocarbons
- 4) wall turbulence strongly affects the quenching process, increasing unburned hydrocarbons
- 5) retarded ignition timing increased unburned hydrocarbons.

The main conclusions drawn from the results are that wall turbulence can significantly increase the effective quench layer thickness and that the key to minimizing wall flame quenching is to reduce turbulence generated near the engine cylinder walls.

ACKNOWLEDGEMENTS

The author wishes to thank all those who made this study possible. Special thanks is given to Professor John W. Daily, the author's principal research advisor, for his timely advice and continuous encouragement throughout this work.

The author is grateful for the help of Mr. H. Stewart and Mr. V. Locke for their outstanding design of the hardware, for Mr. D. Terry, Mr. F. Waymire, Mr. H. Weitzman, and Mr. D. Jensen for their fabrication of the hardware, and for Mr. K. Hom for his outstanding design of electronics and operation of the systems.

Sincerest appreciations are due to Professor A.K. Oppenheim, Professor R.F. Sawyer, Professor M.C. Branch, and Dr. S. Tsuge.

Ms. V. Kemanis' help in typing this work and Ms. R. Palmer's administrative coordination are gratefully acknowledged.

The author is especially thankful for the patience and mental support of his wife, Mie, and his daughters, Ryoko and Bobbie, during this study.

This work would have been in jeopardy if it were not for the exceptional understanding of the staff of the Japan Self Defence Forces, Ground Staff Office, and Professor K. Yamada of the Japan Defence Academy.

This work has been supported by the U.S. Department of Energy under Contract No. W-7405-ENG-48.

TABLE OF CONTENTS

	<u>Page</u>
ABSTRACT	1
ACKNOWLEDGEMENTS	i
TABLE OF CONTENTS	ii
LIST OF FIGURES	iii
LIST OF TABLES	vi
NOMENCLATURE	vii
CHAPTER 1. Introduction	1
CHAPTER 2. Theoretical Considerations	5
2.1 Unburned hydrocarbons and wall flame quenching.	5
2.2 Laminar flame quenching	8
2.3 Turbulent flame quenching in an engine	13
CHAPTER 3. Model Engine Study on Wall Flame Quenching	17
3.1 Experimental approach	17
3.2 Experimental apparatus	17
3.2-1 Engine and instrumentation	17
3.2-2 Optical system	28
a) System description	28
b) Spatial resolution	32
c) Color resolution	34
d) Black-and-white schlieren.	35
CHAPTER 4. Experimental Results	37
4.1 Observation of the wall flame quenching process	37
4.2 Flow and combustion process visualization experiments	42
4.3 Unburned methane measurements	59
CHAPTER 5. Discussion	66
CHAPTER 6. Summary and Conclusions	72
REFERENCES	74
APPENDIX A. Transient Flame Quenching at One Wall	81
APPENDIX B. Wall Quench Volume, Crevice Quench Volume, and Turbulence Volume Fractions	88

LIST OF FIGURES

<u>Figure</u>		<u>Page</u>
2.1	Quenching distances of iso-octane methanol air mixtures	7
2.2	Detail of flame approach to wall describing physical parameters of flame quenching model	11
2.3	Effect of turbulence intensity on quenching distance and Peclet number	15
3.1	Schematic of single compression-expansion machine	18
3.2	Piston head geometries (in mm)	21
3.3	Comparison of piston trajectories between the machine and a real engine, vertical arrows show ignition timing	22
3.4	Comparison of pressure traces between the machine and a real engine with a constant angular velocity	23
3.5	Exhaust intake valve	25
3.6	Gas sampling device	26
3.7	Optical systems	29
3.8	Ray paths in color schlieren system	30
3.9	Spacial uncertainties due to depth of focus effect because of (a) finite size of schlieren light source, and (b) finite width of test section	33
3.10	Color resolution due to finite size of schlieren light source	36
4.1	Cinematographic sequence of schlieren photographs for CH ₄ -Air mixture by spark ignition	38
4.2	Particle velocity at a flame front	40
4.3	Profile of apparent flame front approaching a position at a side wall	41
4.4	Flow pattern during an intake and succeeding compression stroke	43
4.5	Flow characteristics during an exhaust stroke following after a power stroke with combustion	44

<u>Figure</u>		<u>Page</u>
4.6	Interaction between rolled-up vortex and CH ₄ -air flame; equivalence ratio 0.6, line spark ignition, ignition timing at 10 msec BTC, time interval 5 msec, flat piston	46
4.7	Interaction between rolled-up vortex and CH ₄ -air flame; equivalence ratio 0.6, line spark ignition, ignition timing at 10 msec ATC, time interval 5 msec, flat piston	47
4.8	Interaction between rolled-up vortex with the small bevel piston and CH ₄ -air flame; equivalence ratio 0.6, line spark ignition, ignition timing at 25 msec BTC, time interval 5 msec	49
4.9	Interaction between rolled-up vortex with the small bevel piston and CH ₄ -air flame; equivalence ratio 0.6, line spark ignition, ignition timing at 20 msec ATC, time interval 5 msec	50
4.10	Interaction between rolled-up vortex with the large bevel piston and CH ₄ -air flame; equivalence ratio 0.6, line spark ignition, ignition timing at 12 BTC, time interval 5 msec	51
4.11	Interaction between rolled-up vortex with the large bevel piston and CH ₄ -air flame; equivalence ratio 0.6, line spark ignition, ignition timing at TDC, time interval 5 msec	52
4.12	Interaction between rolled-up vortex with a wedge piston and CH ₄ -air flame; equivalence ratio 0.6, line spark ignition, ignition timing at 14 msec BDC, time interval 5 msec	54
4.13	Interaction between rolled-up vortex with a wedge piston and CH ₄ -air flame; equivalence ratio 0.6, line spark ignition, ignition timing at 4 msec ATC, time interval 5 msec	55
4.14	Interaction between rolled-up vortex with a hemispherical squish piston and CH ₄ -air flame; equivalence ratio 0.6, line spark ignition, ignition timing at 17 msec BDC, time interval 5 msec	56
4.15	Interaction between rolled-up vortex with a hemispherical squish piston and CH ₄ -air flame; equivalence ratio 0.6, line spark ignition, ignition timing at 10 msec ATC, time interval 5 msec	57

<u>Figure</u>	<u>Page</u>
4.16 Vortex area A normalized by square of the piston travel X	58
4.17 Normalized vortex area A/X^2 versus Reynolds number $Up X/\nu$	60
4.18 Unburned methane fraction with respect to the initial concentration for combustion with piston withdrawal from TDC	61
4.19 Unburned methane fraction with respect to the initial concentration for single compression-then-expansion combustion as a function of ignition timing	62
4.20 Unburned methane fraction with respect to the initial concentration for a wedge piston for single compression-then-expansion combustion as a function of ignition timing	64
4.21 Unburned methane fraction with respect to the initial concentration for a hemispherical squish piston for single compression-then-expansion combustion as a function of ignition timing.	65
5.1 Contribution of a) wall flame quenching, b) crevice flame quenching, and c) other effects to the observed unburned methane concentration	67
5.2 Wall turbulence plus vortex volume fraction as a function of time; a) piston in compression, b) piston at rest at TDC, c) piston in expansion	68
B.1 Pressure and piston displacement records	90
B.2 Wall turbulence	92

LIST OF TABLES

<u>Table</u>	<u>Page</u>
2.1 Comparison of Quenching Distances Between Calculated One-Wall and Experimental Two-Wall Values	12
3.1 Engine Operating Conditions	19

NOMENCLATURE

A	cross-sectional area of rolled-up vortex
C_1	a constant
C_2	a constant
C_p	specific heat of gas
C_w	specific heat of wall material
d_q	quenching distance between two extruded electrodes
D_1	quench layer thickness subjecting one wall effect
D_{11}	quenching distance between two parallel flat walls
f	a constant
f_s	focal length of schlieren mirror
F	a constant
h	enthalpy
k	thermal conductivity
n	refractive index
P	pressure
Pe	Peclet number
Q	heat of reaction
q''	heat flux
S_u	burning velocity
T	temperature
T_c	contact temperature
T_f	flame temperature
T_f^a	adiabatic flame temperature
T_i	ignition temperature
u	velocity in x direction

u'	turbulence intensity
U_p	piston speed
X	piston travel
x	x coordinate
y	y coordinate
y'	displacement of deflected ray at image of light source

Subscripts

g	gas
L	laminar
o	reference condition
s	source
T	turbulent
u	unburned gas
w	wall
l	corresponding to schlieren mirror 1

Greek letters

α	pressure exponent constant, thermal diffusivity
β	temperature exponent constant, a constant of refractive index
δ	preheating zone thickness
δ_r	reaction zone thickness
ϵ_H	eddy diffusivity
ρ	density
σ	a constant, angle of deflection
ν	kinematic viscosity
ξ	distance travelled by a flame
ω	reaction rate

CHAPTER 1

Introduction

Urban smog is one of the major environmental pollutants, causing eye irritation, visibility reduction, plant damage, ozone formation, and having other deleterious effects. Smog is formed by photochemical reactions of hydrocarbons and NO_x in the atmosphere. Reactive hydrocarbons are oxidized by the action of sunlight with so-called photochemical oxidants, i.e. O_3 , NO_2 , peroxyacetyl nitrate⁽¹⁾. The hydrocarbons and oxides of nitrogen that are responsible for smog formation are injected into the atmosphere by automobiles, aircraft, stationary combustion processes such as in power plants, evaporation of fuels, and other industrial and natural sources. Recent data⁽²⁾ (1974) has shown that of all these sources, 45% of hydrocarbons and 67% of NO_x may be attributed to automobiles, indicating that reduction of automotive emissions may significantly contribute to reduction of smog.

In automobiles, unburned hydrocarbons result from incomplete chemical reactions such as local flame quenching along the cylinder walls⁽³⁻⁷⁾, lack of burning in the piston crevice^(8,9), misfire⁽¹⁰⁻¹⁵⁾, bulk flame quenching^(16,17), and may be reduced by improved engine combustion efficiency.

The work presented here focuses on the unburned hydrocarbon emissions problem, particularly with regard to the emission of hydrocarbons due to wall flame quenching.

In 1957, Daniel⁽⁴⁾, in a pioneering work, took photographs of the flame in the cylinder of a CFR engine and observed that the flame quenched in the vicinity of the engine walls. The wall flame quenching phenomenon has been confirmed by many later investigators⁽⁵⁻⁷⁾ and it has been regarded as one of the major causes of unburned hydrocarbon formation in an automobile engine. Until recent years, most of the studies on hydrocarbon emissions^(3-9, 18-43) were concerned with surveys of the effects of various engine variables such as air-fuel ratio, ignition timing, engine speed, compression ratio, intake manifold pressure, coolant temperature, exhaust back pressure, engine configuration, and so on, and fairly thorough information has been obtained. These engine variables influence the generation mechanisms of hydrocarbons through varying fluid mechanics, thermodynamics, and chemistry. Their effects, however, are coupled in a complex manner so that finding optimal engine operating conditions is not straightforward.

In order to understand engine combustion processes, it seems important to clarify the aerodynamic state in the combustion chamber under various conditions. Both the intake and the compression stroke introduce turbulence into the flow field, the former by the jet action from the intake valve, and the latter due to the vortex roll-up phenomenon^(37, 38, 42, 44) and any other piston induced motion. The flame must propagate through this flow field⁽⁴⁵⁻⁴⁷⁾ and the nature of the turbulence and its location within the cylinder⁽⁴⁸⁻⁵⁰⁾ can have a profound effect on the degree to which reactions are completed. In addition, flow changes near the spark plug have been postulated to be a major cause of cycle to cycle variations⁽⁵¹⁻⁵³⁾ and studies of the engine flow characteristics have been increasingly reported in recent publications. However, in determining flow characteristics

such as turbulence intensities, velocity fields, etc., in an engine, hot wire anemometers have been most widely used. These experiments have been conducted without combustion due to the experimental difficulties, and the flow characteristics within an engine undergoing combustion have not been clearly observed or understood.

The present work has attempted to overcome the experimental difficulties involved in observing the combustion process by utilizing a single compression-expansion model engine, developed by Oppenheim, et al.⁽⁴²⁾. The model engine has a square cross-section which allows a side view of the engine chamber so that the flow patterns which exist during the intake and exhaust strokes and the vortex roll-up and the compression stroke are able to be seen clearly utilizing conventional schlieren optics. The engine has another advantage in that it may be operated in such a manner that we simulate only the intake stroke, or only the compression stroke, or only the compression and expansion stroke, etc. With this system, the effects of engine variables, such as air fuel ratio, ignition timing, and engine configuration on engine cylinder aerodynamics and the combustion processes have been observed.

The major conclusions drawn from this study are summarized as follows:

- 1) quench layer formation is observed along the cylinder walls and its thickness is of the same order of magnitude as that of local thermal boundary layer;
- 2) piston geometry and the intake process can drastically modify the flow characteristics in an engine;
- 3) the rolled-up vortex plays an important role in generating wall turbulence and the process of exhausting unburned hydrocarbons;
- 4) wall turbulence strongly affects the quenching process, increasing unburned hydrocarbons;
- 5) retarded ignition timing increases unburned hydrocarbons.

In Chapter 2, theoretical considerations are discussed. Chapter 3 includes the experimental approach in which the experimental apparatus and procedure are described. In Chapter 4, the experimental results are presented in the form of movies for the flow visualization experiments, and gas chromatograph results for the hydrocarbon experiments. In Chapter 5, the results are discussed. In Chapter 6, the results are summarized and conclusions drawn. The related problems for data reduction are included in the Appendices.

CHAPTER 2

Theoretical Considerations

2.1 Unburned Hydrocarbons and Wall Flame Quenching

When a flame runs into a solid wall, chemical reaction ceases at a certain distance from the wall, leaving a layer of unburned fuel. This distance, or more strictly speaking, the concentration thickness with respect to unburned fuel, is called the quenching distance, or quench layer thickness. The quench layer thickness in an engine can be estimated by converting the volume of emitted hydrocarbons into equivalent unburned fuel volume. Its value deduced from such measured hydrocarbon concentrations is about $30 \sim 100 \mu\text{m}$, which is of the same order of magnitude as quenching distances obtained from laminar flow quenching experiments.

There have been a number of attempts made to determine the quench layer thickness in an engine. For example, Daniel⁽⁴⁾ deduced a quench layer thickness from black-and-white photographs of the quenched region in an engine, and Daniel and Wentworth⁽⁶⁾ conducted an experiment to measure quench layer thickness by using a fast acting sampling valve in the vicinity of the engine wall. Wentworth⁽⁹⁾ demonstrated the relative importance of the piston crevice and wall flame quenching and was able to reduce exhaust hydrocarbons by 47 - 74% with revised designs of the engine piston in which the piston crevice volume was significantly eliminated. The experimental evidence thus shows that the hydrocarbons emitted from an automobile engine are primarily due

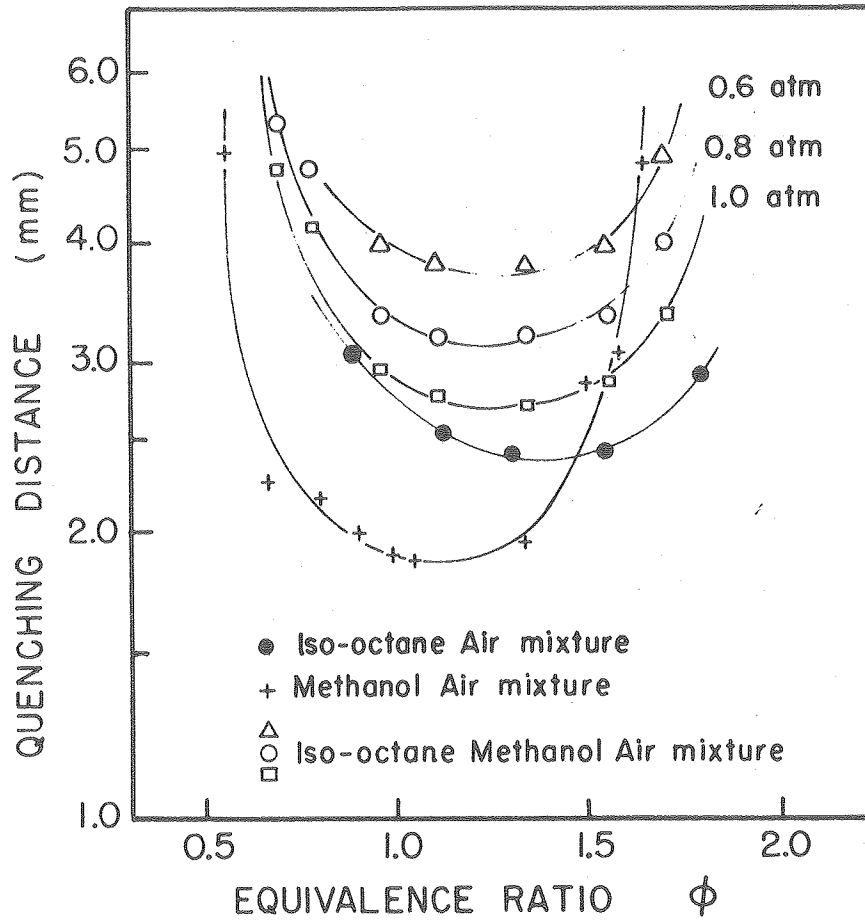
to wall flame quenching and unburned fuel which remains in the piston crevice during the combustion process.

It has been suggested that the contribution of the piston and other crevices to hydrocarbon emissions may be minimized if design problems could be overcome. On the other hand, methods of how to minimize wall flame quenching have not been extensively studied. In fact, quenching mechanisms along engine walls under complicated circumstances have not been understood well. Quenching is a localized phenomenon and the thickness may be different at various locations since conditions such as pressure, temperature, flow field, geometry, etc. are all different in space and time.

Figure 2.1 shows the quenching distance for a mixture of methanol, and methanol-isooctane blends in air⁽⁵⁴⁾, illustrating how the quenching distance for laminar mixtures generally varies⁽⁵⁵⁻⁶⁶⁾. In general, the quenching distance is a strong function of equivalence ratio. The minimum values are attained at an equivalence ratio slightly richer than stoichiometric. Note that the burning velocity is maximum at the corresponding mixture ratio. The quenching distance drastically increases as the mixture approaches both flammability limits. The effect of pressure and temperature (not shown in the diagram) may be shown to follow an empirical equation for quenching distance D_1 as

$$D_1 = F D_{11_0} \left(\frac{P_0}{P} \right)^\alpha \left(\frac{T_0}{T} \right)^\beta \quad (1)$$

where D_{11_0} denotes a reference two-wall quenching distance, α , β , and F are positive constants, and the subscript 0 denotes a reference condition. The quenching distance D_{11_0} can be determined by laminar flow experiments



XBL 787-9685

Figure 2.1 Quenching distances of iso-octane methanol air mixtures (20% methanol in iso-octane by weight) at $T = 100^\circ \text{C}$, in comparison with those of iso-octane air (1 atm, 100°C) and methanol air (1 atm, 100°C) mixtures

for a particular mixture of interest. The values of α and β may vary for different types of fuels⁽⁵⁴⁾. The empirical equation (1) is useful for laminar gas mixtures since the quenching distance may be estimated simply by temperature and pressure which are easily predicted. For this reason, Equation (1) has been used by many investigators. Unfortunately, however, Equation (1) does not take the effect of flow into account, which is expected to play an important role and is of major interest in this study.

The study of wall flame quenching may be systematically divided into two: clarification of flow characteristics with various engine configurations; and corresponding unburned fuel concentration measurements. From the comparison of the results of such experiments, we hope we will find some qualitative information on fluid dynamic effects on flame wall quenching and clarify its mechanisms. Prior to the experimental work, in the following sections, flame quenching phenomena will be discussed for both laminar and turbulent conditions in an attempt to clarify this point with some available theoretical works.

2.2 Laminar Flame Quenching

As pointed out above, lack of understanding of complicated flow characteristics has hampered detailed analyses on engine wall flame quenching. Ferguson and Keck⁽⁶⁷⁾ have hypothesized that wall flame quenching may not be influenced by the existing turbulence and proposed their laminar quenching theory for application to a sparking ignition engine. Their reasoning is based on Daniel's experimental results, that is, the quench layer thickness in an engine is of the same order of magnitude as that of laminar flame quenching devices. Despite questions of the validity of this assumption, a laminar flame quenching

analysis is of great importance since it serves as a reference condition against which to compare experimental results.

The method of theoretical analysis on laminar flame quenching may be categorized into two classes: those beginning with an arbitrary assumption concerning the conditions required for flame propagation, and those which involve direct solution of the conservation equations. The first class employs assumptions for the flame quenching criteria in which either thermal diffusion processes^(68,69) or mass diffusion processes⁽⁷⁰⁾ dominate the phenomenon. This method has been used to obtain correlations for the quenching distance. The second class normally utilizes numerical solutions and provides a better phenomenological description⁽⁷⁰⁻⁷⁹⁾. The work of von Karman and Millan⁽⁷⁴⁾, and of Kirkov and Mursky⁽⁷⁵⁾ are typical descriptions of the problem.

Nevertheless, the solutions derived from simple analysis are useful in discussing the effect of fluid dynamics although they provide intuitive understanding at best. The quenching distance in this method is determined by setting up a criterion at which either the rate of heat loss or the rate of destruction of radical species due to wall effect is equated to their respective rates of generations in the reaction zone of the flame. Friedman⁽⁶⁸⁾ first demonstrated the thermal flame quenching theory for a flame passing through two parallel flat plates and was able to show that the quenching Peclet number, defined by two wall quenching distance D_{11} , burning velocity S_u , and thermal diffusivity α behaves as follows:

$$\frac{D_{11}S_u}{\alpha} = \frac{1}{f} \left(\frac{T_f^a - T_j}{T_j - T_u} \right)^{\frac{1}{2}} \quad (2)$$

where f is a geometric constant, T_f^a is adiabatic flame temperature,

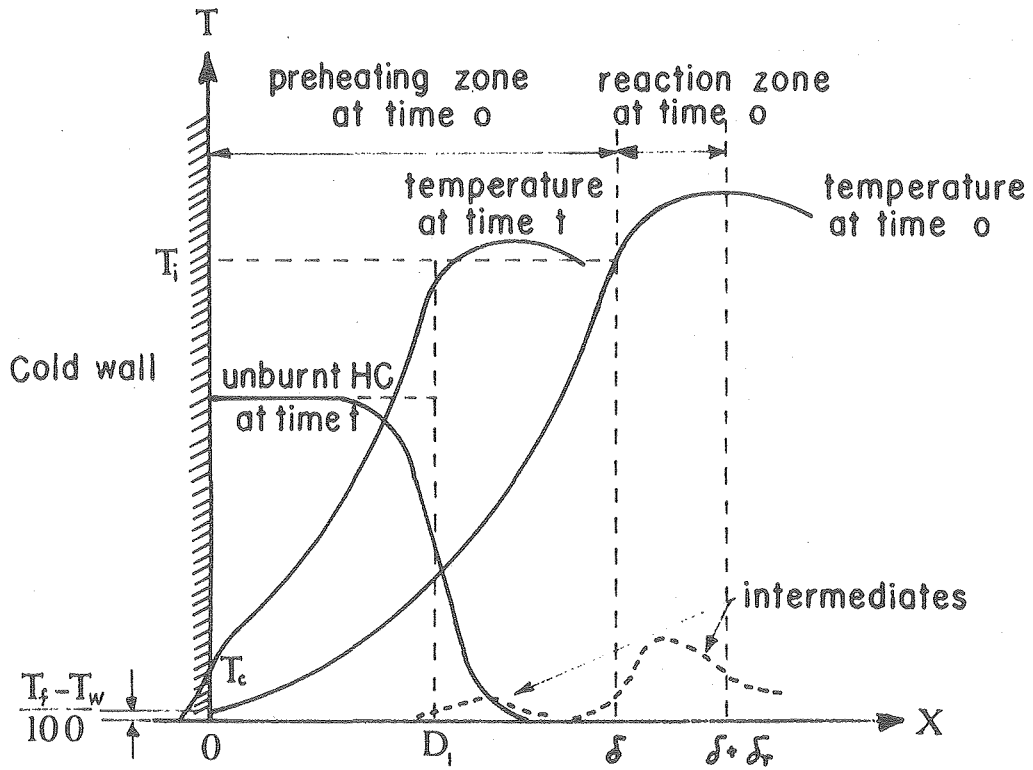
T_i is ignition temperature, and T_0 is the unburned gas temperature. Notice that the flame in this case is subject to the effect of two walls and the quenching distance predicted by Equation (2) may then be associated with the piston crevice flame quenching. Wall flame quenching involves a single wall. This case has been analysed by Ishikawa and Branch⁽⁸⁰⁾ for a system similar to that of Kirkov and Mursky introduced above, (Figure 2.2). The energy equations including heat transfer in a solid wall were analytically solved by appropriate simplifications and the quenching Peclet number was obtained as follows (see Appendix A):

$$\frac{D_1 S_u}{\alpha} = 4.6 + \ln \left(\frac{T_f^a - T_f}{T_f - T_w} \right) \quad (3)$$

where D_1 denotes a quenching distance subjecting one wall effect, T_f the quenching flame temperature, and T_w wall temperature. It is remarkable that Equations (2) and (3) have similar forms. The first term on the right hand side of Equation (3) is attributed to the definition of the thickness of the preheating zone δ ⁽⁸¹⁾ as the distance between two positions corresponding to ignition temperature T_i and $(T - T_c)/(T_i - T_c) = 1/100$ (see Figure 2.2). The corresponding Peclet number based on the preheating zone thickness becomes

$$\frac{\delta S_u}{\alpha} = 4.6 \quad (4)$$

The logarithmic term in Equation (3) is normally negative so that Equation (3) yields a quenching distance slightly smaller than the preheating zone thickness. Some example calculations using Equation (3) are listed in Table 2.1 in which the calculated quenching distance D_1 is about four tenths of the experimental data of two wall quenching



XBL 787-9684

Figure 2.2 Detail of flame approach to wall describing physical parameters of flame quenching model

Table 2.1 Comparison of Quenching Distances Between Calculated One-Wall and Experimental Two-Wall Values ($T_w = 300^\circ\text{K}$, Stoichiometric Mixture)

Chosen Values of the Parameters						
Fuel	T_f^a (K)	T_f (K)	α (cm ² /sec)	S_u (cm/sec)	Calculated	Experimental
					Values	Values
					D_1 (cm)*	D_{11} (cm)**
Hydrogen	2400	2350	3.20	306	0.024	0.057
Methane	2236	2000	1.13	39	0.095	0.235
Propane	2250	2000	1.10	45	0.071	0.207
Benzene	2306	2100	1.15	47	0.070	0.192

* Gas properties were taken from Reference (94)

** From Reference (66), p. 178.

distance D_{11} . The ratio D_1/D_{11} has not been uniquely determined but given values in the range $0.2 \sim 0.5$ (66,82). This may be due to a difference in temperatures at which gas properties are calculated for quenching distances.

2.3 Turbulent Flame Quenching in an Engine

The flow characteristics in an engine are not easily determined. This is because neither experimental nor predictive techniques have been well established for engine flow with complicated geometries. The question of how the flow field influences wall flame quenching has thus not been completely resolved. It is clear that changes in temperature and pressure will affect the quenching, but how large an effect will turbulence have on the process?

In either Equation (2) or Equation (3), the quenching Peclet number is shown to be a weak function of temperatures such as adiabatic flame temperature, wall temperature and so on. In addition, the values of these temperatures may change due only to gas properties and thermodynamic state of the mixture and may not be subject to fluid dynamic conditions. Therefore, the quenching Peclet number may take nearly a constant value for identical mixtures. The burning velocity and thermal diffusivity are, however, strongly influenced by turbulence of the mixture. The burning velocity may increase in a manner, $S_u \sim \sqrt{u'}$, (85) where u' is turbulent intensity. On the other hand, the effective thermal diffusivity should be a sum of the molecular thermal diffusivity and eddy diffusivity, ϵ_H . The eddy diffusivity may increase with turbulence in a manner, $\epsilon_H \sim u'$ which is apparent from Reynolds analogy. Therefore, if this crude consideration is allowed for the results of laminar theories, the quenching distance may increase with turbulence

in a manner, $D_T \sim \sqrt{u'}$.

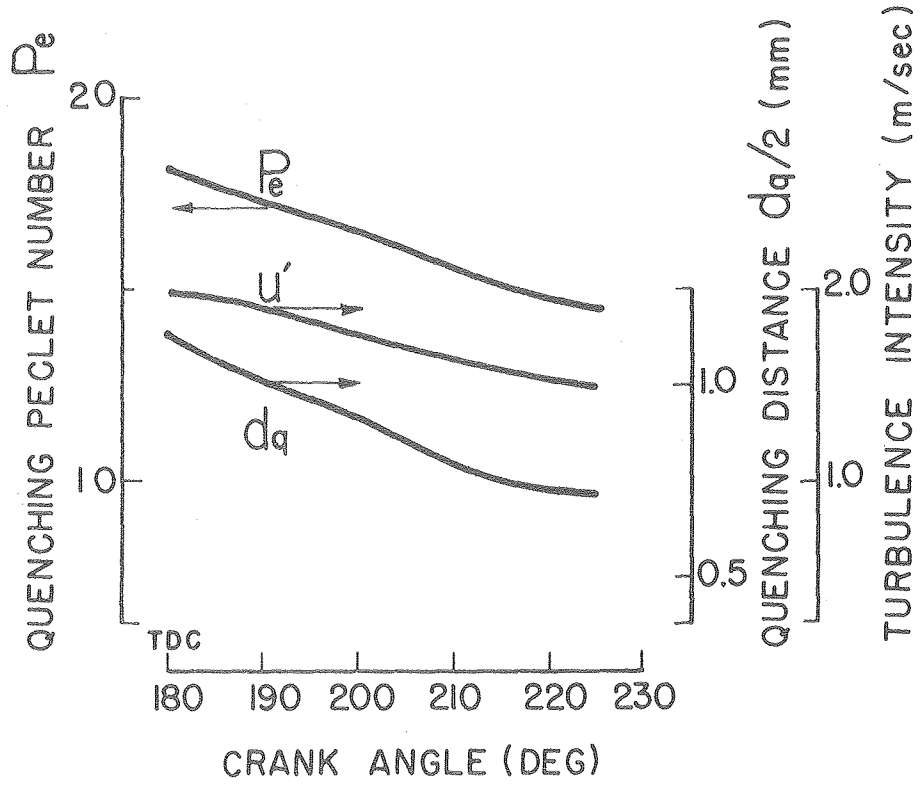
There has been little work done on turbulent quenching. However, Ballal and Lefebvre's work⁽⁸³⁾ has demonstrated that the quenching distance in turbulent flow can be substantially different than that for laminar flow. Their results may be rewritten in the form of a Peclet number as

$$\frac{S_L \text{ (or } S_T) d_q}{\alpha} = \frac{C_1}{1 - C_2 \left(\frac{u'}{S_L \text{ (or } S_T)} \right)} \quad (5)$$

where S_L and S_T denote burning velocity (laminar or turbulent), d_q quenching distance, and C_1, C_2 positive constants where $C_2 < 1$. The conclusion they have drawn is that quenching distance increases with increases in thermal diffusivity and turbulence intensity, and decreases with an increase in burning velocity. The quenching distance d_q in Equation (5) is the distance between two electrodes extruded in a free stream. Although the conditions are somewhat different between Ballal and Lefebvre's system and an engine, Equation (5) does imply that wall turbulence may well increase the quenching distance.

Figure 2.3 utilized Equation (5) to show how the quench layer thickness might vary in an engine for crank angles near top dead center. It has been assumed that the quench layer thickness is half the value of the quenching distance between Ballal and Lefebvre's two electrodes d_q . The values of C_1 and C_2 used in Equation (5) are 10 and 0.63 respectively according to Ballal and Lefebvre⁽⁸³⁾. The laminar burning velocities were taken from Babu and Murthy's numerical calculation⁽⁸⁴⁾ simulating SI engine combustion and the turbulent burning velocity was calculated by the equation⁽⁸⁵⁾

$$S_T = S_L + \sqrt{2S_L u'} \quad (6)$$



XBL 787-9679

Figure 2.3 Effect of turbulence on quenching distance and Peclet number

The turbulence intensities corresponding to the above crank angles were taken from Lancaster's experimental results⁽⁵⁰⁾. Figure 2.3 shows that the quench layer thickness increases by about 60% as the turbulence intensity increases by 33%. This implies that the key to minimizing wall flame quenching is to reduce the wall turbulence.

CHAPTER 3

Model Engine Study on Wall Flame Quenching

3.1 Experimental Approach

The flow characteristics in an engine may vary with different engine geometries but how that difference effects the combustion process has not been completely understood. Because of complexities in engine processes, it is not possible to predict a priori the precise flow characteristics within an engine. Because of this, visualization of the phenomena would provide useful information for analysis. Previous visualization experiments have been performed under conditions in which only a top view of the piston was possible^(3,4,86). The unique aspect of our apparatus is that we may observe the combustion process from the side.

3.2 Experimental Apparatus

3.2-1 Engine and instrumentation

The single compression-expansion model engine has been described in detail in reference (42). Figure 3.1 shows a schematic of the engine system which has a stainless steel test section with a square cross-section, 3.81 x 3.81 cm, with side windows of quartz. Operating conditions of the model engine are listed in Table 3.1 in comparison with a CFR engine. Five piston configurations have been prepared in an attempt to vary the flow characteristics, that is, a conventional flat piston, two beveled pistons, a wedge piston, and a hemispherical

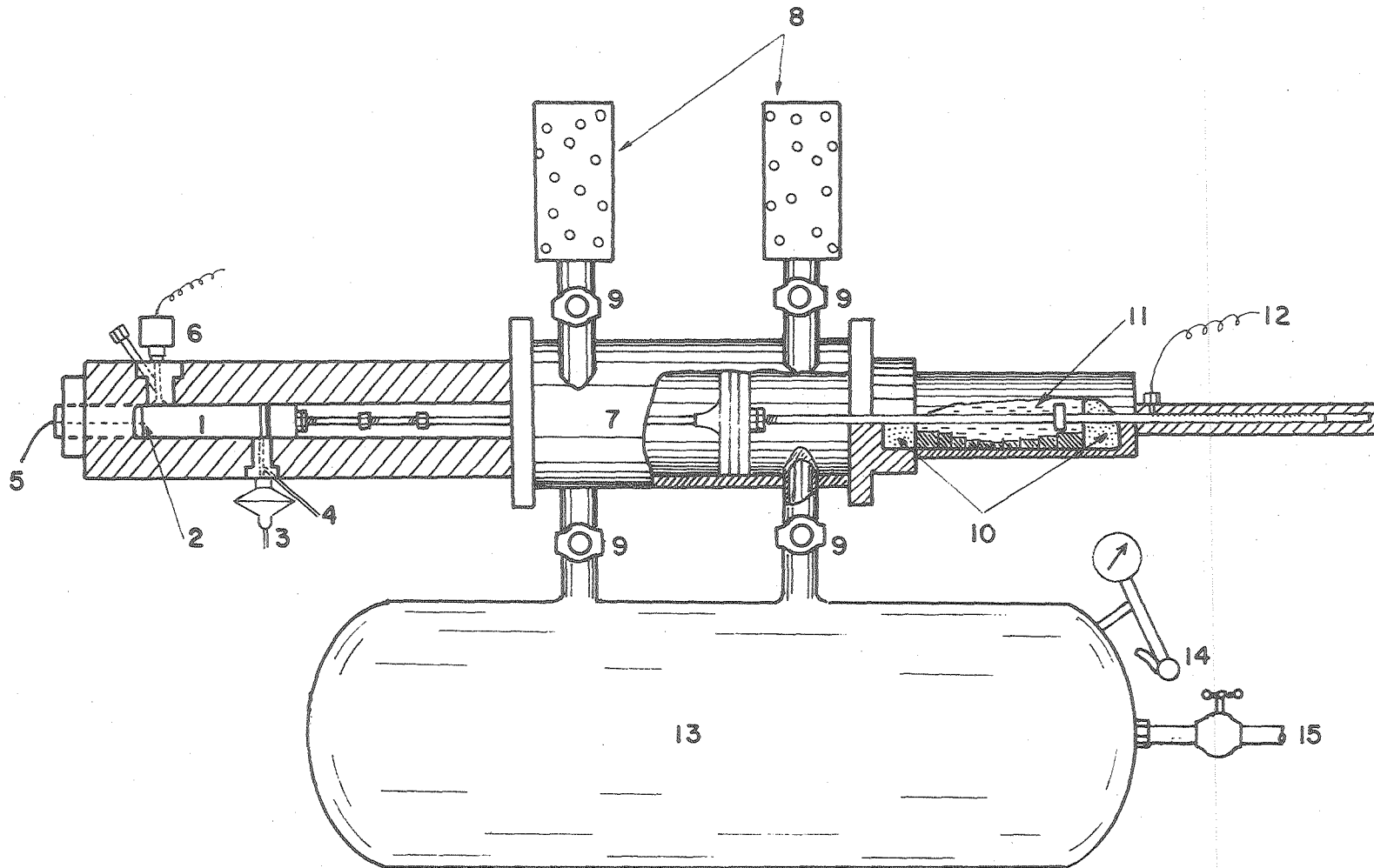


Figure 3.1 Schematic of single compression-expansion machine; 1 - Combustion chamber, 2 - Line igniter, 3 - Inlet valve, 4 - Inlet gas tubing, 5 - High voltage wiring, 6 - Exhaust valve, 7 - Driver section, 8 - Mufflers, 9 - Solenoid valves, 10 - Shock absorbers, 11 - Snubber port, 12 - Magnetic pick-up, 13 - Compressed air tank, 14 - Air release valve, 15 - House air inlet

XBL 784-8138

TABLE 3.1 Engine Operating Conditions

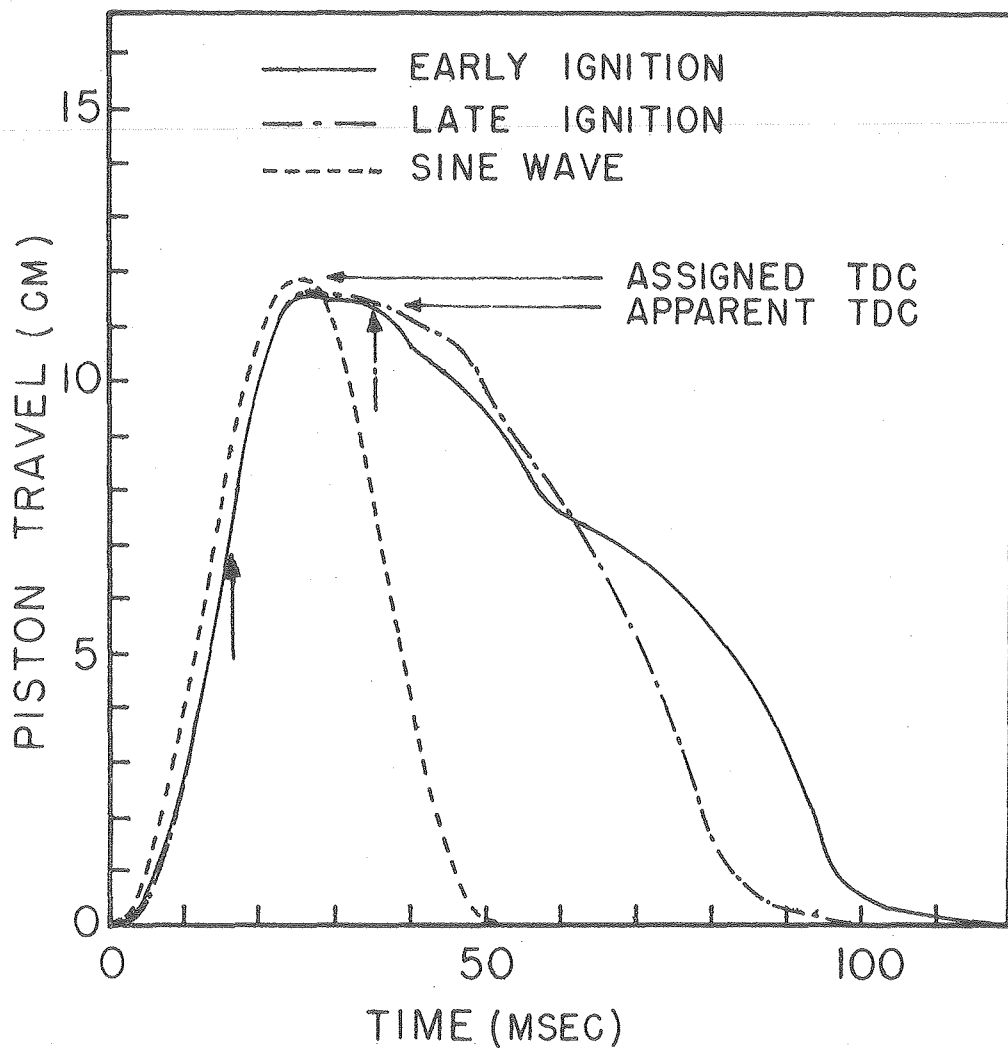
	<u>Model Engine</u>	<u>CFR Engine*</u>
cross-section of cylinder	14.52 cm ²	53.52 cm ²
stroke	11.90 cm	11.43 cm
unswept volume	37.31 cm ³	101.96 cm ³
compression ratio	6.0 ± 0.7	6.0
stroke to bore ratio	3.13	1.38
equivalent engine speed	1200 rpm	—
piston crevice volume		
flat piston	0.42 cm ³	0.754 cm ³
bevel pistons	0.42 cm ³	—
wedge piston	0.74 cm ³	—
hemispherical squish piston	0.35 cm ³	—
cylinder head crevice volume	0.33 cm ³	—
distance from valve center line to cylinder head	1.1 cm	—

* typical values

squish piston which are illustrated in Figure 3.2. The pneumatically driven piston is designed to simulate constant angular velocity crank shaft rotation. The air pressure imposed on the driver section is 6.2 atm, while that of the test section varies from 0.5 to 25 atm. The piston area ratio of the driver section and the test section is 28.7 so that the piston can be driven by compressed house air. The engine is operated by an electronic control system. The ignition timing and the valve opening timing can be pre-set.

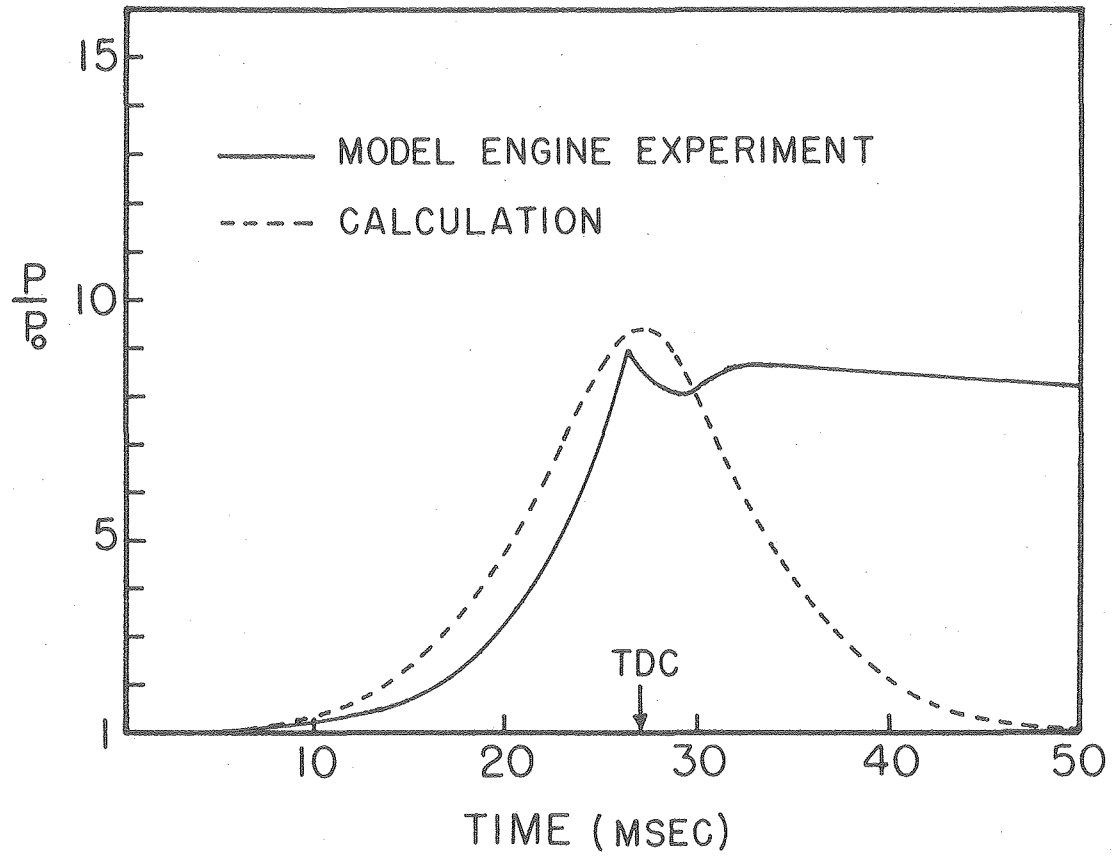
The piston can be run in a sequence of motions; that is, compression, expansion, and again compression. The piston trajectory in operation may deviate from a sine wave trajectory, which is originally set up without pressurization in the test section, since the pressure in the test section either opposes or adds to the piston motion. In fact, the piston in compression bounces once due to the compressed air acting as a spring at a location of about 97 percent of the stroke before it reaches the TDC; thereafter it creeps quickly up to TDC. Depending on the pressures in the test section and the driver section, the apparent compression ratio varies from run to run with about a 15% deviation. Figure 3.3 shows an example of piston trajectories. It should also be pointed out that if combustion takes place way after TDC there is an unavoidable time lag of about 30 to 40 msec at best which the piston stays at TDC. This is associated with the performance of the activating solenoid valves at the driver section.

The dual-beam oscilloscope provides a photographic record of piston travel, pressure of the test section, and ignition timing mark. Figure 3.4 shows an example of measured pressure variation. Also shown in the calculated isentropic pressure variation for a sine wave piston



XBL 784-8137

Figure 3.3 Comparison of piston trajectories between the machine and a real engine; vertical arrows show ignition timing



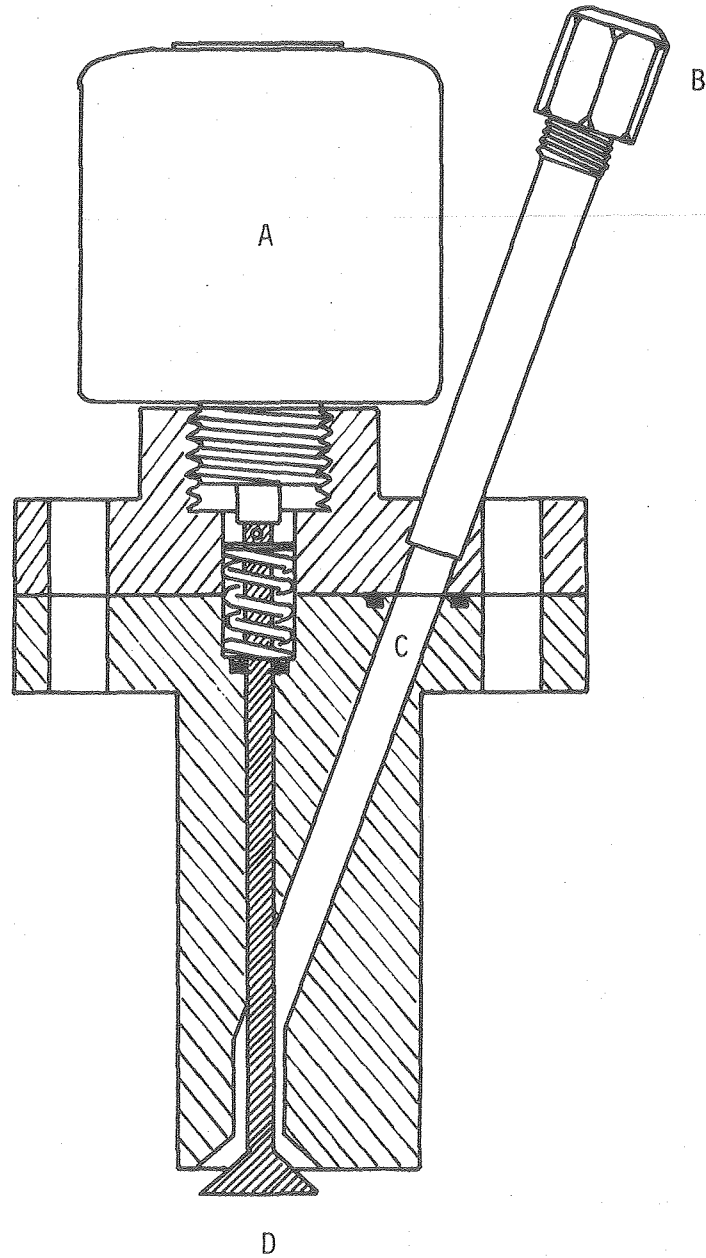
XBL 784-8145

Figure 3.4 Comparison of pressure traces between the machine and a real engine with a constant angular velocity

motion. As is seen in Figure 3.3, the calculated pressure deviates from that measured as the pressure increases, which may be attributed to leakage through the piston-cylinder interface. For the present work, this leakage has been kept as low as 5% of initial mass of the mixture.

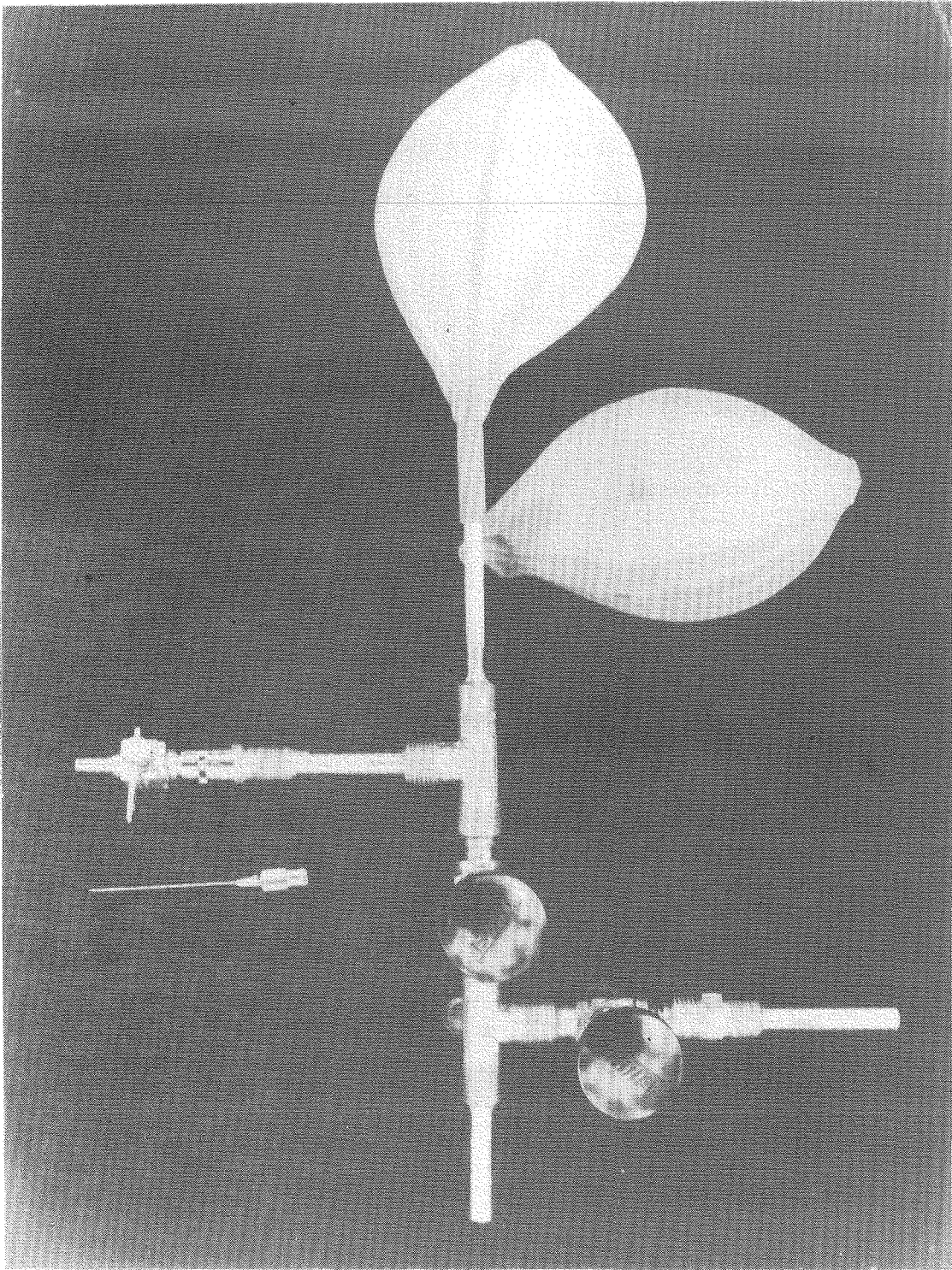
The engine is equipped with a simulated exhaust/intake valve and a burned gas sampling device which are illustrated in Figures 3.5 and 3.6. The valve is operated by a fast-acting solenoid valve. The opening stroke can be varied within 3 mm, which is fully executed in about 4 milliseconds. The burned gas sampling device is designed so that the burned gas is collected into the sampling collector at atmospheric pressure. The sampling device can be disconnected from the exhaust valve and the exhaust let out to atmospheric pressure when simulating actual engine operating conditions. It has an adaptor for a hypodermic syringe which is used to extract the gas sample from the device and inject it into a gas chromatograph. The sample device can be evacuated to 12 mm mercury, which eliminates possible interference due to leakage of fresh charge through the exhaust valve. An extensive study of uncertainty in chromatograph results has shown that drift and random uncertainties were negligible, less than 0.1% of the reading reported.

Ignition is accomplished by means of a line igniter⁽¹⁷⁾ which provides a two-dimensional flame front so that analysis of the schlieren image is simplified considerably. The gas mixture, which is methane air, is provided by a mixing device as reported in reference (87). The fresh gas mixture is introduced into the engine chamber through a pintle valve which is pneumatically operated. The pintle valve is designed so as to eliminate any possibility of unburned hydrocarbons



XBL 784-8136

Figure 3.5 Exhaust intake valve; A - Fast acting solenoid valve, B - Selastic fitting, C - Exhaust port, D - Exhaust valve



XBB 784-4496

Figure 3.6 Gas sampling device

remaining in the valve assembly. The present mixing device is very sensitive to the pressure loss between the hypodermic needles and the atmosphere since the flow at the needle is not choked. Therefore, care must be taken to prevent the introduction of any change in the flow system; otherwise, the resulting mixture ratio will be erroneous.

The gas chromatograph used is a Beckman GC/2 with a thermal conductivity detector. For data processing, a computing integrator for chromatography, AUTOLAB-System IV, is used.

3.2-2 Optical System

a) System description

Figure 3.7 shows the schlieren system. The schlieren photographic technique has been widely utilized to study various combustion processes. The techniques are extensively summarized in the literature⁽⁸⁸⁻⁹¹⁾. However, not clearly described in any of the literature are details about the application of the schlieren method for quantitative distance measurements, nor, to the author's knowledge, has the technique been used for studying wall quenching. We will therefore discuss in detail how our color schlieren system works and examine spatial and color resolution questions.

Figure 3.8 shows typical ray paths of deflected and undeflected rays, where the mirrors are replaced by lenses for the purpose of illustration. The rays, emanating from a point white light source S, are collimated by lens L₁, pass through the test section, and are focused by lens L₂ to make the image of the source S at the focal length f₂ of L₂. The focusing lens L₃ and the camera film are arranged in such a way that the test section is imaged onto the film. The color stop is set up exactly at S', the image of the source S. If a disturbance in density of the gas at point A in the test section occurs due to combustion, a ray λ passing the point A deflects toward higher density by an angle θ corresponding to

$$\theta = \frac{1}{n_o} \int_0^L \left(\frac{dn}{dy} \right)_y dx = \frac{\beta}{\rho_o} \int_0^L \left(\frac{d\rho}{dy} \right)_y dx \quad (7)$$

where n is the index of refraction, dn/dy its gradient, ρ the gas density, L the depth of the gas and β a non-dimensional constant having a value 0.000292 for air at S.T.P. The subscript, o, indicates conditions

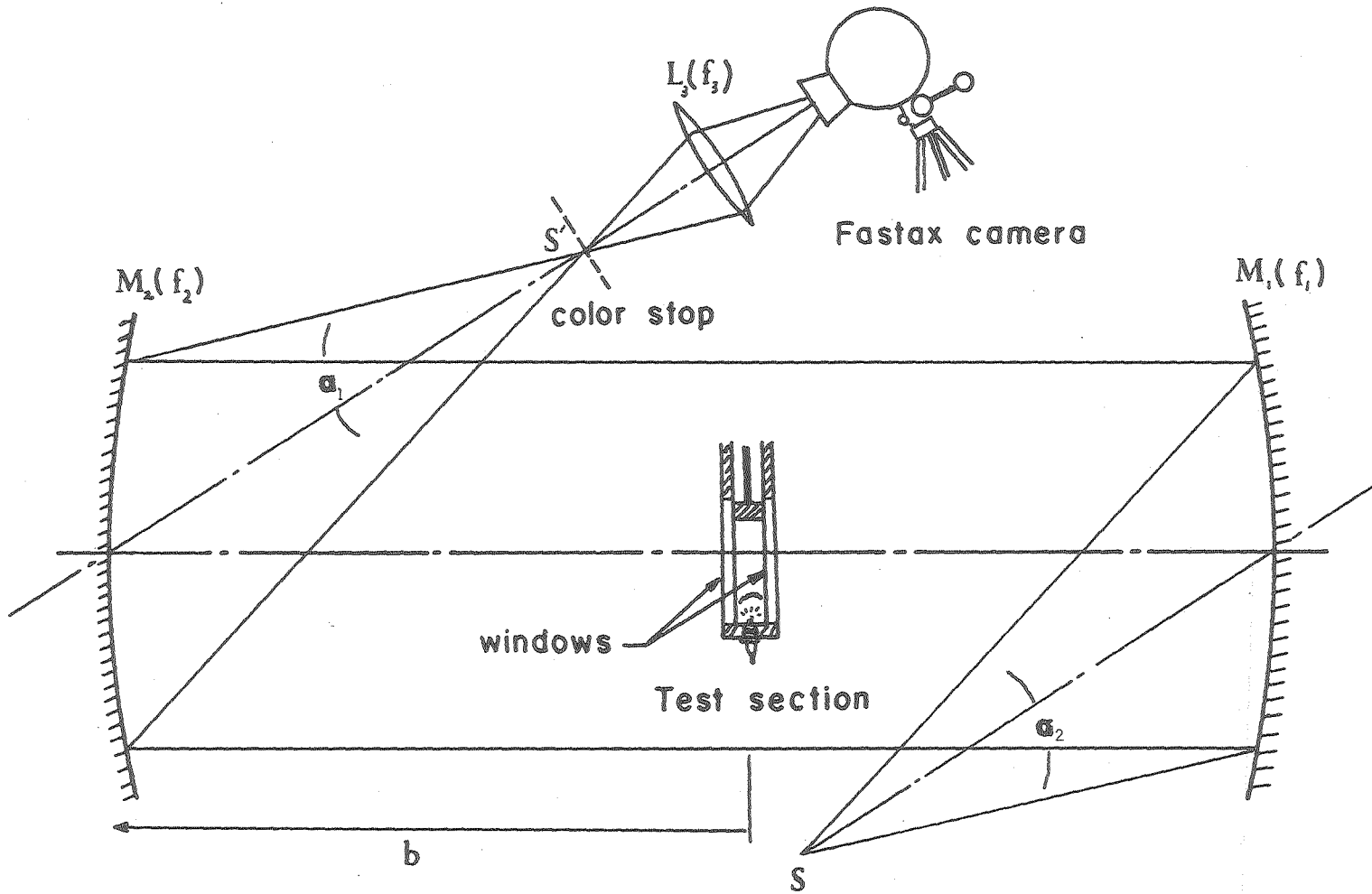
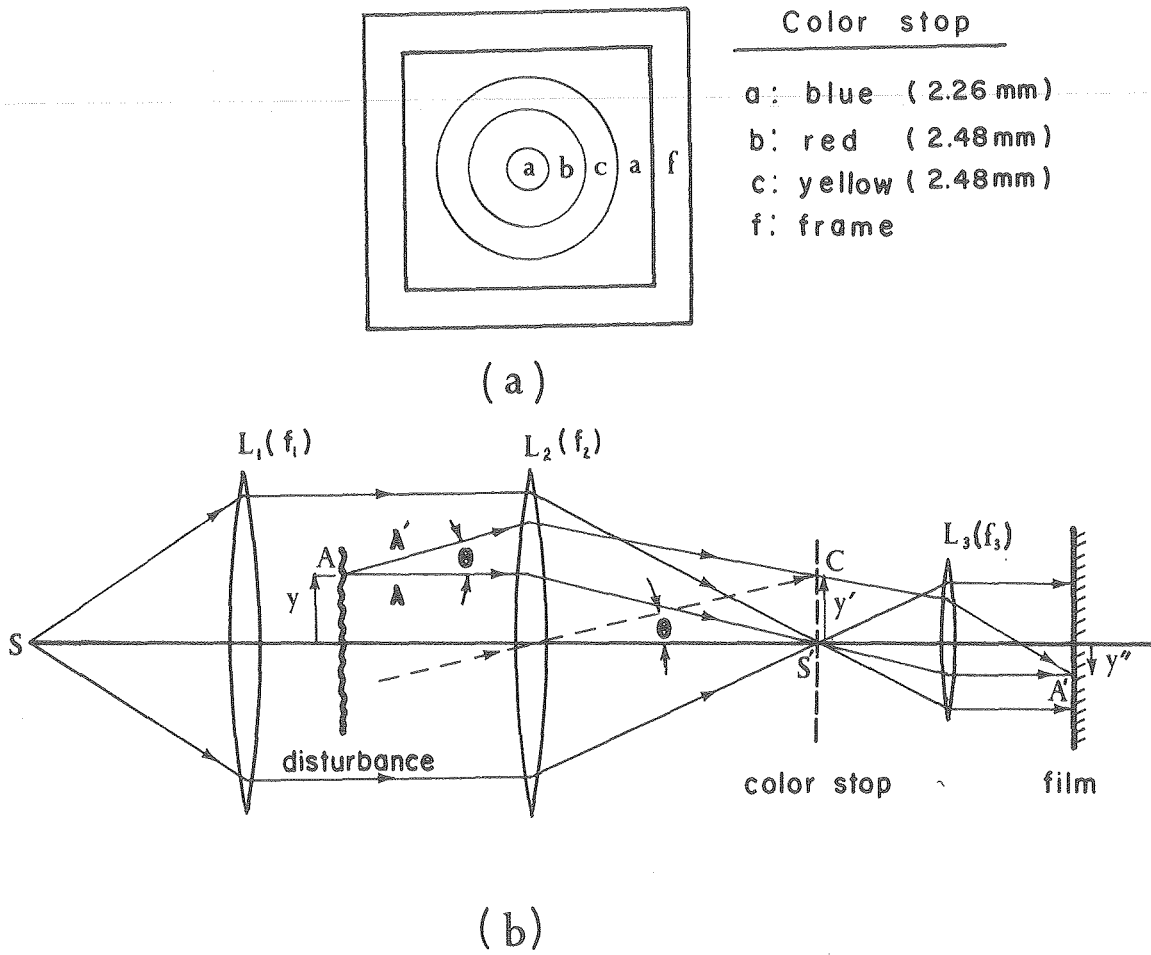


Figure 3.7 Optical systems. $f_1 = f_2 = 3.94$ m, $f_3 = 20$ cm, diameter of mirror XBL 787-9680 = 305 mm, $\alpha_1 = \alpha_2 = 2.7$ deg, $M_1M_2 = 9.30$ m, $b = 3.94$ m.



XBL 787-9681

Figure 3.8 Ray paths in color schlieren system

at S.T.P. In the case of uniform conditions we can determine $\frac{d\rho}{dy}$ exactly. The deflected ray λ' will pass through a point C on the color stop. The displacement $\overline{S'C} = y'$ is simply related to θ by

$$y' = f_s \tan\theta \approx f_s \theta \quad (8)$$

At the stop, the ray λ' becomes colored at point C. The colored ray will then be imaged by lens L_3 to the same point as the undeflected ray A. Thus, by observing the color on the film the deflection at point A can be determined. Here it has been assumed that the refractive deviation of the ray λ' from the undeflected ray λ at the point A is very small. The density gradient at point A can then be calculated by

$$\left(\frac{d\rho}{dy}\right)_y = \frac{\rho_u y'}{B L f_s} \quad (9)$$

Assuming ideal gas behavior, the temperature gradient is also given by

$$\frac{1}{T^2} \frac{dT}{dy} = \frac{y' P_u}{\beta L f_s T_u P} \quad (10)$$

where the minus sign is dropped since it merely indicated the direction of deflections.

To determine the temperature gradient directly, temperature and pressure should be known. Although the pressure can be measured, it is difficult to measure the temperature distribution, and so is its calculation. However, if one rewrites Eq. (10) as

$$\frac{d(1/T)}{dy} = \frac{y' P_u}{\beta L f_s T_u P} \quad (11)$$

it is not necessary to have the value of temperature.

b) Spatial Resolution

The spatial resolution attainable with the schlieren system limits the range of experimental conditions which can be examined. Uncertainties in position arise from optical aberrations, depth of focus difficulties, diffraction, and film resolution.

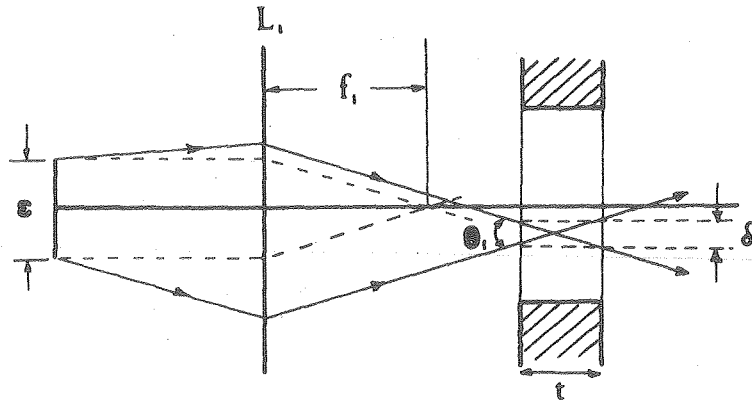
Optical aberrations include spherical aberrations, coma, and astigmatism. For our optics none of these effects limit resolution. Spherical aberrations are on the order of 3 mm resulting in negligible spatial uncertainty. Coma, is also small for our apparatus. The most severe restriction placed on the optical system is that due to astigmatism. For example, the separation of the astigmatic S and T planes at the schlieren stop for the configuration reported here was about 3 cm. However, this also produces a negligible spatial uncertainty. Hosch and Walters ⁽⁹²⁾ report exact ray tracing results that support the above results.

The depth of focus effect arises because of the finite width of the test section and the finite size of the schlieren light source. This effect is illustrated in Figure 3.9a. The positional uncertainty due to this effect is approximately equal to

$$\delta \approx \theta_1 t \approx \frac{e}{f_1} t \quad (12)$$

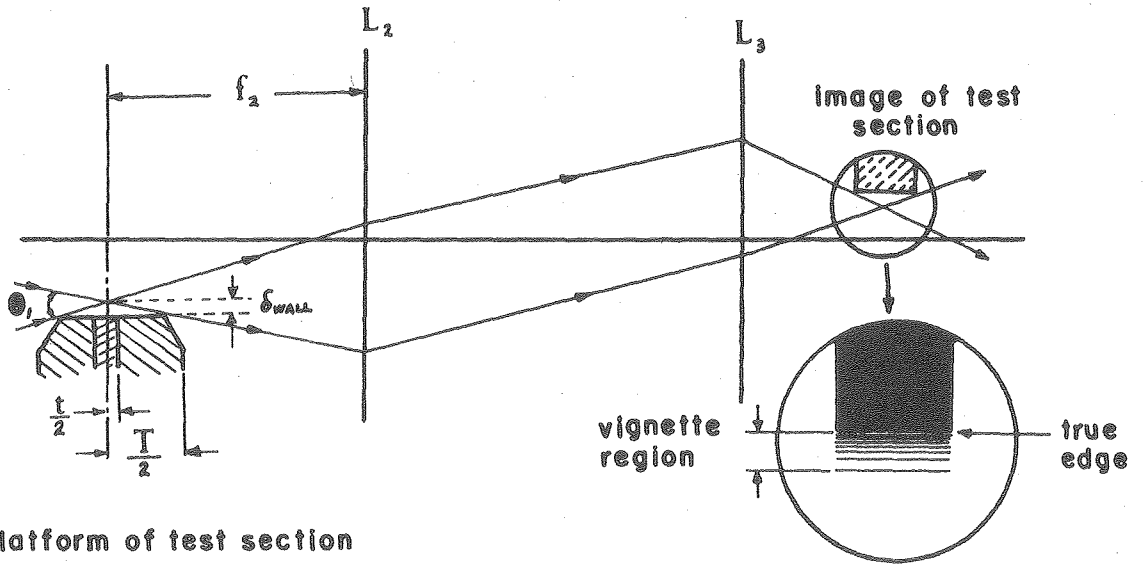
For our optics $\delta \sim 20\mu$ which is clearly negligible. It is important that the camera film be placed exactly at the image plane of the test section, i.e., that the system be well focused.

There is an additional uncertainty in the position of the wall due to the nature of the windows on the test section which is illustrated in Figure 3.9b. This results in a vignetting of light over a region



refractive index field
of gas phase

(a)



platform of test section

(b)

Figure 3.9 Spatial uncertainties due to depth of focus effect because of (a) finite size of schlieren light source, and (b) finite width of test section XBL 787-9682

$$\delta_w \approx \theta_1 T/2 = \frac{\epsilon}{f_1} \frac{T}{2} \quad (13)$$

For our optics $\delta_{wall} \sim 50\mu$ but the uncertainty in wall position should be less subject to diffraction since the actual wall images as the edge of the dark region.

The effect of density gradients is to deflect these rays. If the angular deflection is sufficiently large, then there will be some uncertainty as to the source of the ray. This uncertainty will be of the order of θt where θ is the deflection angle due to the schlieren effect. We measure deflection angles on the order of 0.0025 radians, which leads to a positional uncertainty of about 100μ .

Diffraction effects are also small for our system. The diffraction limited resolution is about 30μ at the test section.

For the results reported, film resolving power limits resolution. The film, KODAK Ektachrome 7241EF, can resolve 32-50 lines/mm, or 20-30 μ . Because of image contraction, this corresponds to 400-600 μ at the test section for the results reported.

c) Color Resolution

Any uncertainty in color can lead to uncertainty in the calculated ray deflection angle and thus the temperature gradient. The primary cause of color uncertainty is the finite size of the source as was illustrated in Figure 3.9. The source images onto the stop as a spot of size $(f_1/f_2)S$. As a ray is deflected, passing through the various colors of the stop, the colors mix and it is difficult to interpret the results. One method of overcoming this problem is to make the color bands slightly larger than the source image. Thus, for a short distance,

the ray will take on a pure color, allowing an exact determination of the deflection. Unfortunately, this results in a wide color spacing which in turn means that we can accurately determine the deflection at only a few locations in a flame front.

This difficulty is illustrated in Figure 3.10 which shows the temperature gradient as a function of temperature and color for a typical color stop. There is an uncertainty in dT/dy due to both the uncertainty in color and in T . In order to improve the color resolution the neighboring colors are separated by black ribbons, which eliminate all light which is not of a pure color (shaded portion of Figure 3.10). The schlieren image is much clearer with better definition of the colors. This change has been helpful in making quantitative measurements.

The conclusions one must reach about the color schlieren method is that it is best suited for qualitative flow visualization.

One of the difficulties in studying quench layers is that there is, in fact, no agreed upon definition of the layer thickness. In fact, the thickness, if there is a unique one, is time varying. The commonly reported thicknesses are quite arbitrary, depending on the experimental configuration at hand or the particular analysis.

d) Black-and-white schlieren

Besides the color schlieren technique, the black-and-white schlieren technique has also been used with the same optical system. The only difference is the stop which has an aperture with the same size as the image of the light source, passing all undeflected light but blocking all deflected light. It turns out that black-and-white schlieren photography with this stop yields better sensitivity and is more appropriate for observation of flows with weak density gradients compared to color schlieren photography.

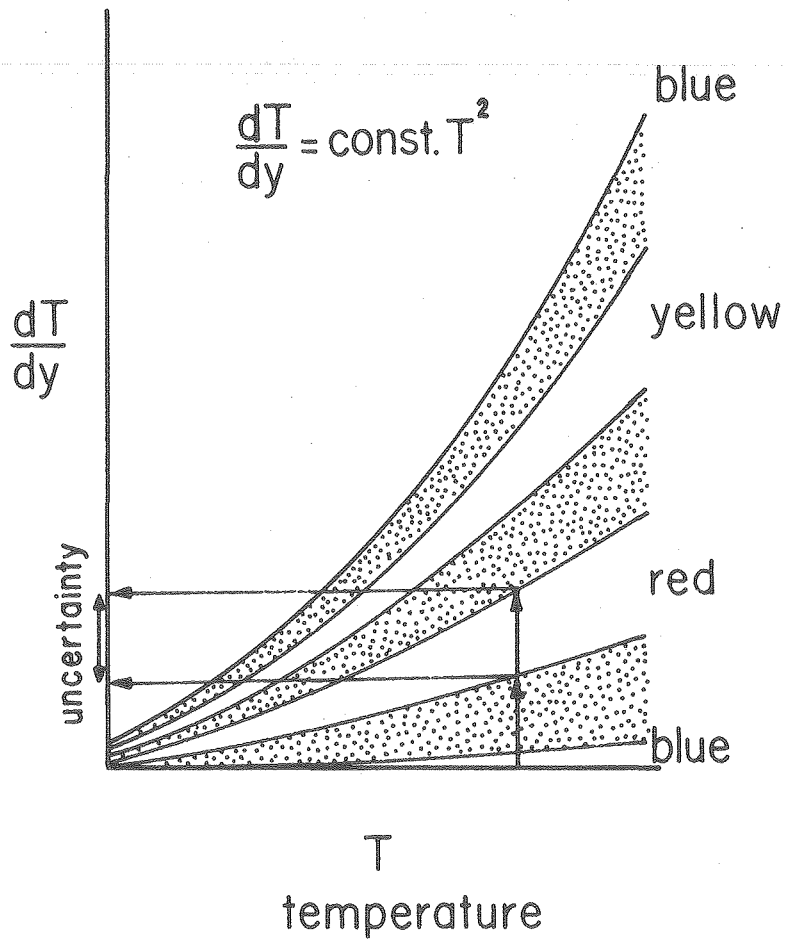


Figure 3.10 Color resolution due to finite size of schlieren light source

XBL 787-9683

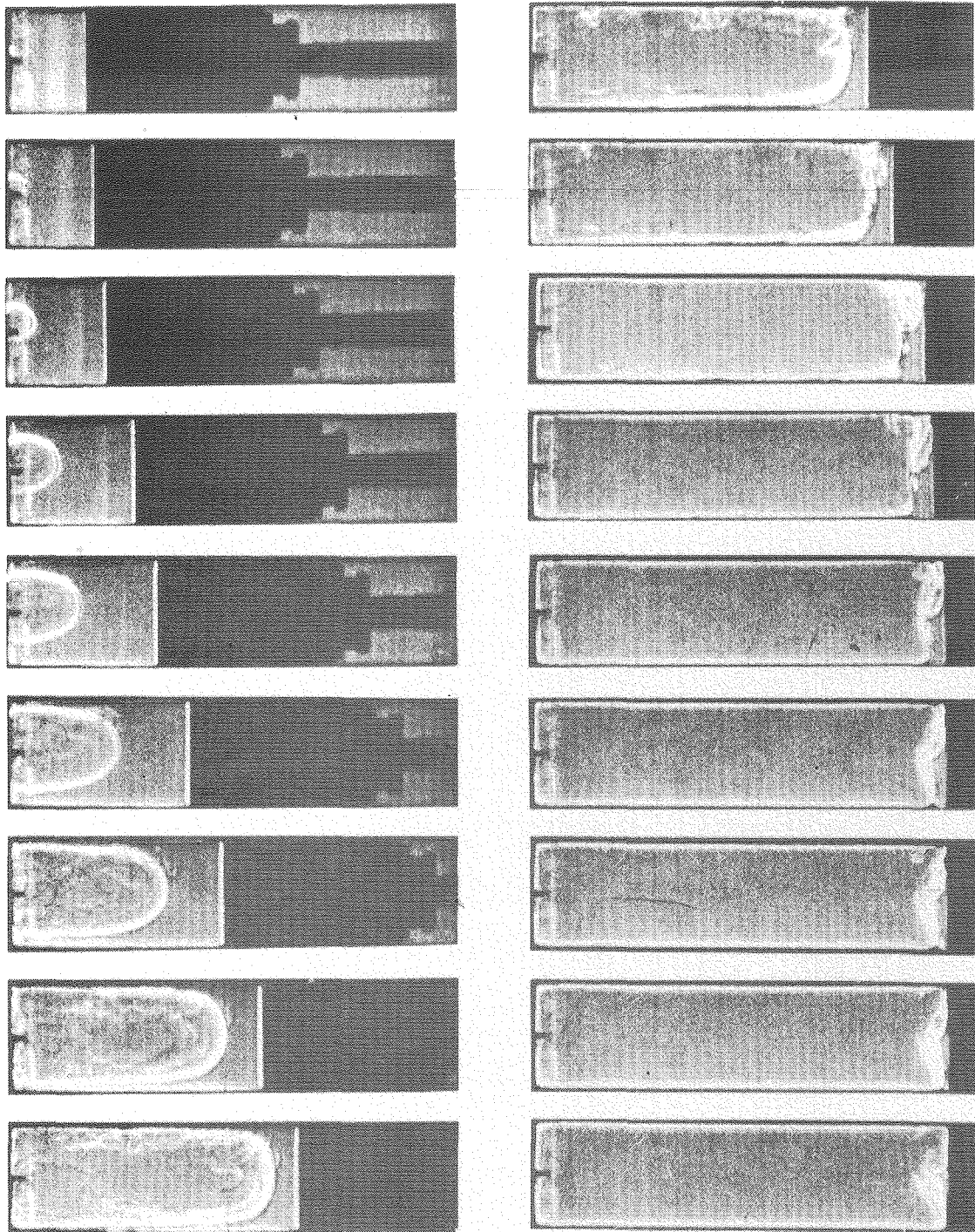
CHAPTER 4

Experimental Results

4.1 Observation of the Wall Flame Quenching Process

As discussed in Section 3.2-2, the width of the test section along the light path limits the observable distance from the wall. The quenching distance has to be larger than this limiting distance if it is to be observed. Calculations based on simple correlations such as Equation (1) predict quench layer thicknesses of about 100 μm in engines. This is too small to be observed by our schlieren system, but the quenching distance may be enlarged by reduction of either pressure or temperature and this can be accomplished in an engine by withdrawing the piston from TDC while starting at atmospheric pressure.

Figure 4.1 shows a typical photograph taken at the camera speed of 7000 frames per second after the cylinder was first filled with a premixed methane-air charge and the piston brought to top dead center at one atmosphere. The mixture is ignited as soon as the piston starts to withdraw (~ 2 msec ATDC) and the flame expands with a hemispherical shape until the walls are reached. The flame then elongates and begins to accelerate along with the acceleration of the piston. The quenching process occurs on all the surfaces of the chamber. The earliest quenching takes place on the cylinder head, followed by quenching of the flame propagating past the sidewall, and finally extinguishing on the piston face.



XBB 787-8802

Figure 4.1 Cinematographic sequence of schlieren photographs for CH_4 -Air mixture by spark ignition; piston withdrawn from TDC, equivalence ratio unity, initially 1 atm and room temperature, time interval 2 msec

Even on the cylinder head there is a strong coupling between fluid mechanics, heat transfer, and chemistry. The velocity of the flame front parallel to the cylinder head wall is about 120 cm/sec in laboratory coordinates. As discussed in ref. (43), the laminar flame speed is (with respect to the unburned gas) only about 40 cm/sec. Thus, the flame propagates toward the wall through a large velocity gradient. This is also true along the side walls as is shown in Figure 4.2 where the particle velocity at the flame front and parallel to the wall is plotted at a time of 13 msec after ignition. The particle velocity profile implies that the flame front near the wall moves faster than the center position and the flame shape becomes flattened from the hemispherical shape. This trend can be clearly seen in Figure 4.1.

With the exception of the cylinder head surface, it is possible to plot lines of constant color, or density gradient, as a function of time wherever the flame is laminar. This has been done in Figure 4.3 for a point 2.54 cm from the cylinder head. Also plotted in Figure 4.3 are the thicknesses of the thermal boundary layers that develop as a result of expansion cooling and the calculated quench layer thickness. The calculated quench layer is based on the empirical Equation (1) with suitable values for the constants, which reduces to

$$D_1(\text{mm}) = 14.8 P(\text{BAR})^{-0.52} T(\text{K})^{-0.50} \quad (14)$$

This calculated quench layer thickness is based on the value D_{110} obtained by flame extinguishment tests and one would expect order of magnitude agreement with observed quench layer thicknesses. From Figure 4.3 it is clear that there is no well defined quench layer thickness that can be defined from the schlieren results. The quenching process is, in fact, a diffusional process and one expects smooth variation of

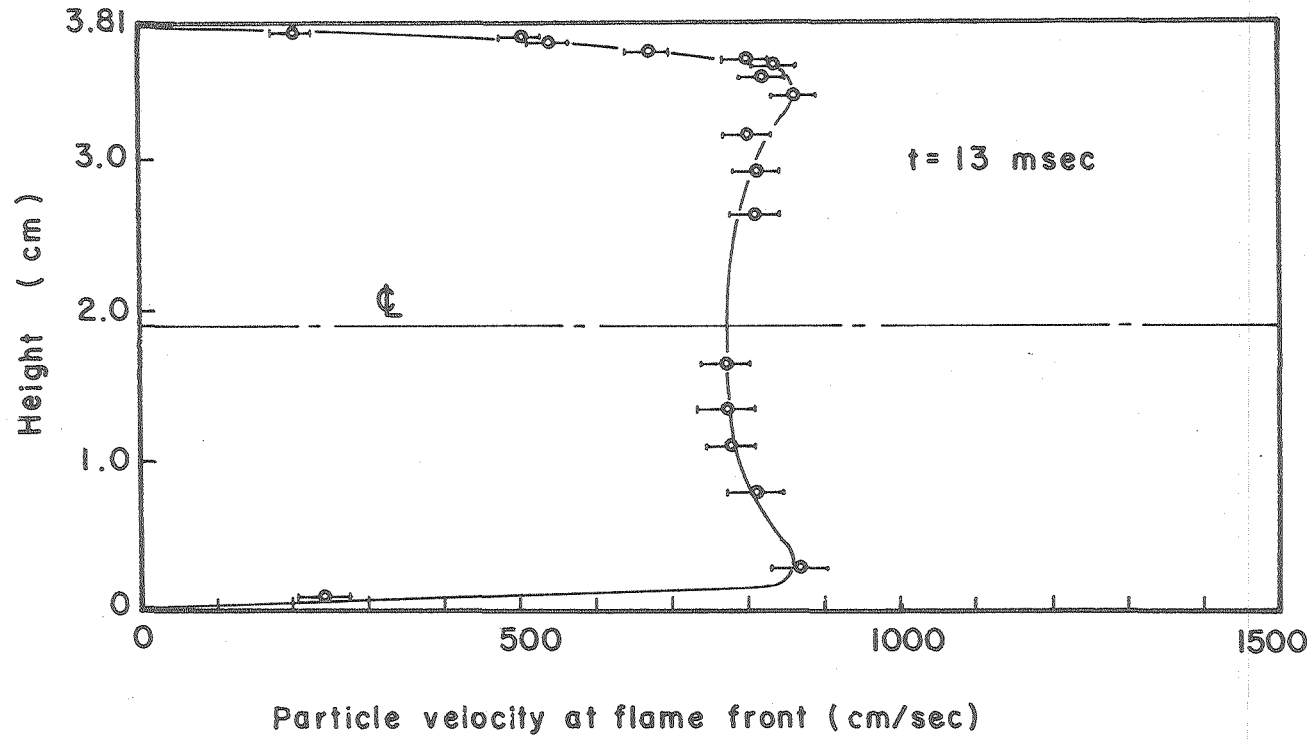


Figure 4.2 Particle velocity at a flame front

XBL 787-9675

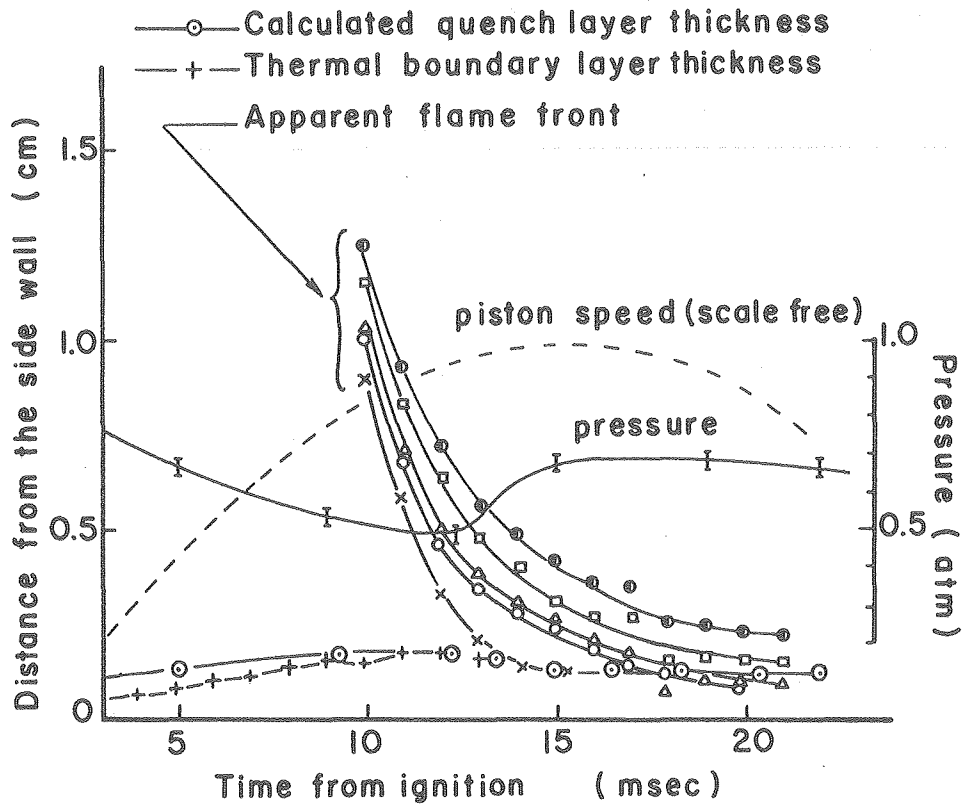


Figure 4.3 Profile of apparent flame front approaching a position at a side wall, 2.54 cm away from the cylinder head. Symbols of schlieren colors; x-interface of base blue and purple (flame front), 0-interface of purple and yellow, Δ-center of bright yellow region, □ -center of bright red in flame, ⊙-interface of red in flame and purple in flame. (case d)

XBL 787-9676.

the properties over the layer. However, the quenching process is occurring over a region of the size anticipated.

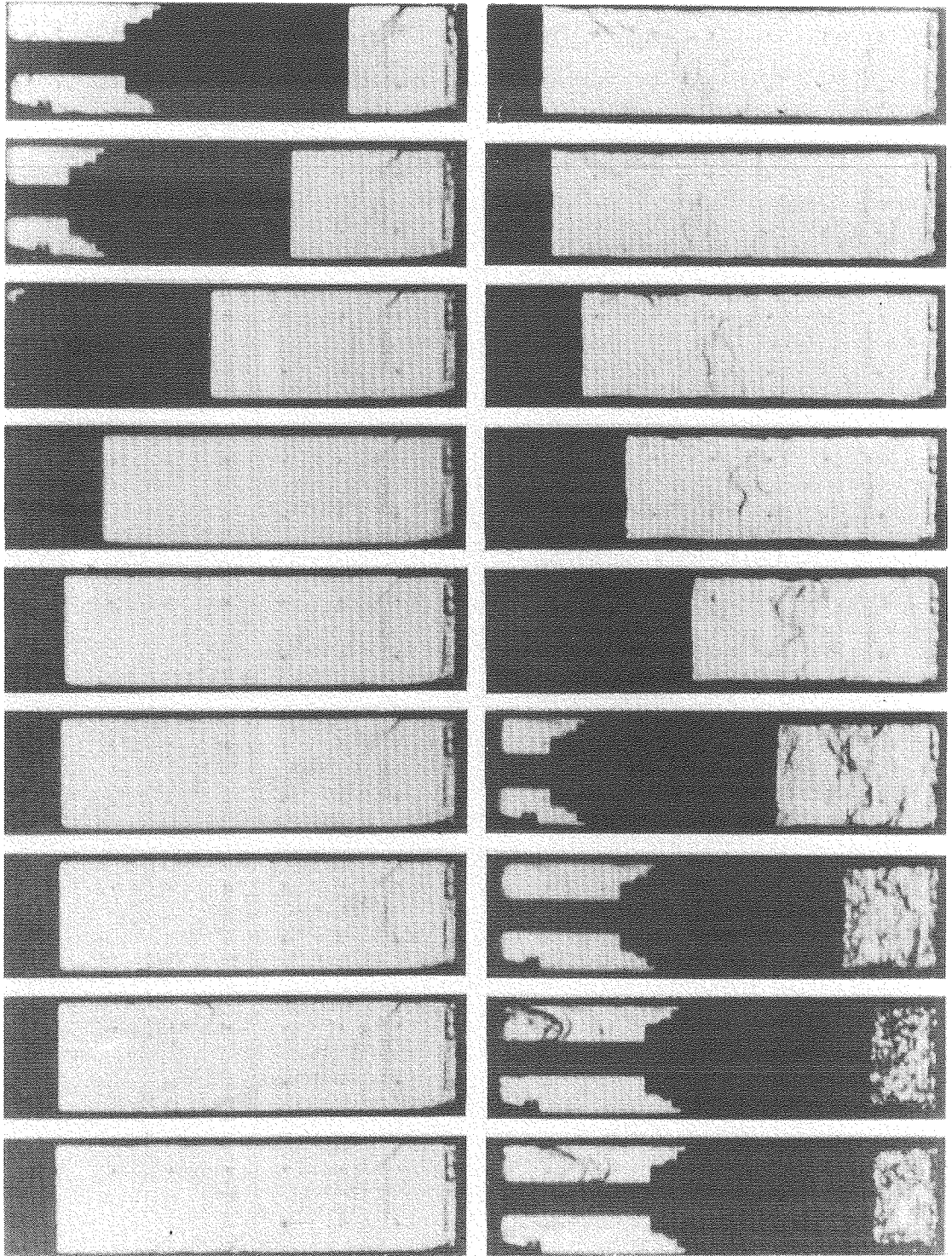
It should also be noted that the thermal boundary layers are of the order of the quench layer region thickness. Thus, there is interaction between the thermal boundary layers and the quenching process.

Lastly, notice that wall turbulence can be induced by the piston motion.

4.2 Flow and Combustion Process Visualization Experiments

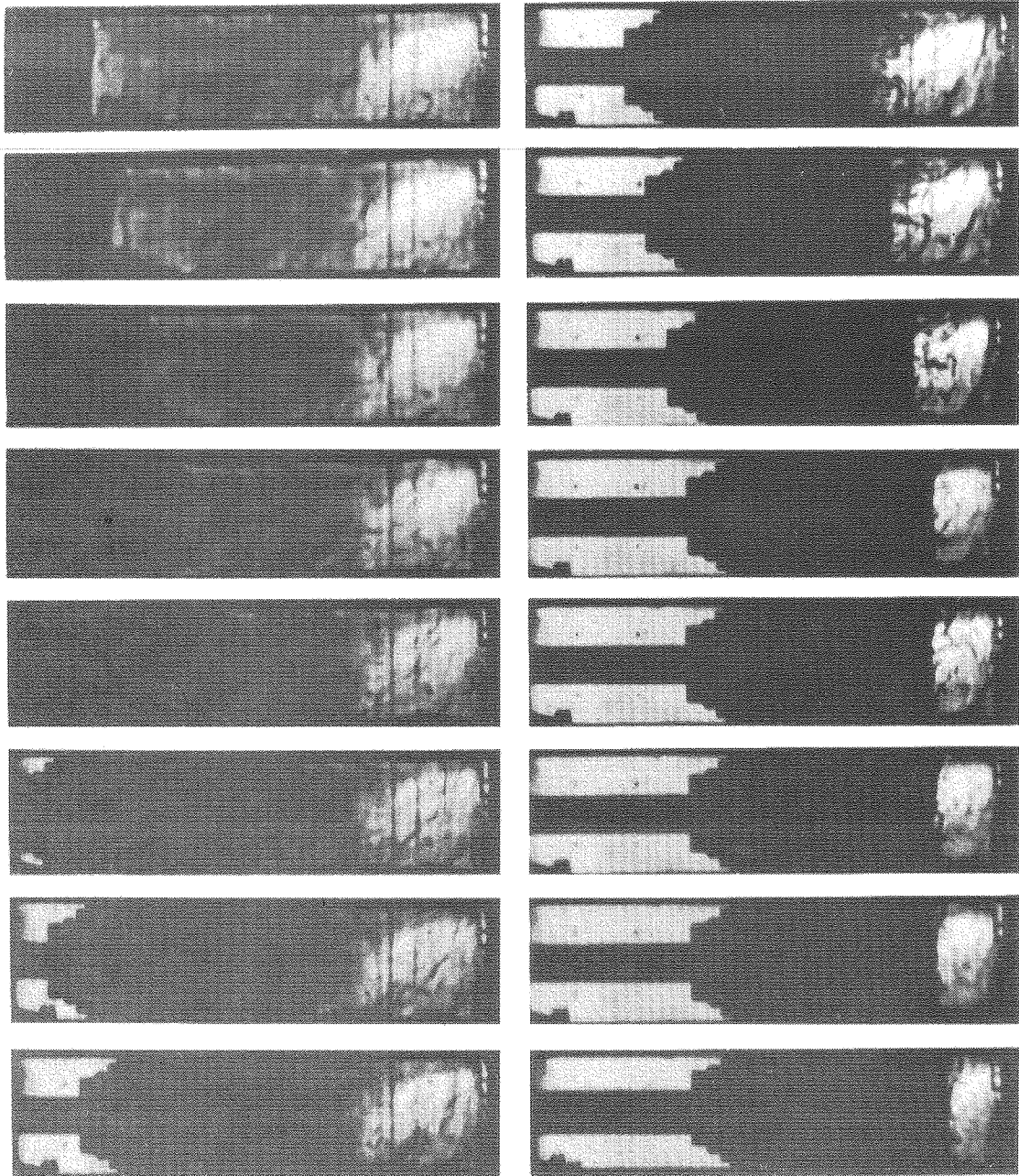
As mentioned in Chapter 1, a series of experiments has been conducted to examine the effect of geometry, equivalence ratio, and ignition timing on unburned hydrocarbons. The experiments involve running the machine through a compression and expansion stroke, and making measurements of unburned methane concentration after a sufficient period of time has allowed mixing of the products of combustion within the cylinder. Schlieren movies of each configuration have also been taken and flame sequences from the movies are shown in Figures 4.4-4.15.

Figure 4.4 shows a schlieren record for simulation of the intake and compression strokes in our machine. Although the initial motion is highly directed, by the time significant compression has occurred the turbulence appears to be fairly homogeneous. The characteristic size of the turbulence as measured by the observed grain diameters, drops from about 0.5 - 0.6 mm to 0.2 - 0.3 mm at TDC in rough agreement with the results of Dent and Salama's⁽⁴⁸⁾ hot wire experiments. There is some interaction between this turbulence and the roll-up vortex as well. Figure 4.5 shows a typical exhaust flow pattern. The roll-up vortex interacts with turbulence of the burned gas as soon as it forms.



XBB 784-4495

Figure 4.4 Flow pattern during an intake and succeeding compression stroke

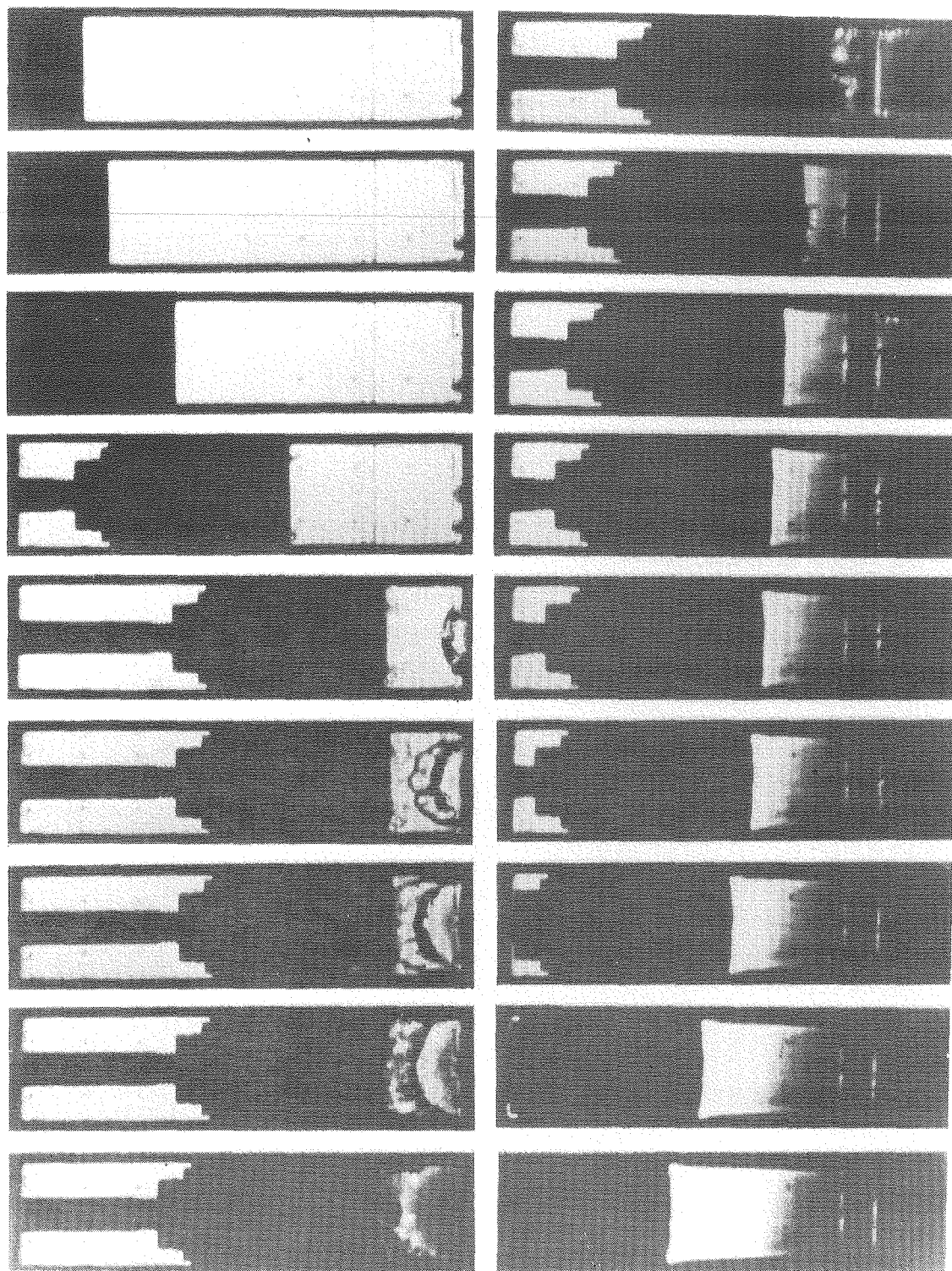


XBB 787-8801

Figure 4.5 Flow characteristics during an exhaust stroke following after a power stroke with combustion

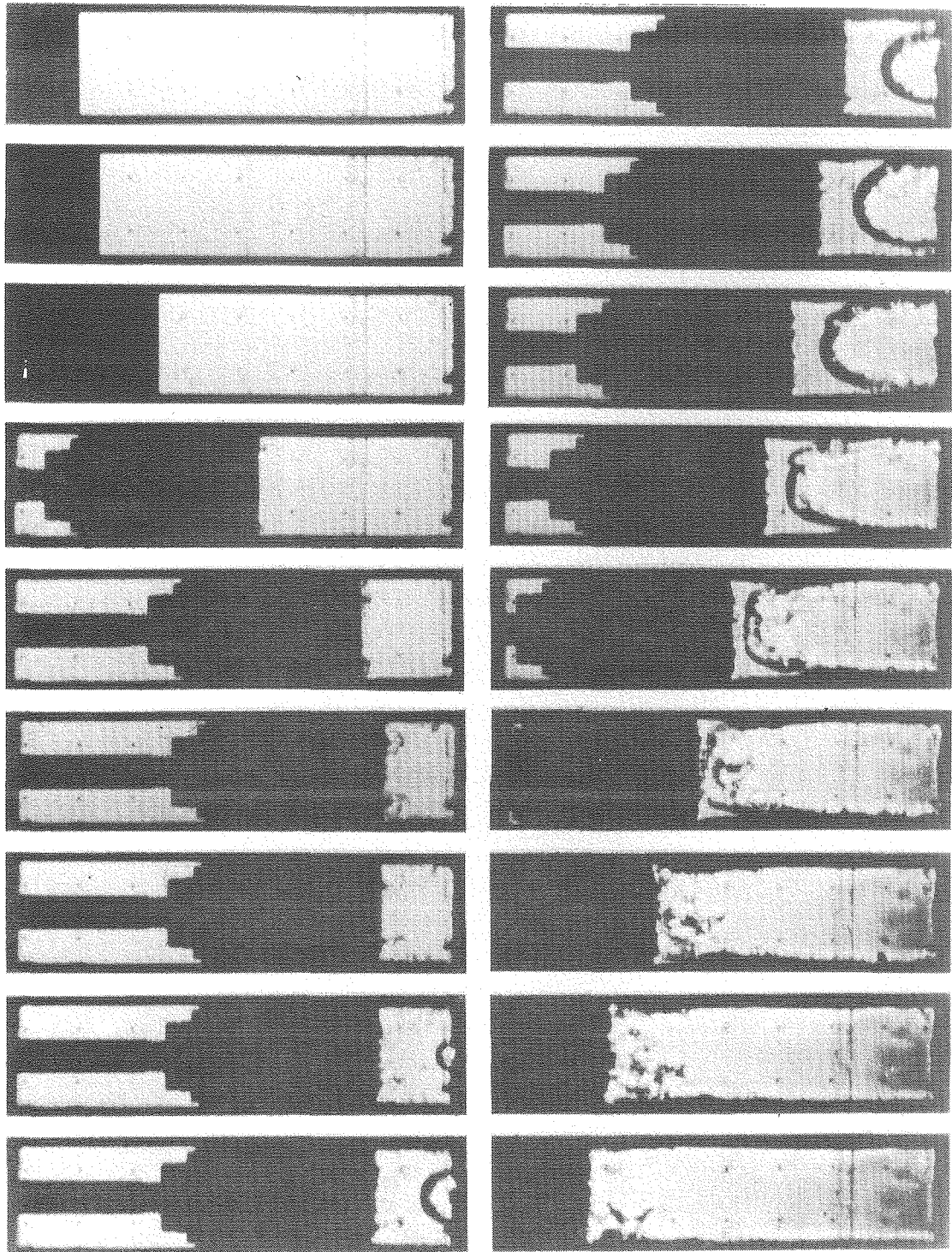
The vortex near the exhaust valve is elongated and is swallowed into the exhaust valve before the exhaust stroke is completed. As the piston approaches TDC the vortex diffuses out and exhaust into the valve.

Figures 4.6 and 4.7 show the flow patterns for the flat piston and correspond to early and late ignition respectively. In both cases the vortex roll-up occurs in what was initially a quiescent environment. The size of the vortex keeps increasing, even after top dead center. The boundary layer, which grows along the wall due to the bulk motion induced by piston movement, may be seen clearly. It is interesting to note that as the vortex diverges after top dead center, the boundary layers along the walls become turbulent almost instantly. This may be caused by the interaction of the boundary layer and reverse flow that is induced by the growth of the vortex. The essential difference between the early ignition and late ignition cases is that with early ignition the flame propagates throughout the chamber in a turbulence free environment, with the exception of the vortex region, and consequently, the wall quenching process is laminar over most of the cylinder. In the late ignition case, a substantial fraction of the cylinder is highly turbulent, which significantly modifies the flame wall quenching process. Furthermore, in the late ignition case, the cylinder pressure has begun to drop due to piston withdrawal, and the flame must propagate at a lower overall pressure than for early ignition. As will be demonstrated below, this has a significant effect on the total unburned hydrocarbons present after combustion is completed. Although it is speculation at best, it may be that the formation of moisture on the cylinder walls as the piston withdraws is an indication of the degree to which combustion



XBB 784-4495

Figure 4.6 Interaction between rolled-up vortex and CH₄-air flame; equivalence ratio 0.6, line spark ignition, ignition timing at 10 msec BTC, time interval 5 msec, flat piston



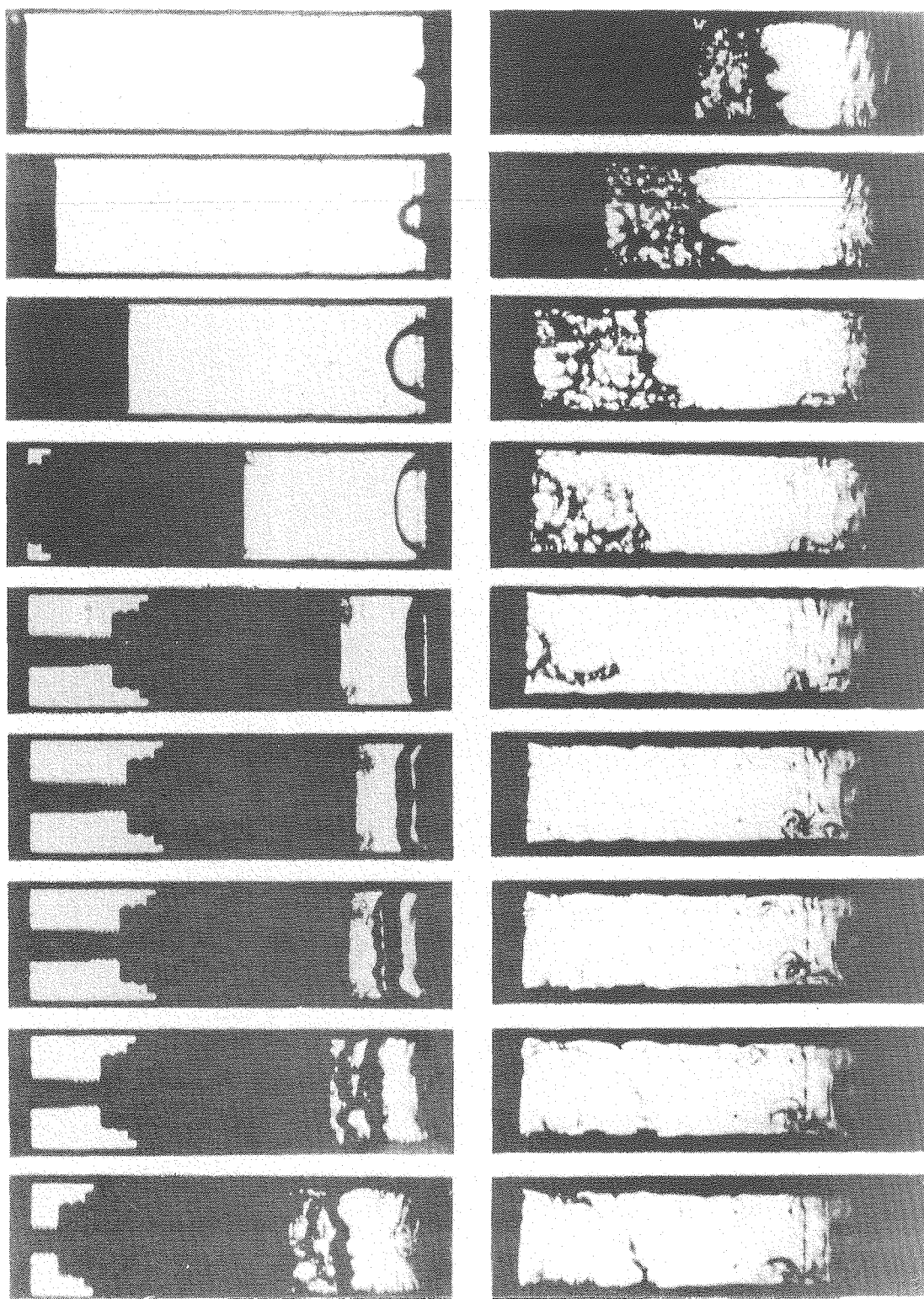
XBB 784-4493

Figure 4.7 Interaction between rolled-up vortex and CH₄-air flame equivalence ratio 0.6, line spark ignition, ignition timing at 10 msec ATC, time interval 5 msec, flat piston

has been completed. In the late ignition case, it may be observed that near the piston no water condenses on the walls, indicating the presence of a quenched region.

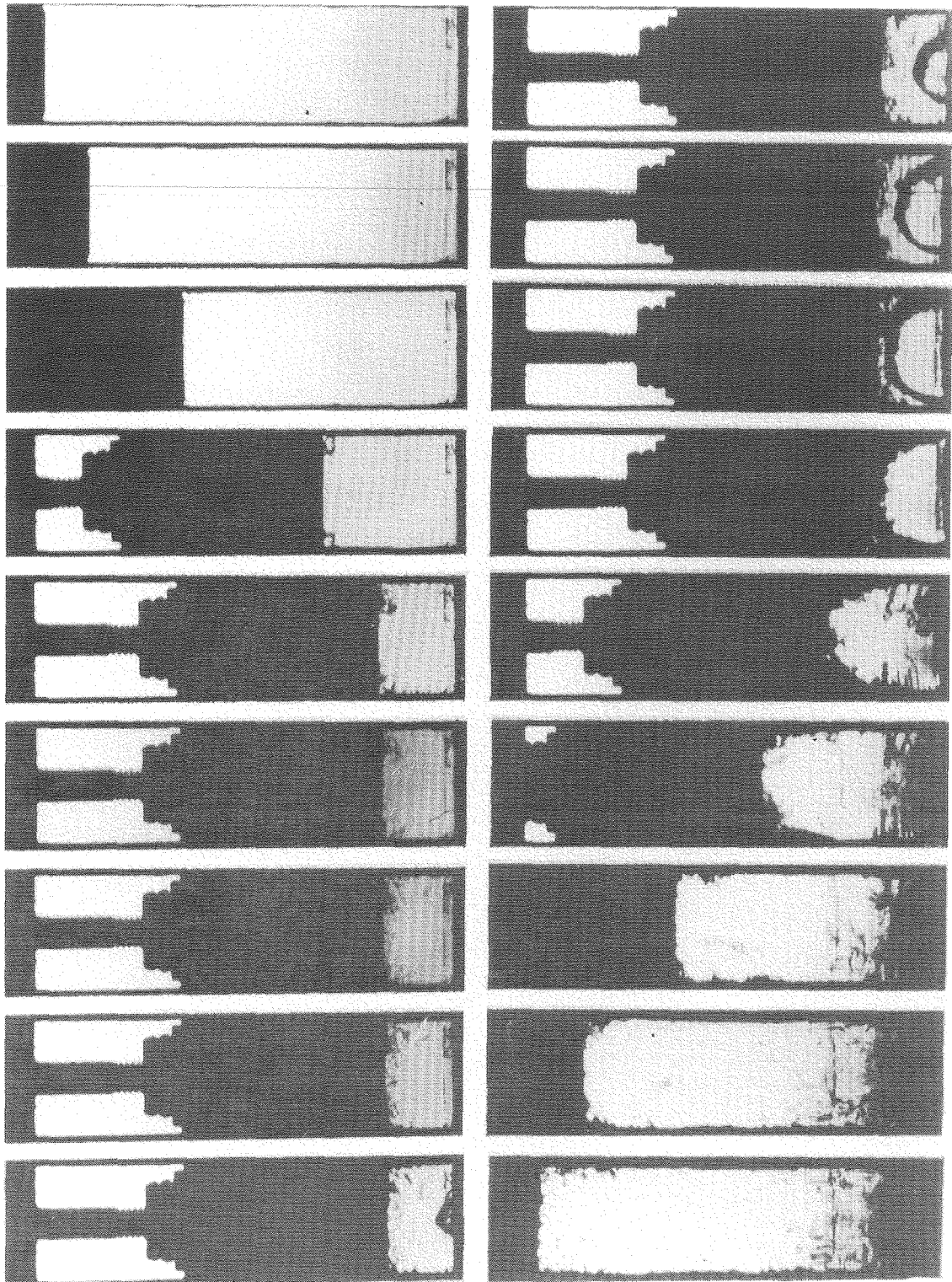
Figure 4.8 shows the flow pattern generated by the piston which is beveled at the same scale as that of Wentworth⁽⁹⁾. Ignition occurred very early, about 25 milliseconds before top dead center. The vortex grows in a manner somewhat similar to the flat piston case. However, as can be seen, the vortex is squeezed towards the center of the piston head, and its scale is slightly smaller than that of the regular flat piston. The figure shows a typical interaction between the flame and wall turbulence. When the flat flame front reaches the edge of the turbulent region, the flame degenerates along the walls. It appears that the bulk of the turbulence is along the walls, the corners, and the piston face. The turbulent flame speed appears to be about $2\frac{1}{2}$ times that of the laminar flame speed. Figure 4.9 is for late ignition timing.

In Figures 4.10 and 4.11 we show a movie frame sequence at the same conditions as in the previous paragraph, except for a thicker bevel. The quantitative results are extremely interesting. The main feature of this piston is that the vortex roll-up size is limited by the size of the triangular region defined by the cylinder walls and the wedge. Regardless of operating conditions, the vortex never leaves the wedge region. It is therefore much smaller than that of the normal piston. Unlike the normal piston, the roll-up vortex does not grow once the cylinder has come to top dead center. Another interesting aspect of the movie is that during the expansion stroke, gas that was entrained in the piston wall crevice feeds out into the vortex that remains in



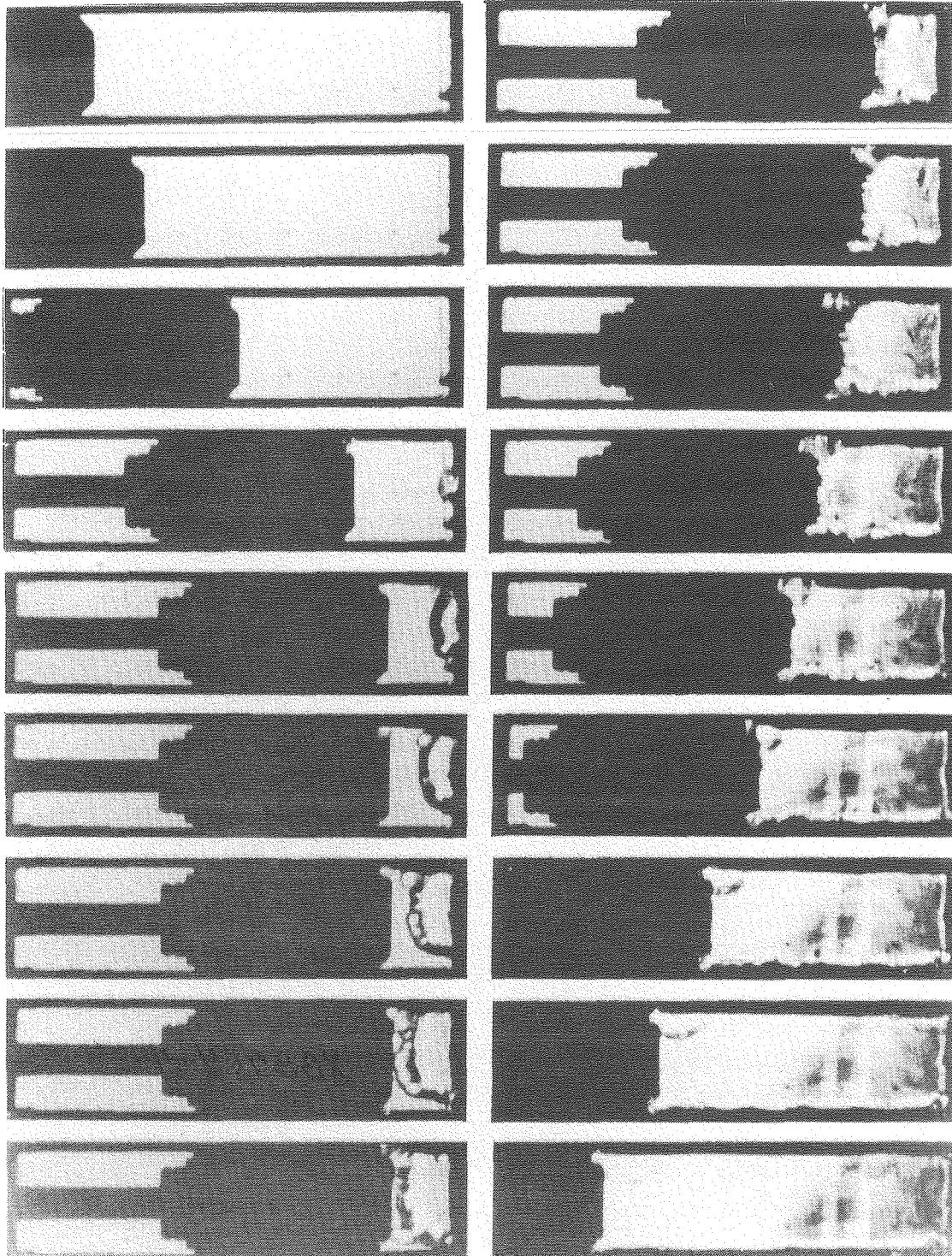
XBB 784-4492

Figure 4.8 Interaction between rolled-up vortex with the small bevel piston and CH_4 -air flame; equivalence ratio 0.6, line spark ignition, ignition timing at 25 msec BTC, time interval 5 msec



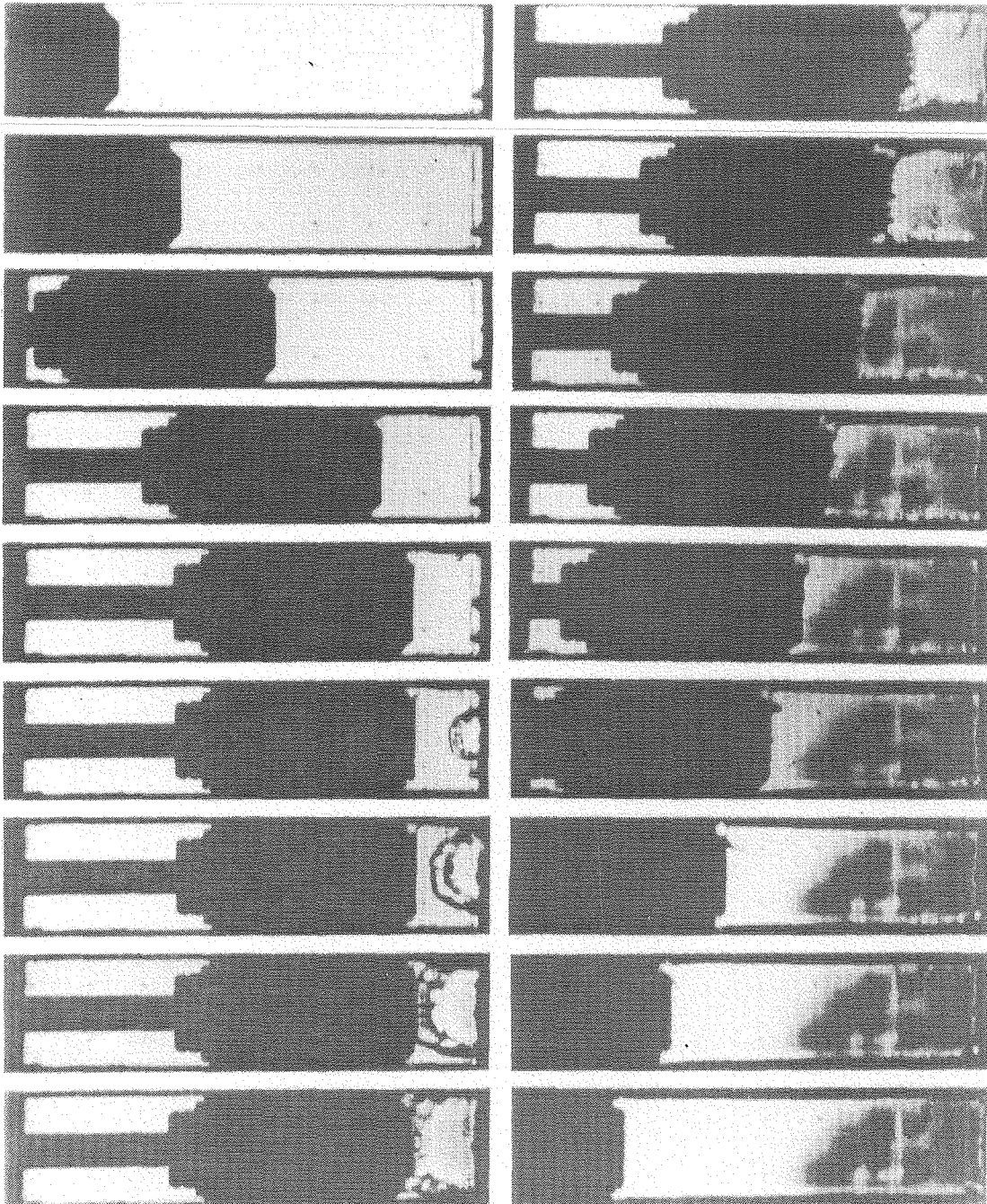
XBB 784-4491

Figure 4.9 Interaction between rolled-up vortex with the small bevel piston and CH₄-air flame; equivalence ratio 0.6, line spark ignition, ignition timing at 20 msec ATC, time interval 5 msec



XBB 784-4489

Figure 4.10 Interaction between rolled-up vortex with the small bevel piston and CH₄-air flame; equivalence ratio 0.6, line spark ignition, ignition timing at 12 BTC, time interval 5 msec



XBB 784-4490

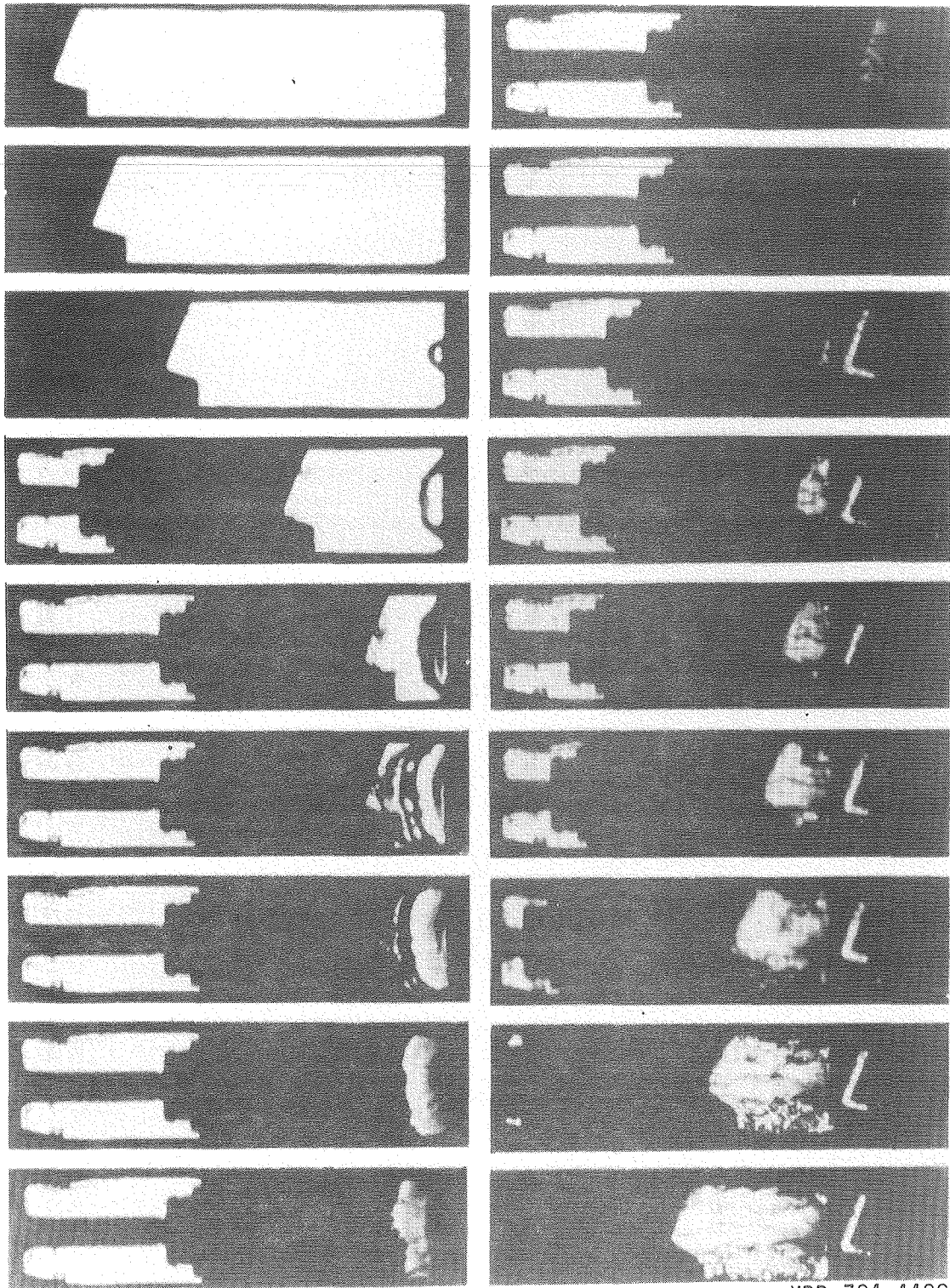
Figure 4.11 Interaction between rolled-up vortex with the large bevel piston and CH₄-air flame; equivalence ratio 0.6, line spark ignition, ignition timing at TDC, time interval 5 msec

the wedge area. This implies that with the beveled piston, the majority of unburned hydrocarbons may remain in the crevice and vortex region.

Figures 4.12 and 4.13 show the flow patterns induced by the wedge piston for early and late ignition. As can be seen, the flow patterns are quite different than those of the more conventional pistons. The vortex on the slant wall detaches from the wall early in the stroke and moves down the ramp. The vortex on the flat land never seems to form strongly, and finally couples with what looks like a small recirculating zone hanging off the corner of the land. It is apparent that there is a large scale circulation induced by the wedge. As we shall see below, there is a region of ignition timing near top dead center where there is significant misfire, implying high velocities in the ingiter region.

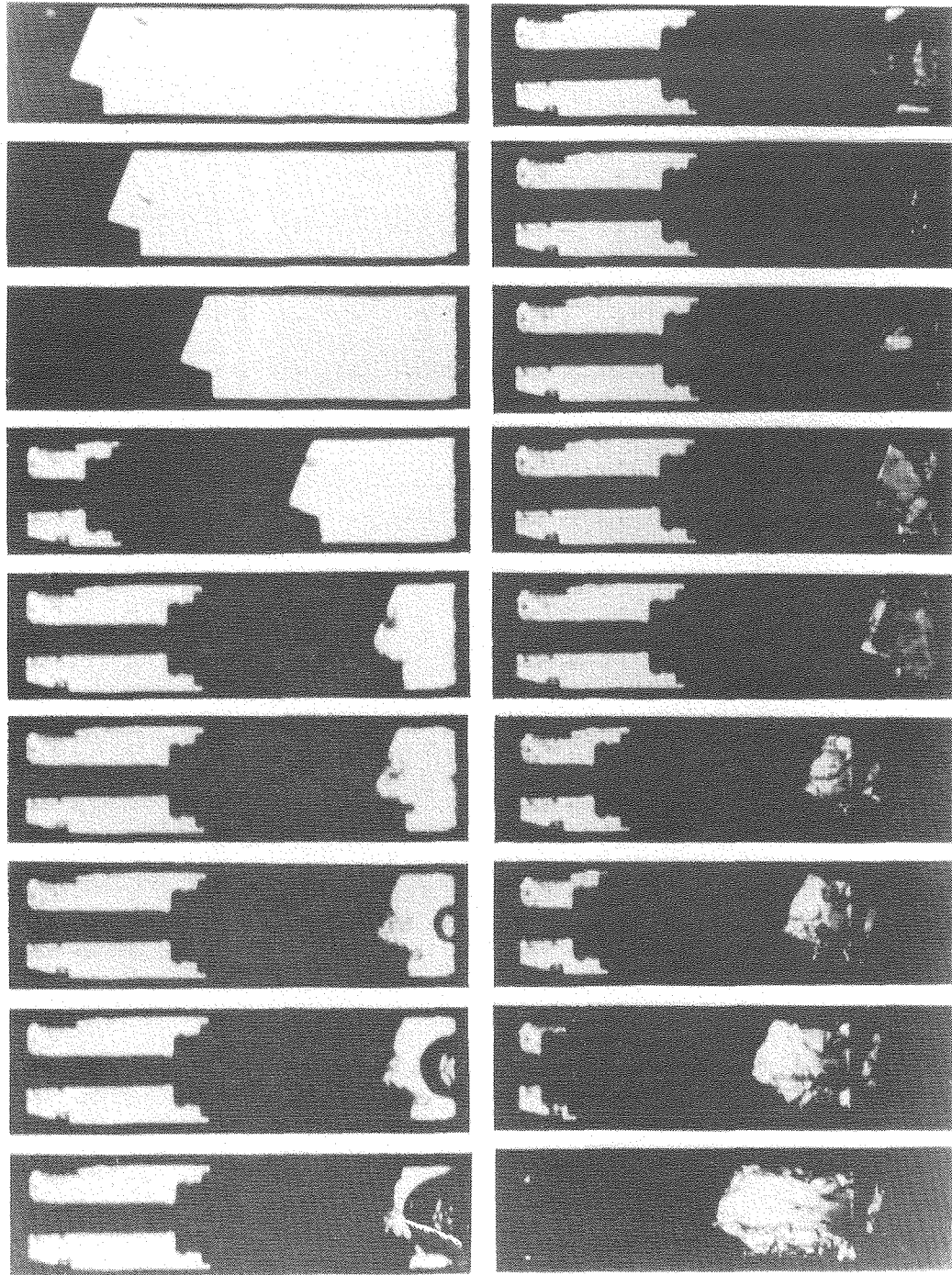
Figures 4.14 and 4.15 show the flow patterns for the hemispherical squish piston for early and late ignition time. Vortices form both along the wall and in the cup. The roll-up vortex gradually fills the almost V-shaped interface between the piston and the wall, but unlike the situation with the flat piston with a large bevel, the vortex continues to grow after top dead center.

The effect of operating conditions on the vortex size is illustrated in Figure 4.16, in which vortex area, normalized by the square of the piston travel, is compared for the compression strokes of the flat piston, and two bevel pistons, and the exhaust of the regular piston. The exhaust motion here is run for a quiescent burned gas so that there is no turbulence interference for the roll-up vortex⁽⁹³⁾.



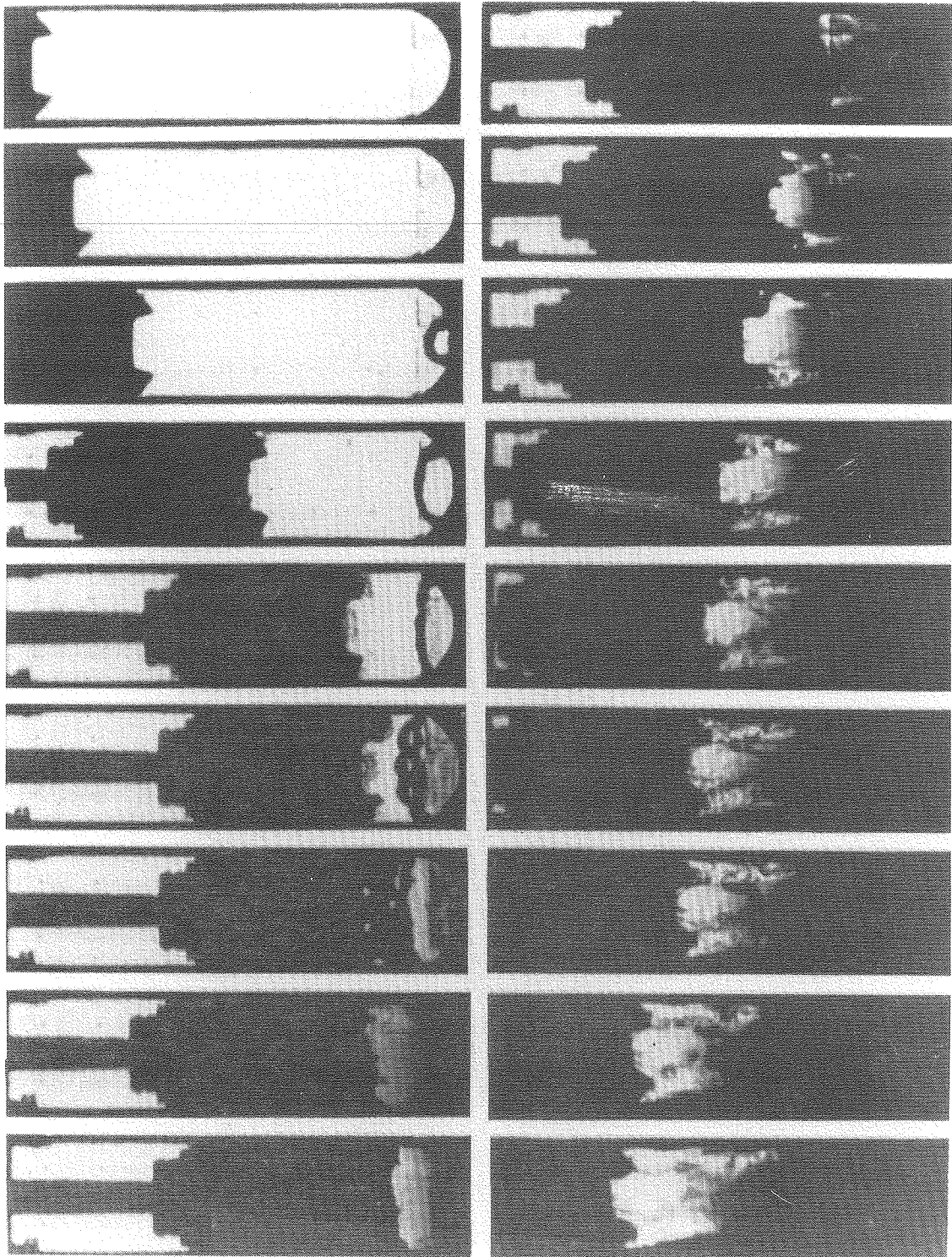
XBB 784-4488

Figure 4.12 Interaction between rolled-up vortex with a wedge piston and CH₄-air flame; equivalence ratio 0.6, line spark ignition, ignition timing at 14 msec BDC, time interval 5 msec



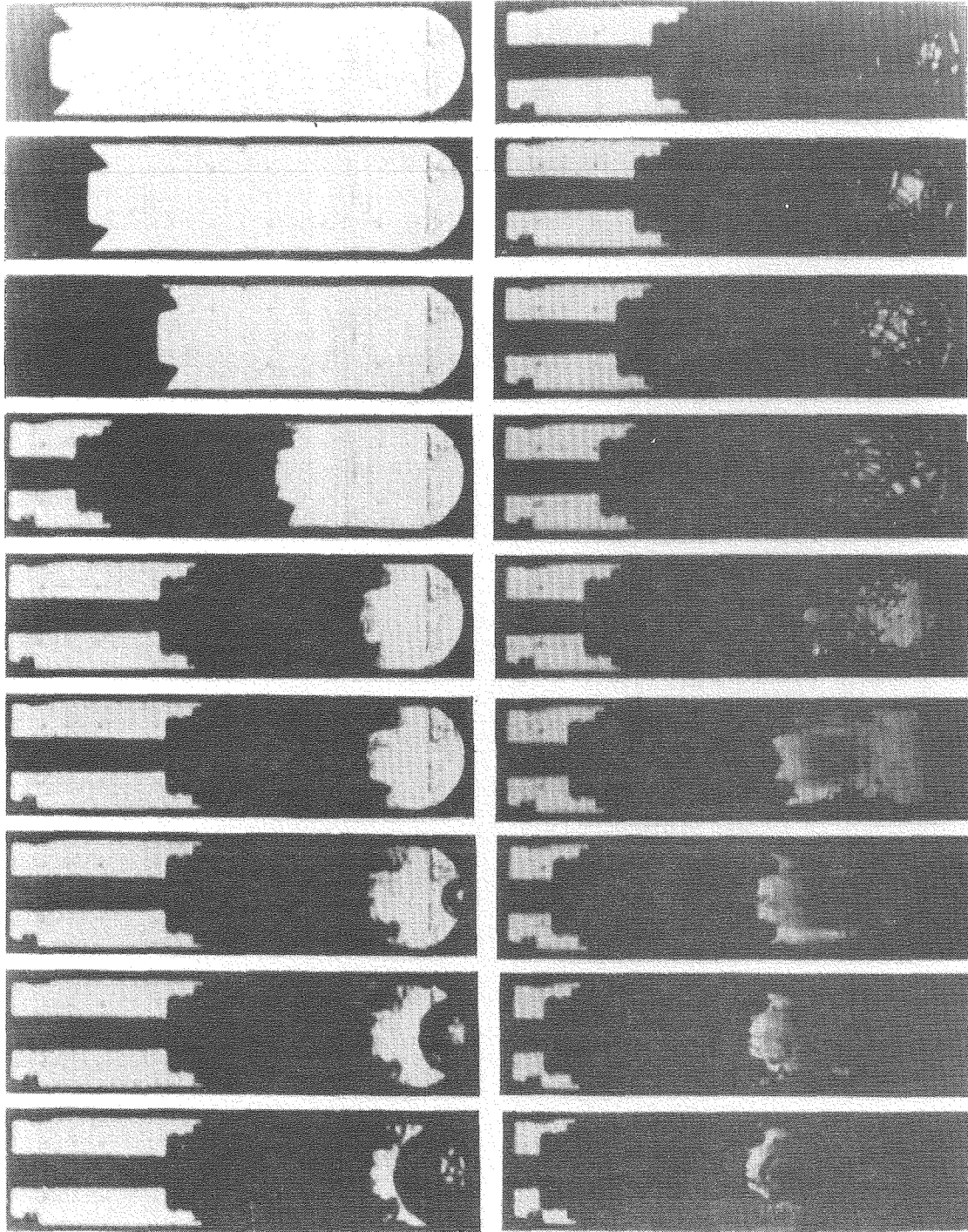
XBB 784-4487

Figure 4.13 Interaction between rolled-up vortex with a wedge piston and CH₄-air flame; equivalence ratio 0.6, line spark ignition, ignition timing at 4 msec ATC, time interval 5 msec



XBB 784-4486

Figure 4.14 Interaction between rolled-up vortex with a hemispherical squish piston and CH₄-air flame; equivalence ratio 0.6, line spark ignition, ignition timing at 17 msec BDC, time interval 5 msec



XBB 784-4485

Figure 4.15 Interaction between rolled-up vortex with a hemispherical squish piston and CH₄-air flame; equivalence ratio 0.6, line spark ignition, ignition timing at 10 msec ATC, time interval 5 msec

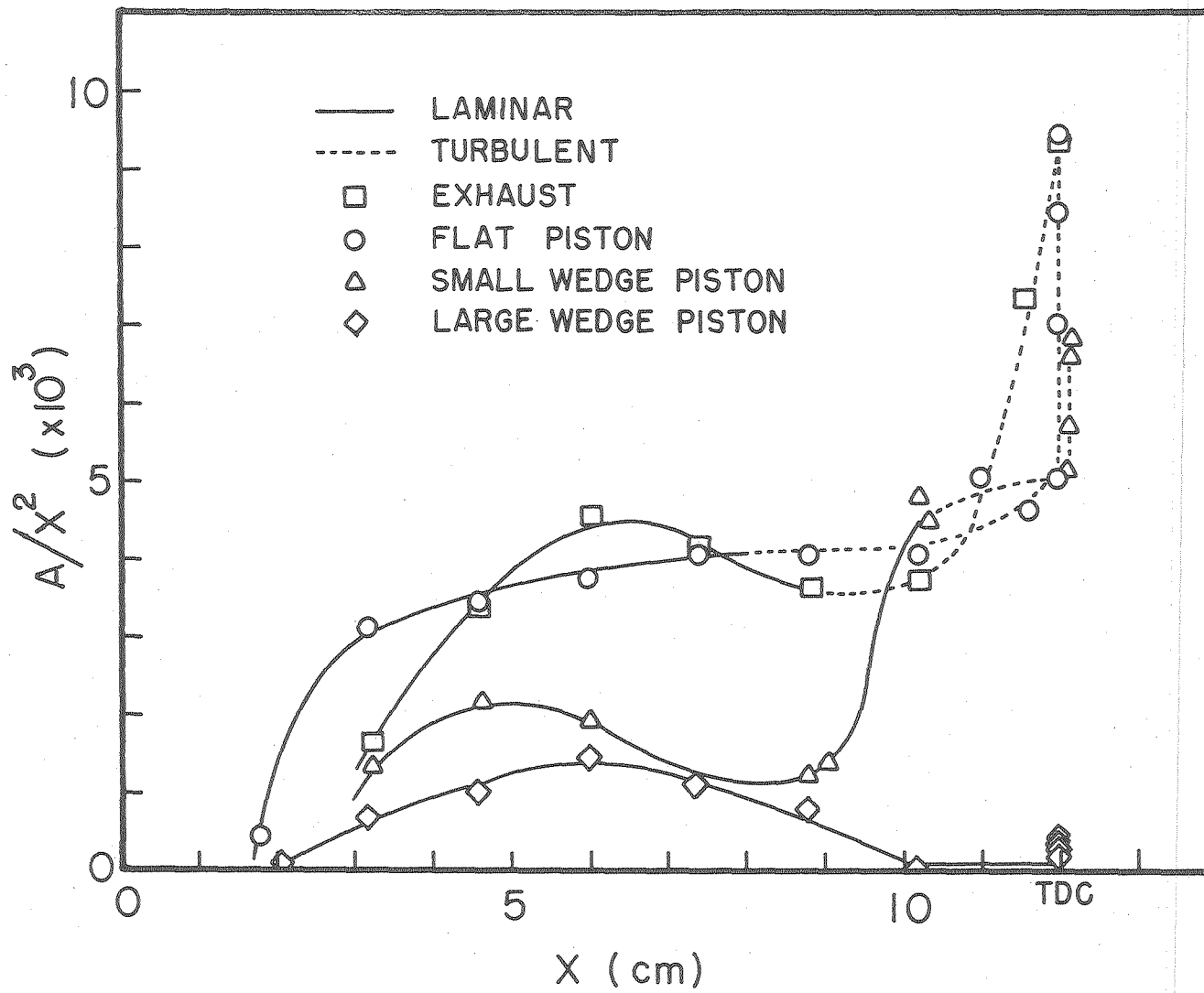


Figure 4.16 Vortexarea A normalized by square of the piston travel X. XBL 783-7876
 The engine speed $U_p = 623 \sin 104.7t$ cm/s.

In Figure 4.17, the same results are plotted with the water data of Tabaczynski et al.^(37,44) and Daneshyar et al.⁽³⁸⁾. As can be seen, the data for the flat piston fall within the turbulent region encompassed by Tabaczynski's data. Our data, which are for air-methane, were taken at much higher angular momentum than reported by the other workers (104 radians/sec as compared to less than 18 radians/sec). The data with a Reynolds number less than 5×10^4 correspond to the laminar vortex, showing that transition of the vortex for the gas mixture is delayed as Daneshyar et al.⁽³⁸⁾ anticipated. However, the agreement with the water experiments is notable.

4.3 Unburned Methane Measurements

Hydrocarbon measurements have been made for all five piston configurations and the results are presented in Figures 4.18 - 4.21. The first condition corresponds to the piston withdrawal as shown in Figure 4.1. The second set of experiments consists of combining the compression and expansion stroke similar to that discussed in the previous section.

Figure 4.18 shows the percentage of unburned methane for the piston withdrawal case. The figure shows no effect of ignition timing. Also shown is the effect of stoichiometry on percent unburned methane, and as may be seen, there is little effect. This may be explained by qualitative arguments in that as the equivalence ratio becomes leaner, the quench layer becomes thicker, while at the same time the total concentration of methane is decreasing. The two have a counter-balancing effect.

Figure 4.19 shows the percentage of methane unburned for the three flat pistons. There is a general trend in which unburned methane

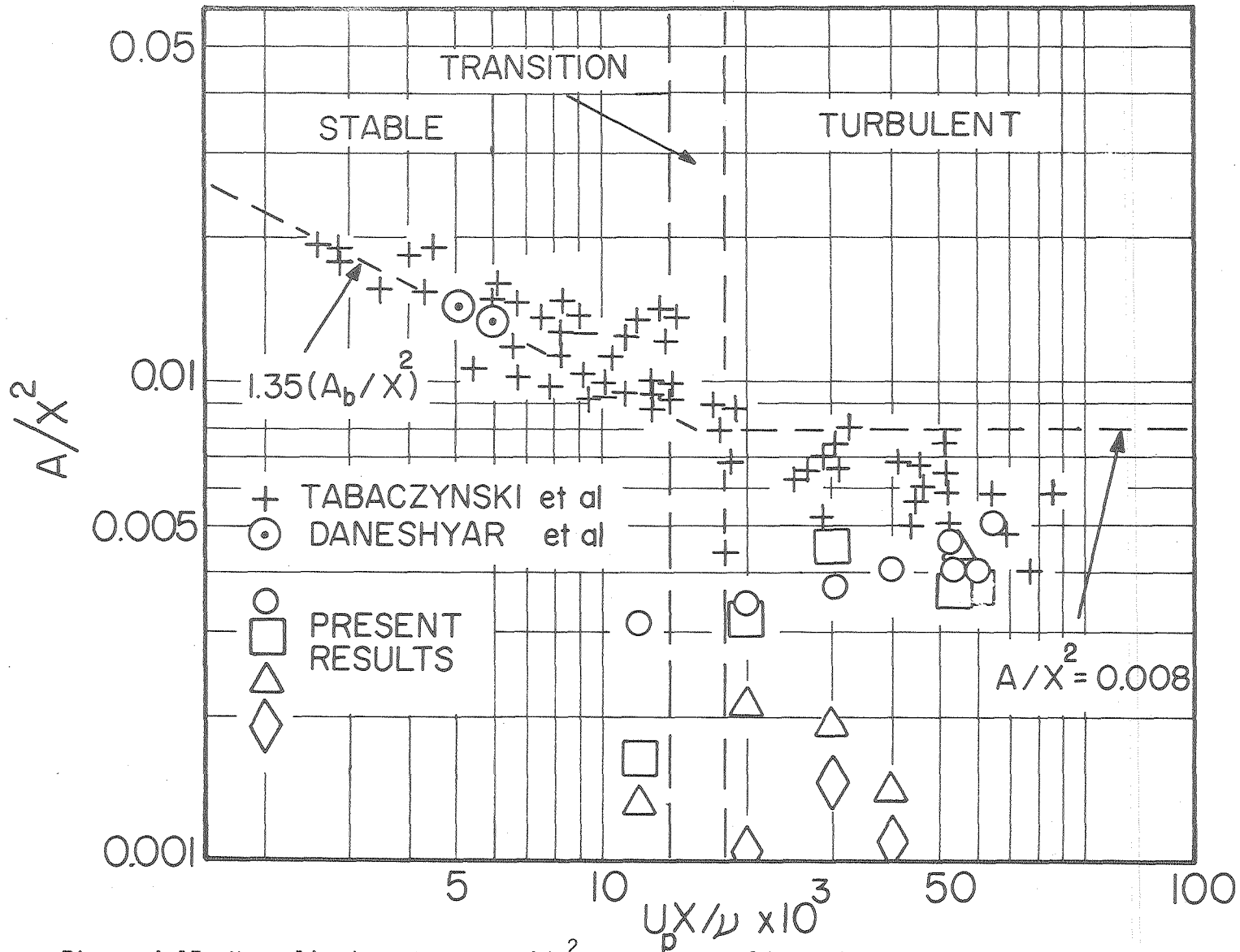


Figure 4.17 Normalized vortex area A/X^2 versus Reynolds number $U_p X / \nu$. Comparison is made with the data taken from Ref. 38 and Ref. 44. Data points correspond to those in Figure 4.16 with identical symbols

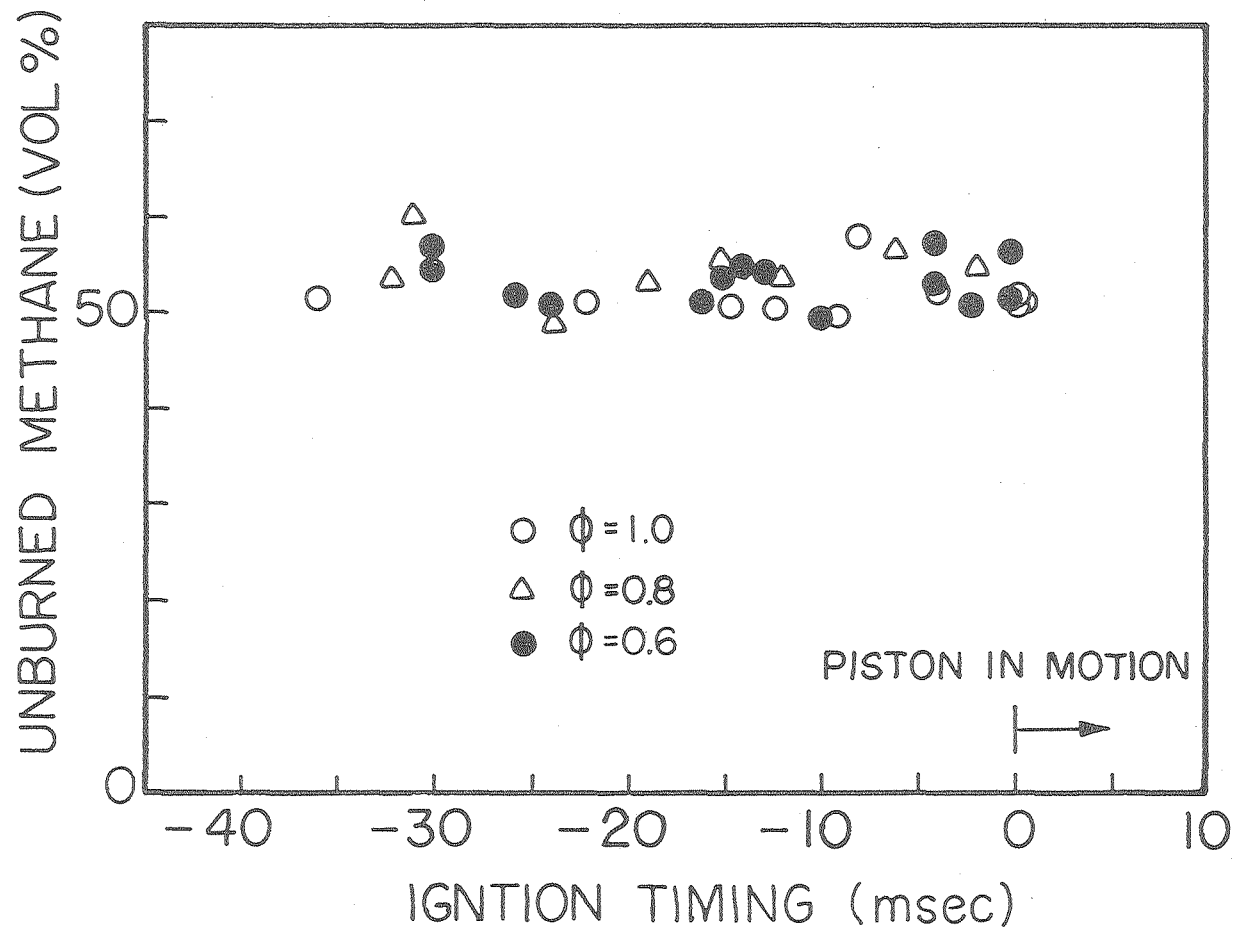


Figure 4.18 Unburned methane fraction with respect to the initial concentration for combustion with piston withdrawal from TDC; initial pressure 1 atm, room temperature XBL 783-7878

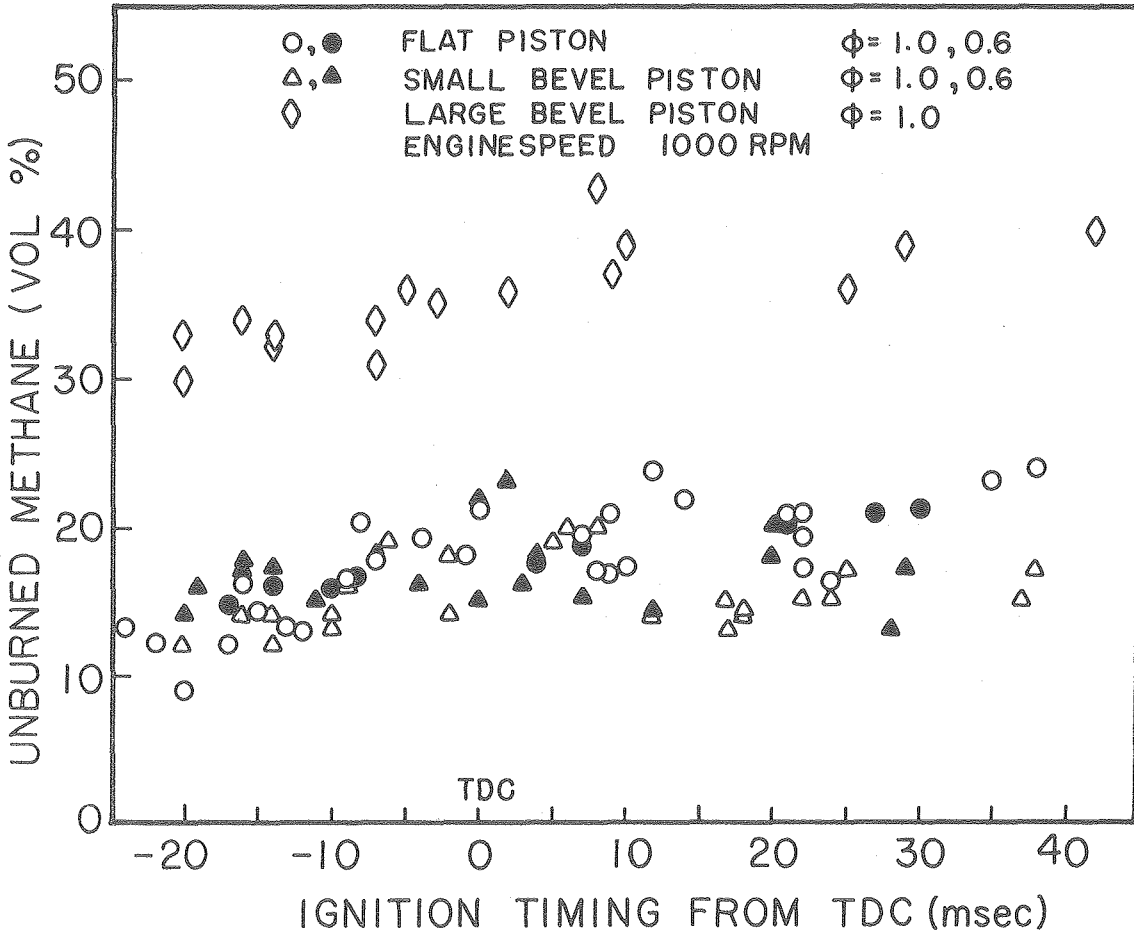


Figure 4.19 Unburned methane fraction with respect to the initial concentration for single compression-then-expansion combustion as a function of ignition timing

XBL 784-8139

increases as ignition is delayed, and then remains approximately constant after TDC. The piston with a large bevel has appreciably higher unburned methane but experiments have shown that quenching increases substantially in such triangular regions.

Figure 4.20 shows similar results for the wedge piston with an important difference being that there is a region of misfire where both the stoichiometric mixture and lean mixture combustion occur erratically. Data points are plotted only for cases where combustion occurs. For the lean mixture the misfire region is quite wide and may be divided into two regions. Over the first region no combustion occurs, while for later timing there is occasional firing. (At late timing no ignition occurs either.)

Figure 4.21 shows the results for the hemispherical squish piston. The trend is similar to that of the other cases. For this case some misfire has been observed for late ignition, but on an irregular basis. Both the wedge and squish pistons have higher unburned methane concentrations than the flat piston. Again the unusual shapes may increase quenching. The sudden generation of wall turbulence seen for the flat piston does not occur for the wedge or hemispherical squish pistons.

None of the results show a strong effect of equivalence ratio. This may be explained by noting that while the quench layer thickens at leaner mixtures, the total methane concentration is also decreasing. Thus, the two effects balance. As an experiment to study possible biasing introduced by our sampling technique we have run the only asymmetric piston in both positions. There was no change in the results.

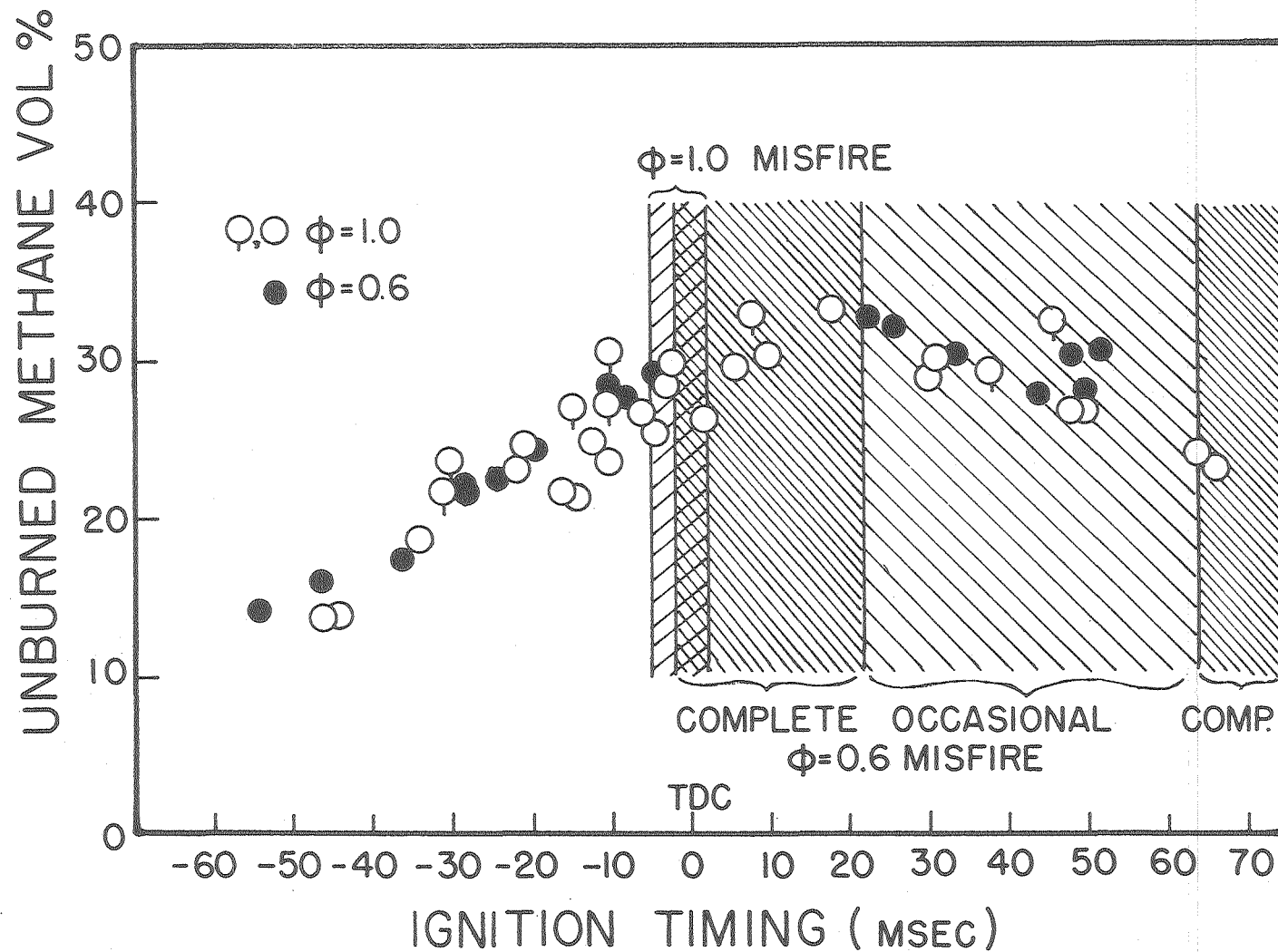


Figure 4.20 Unburned methane fraction with respect to the initial concentration for a wedge piston for single compression-then-expansion combustion as a function of ignition timing

XBL 784-8141

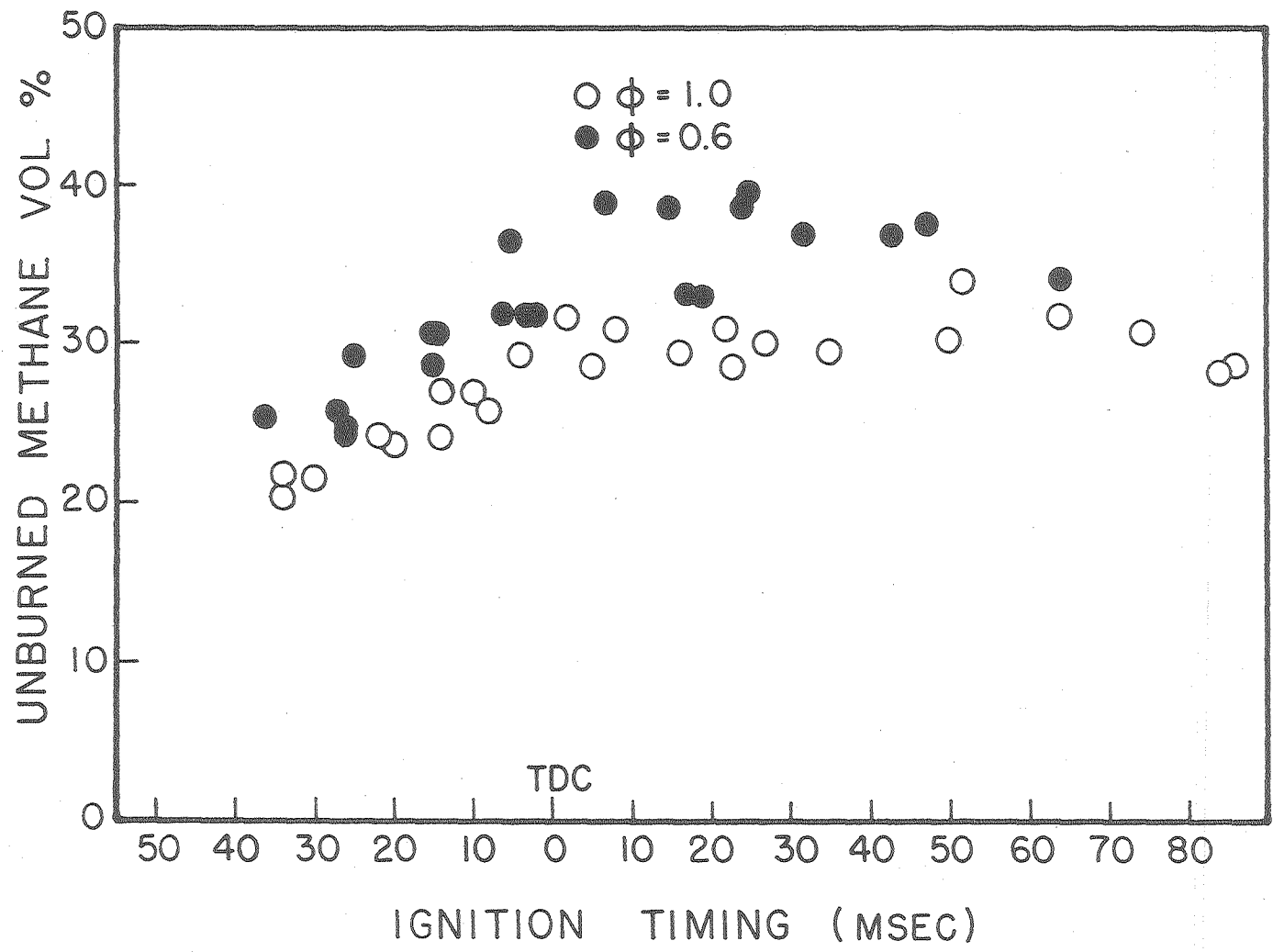


Figure 4.21 Unburned methane fraction with respect to the initial concentration for a hemispherical squish piston for single compression-then-expansion combustion as a function of ignition timing XBL 784-8144

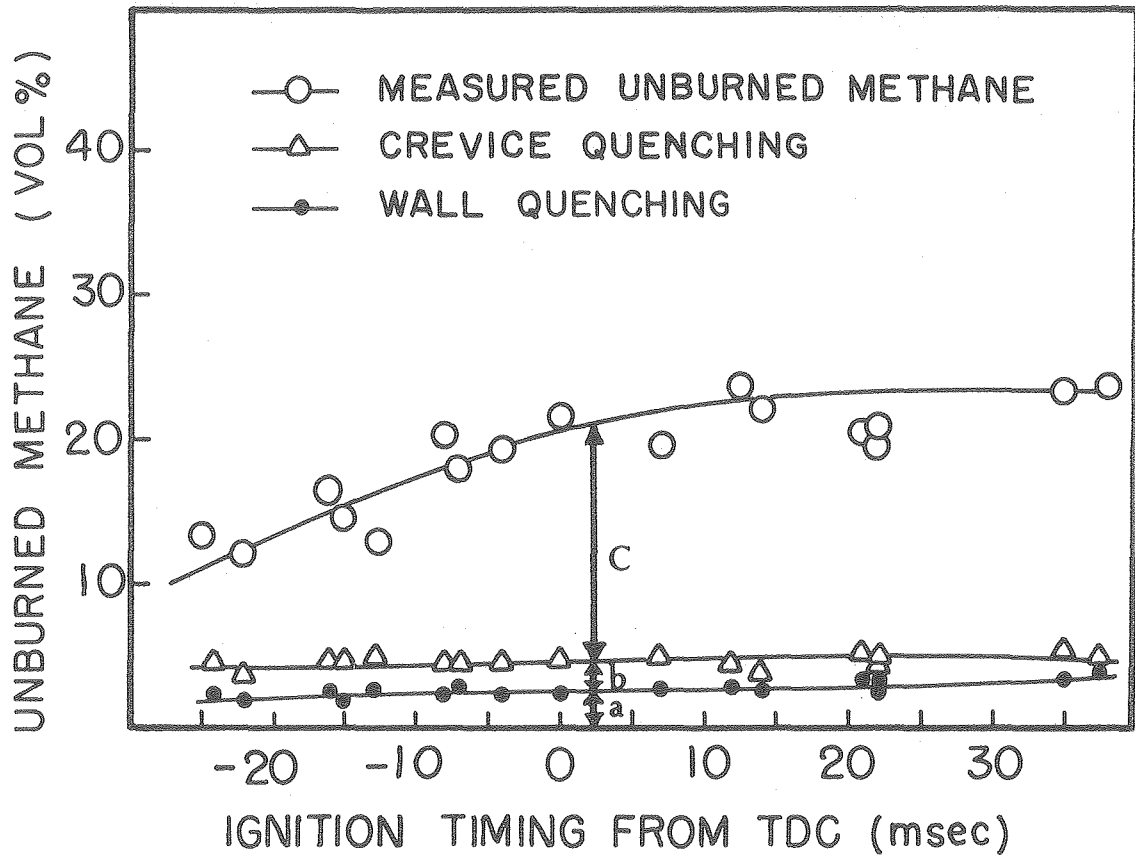
CHAPTER 5

Discussion

As discussed in the Introduction, there is a large body of work which leads to the conclusion that unburned hydrocarbons remain in an engine cylinder due to incomplete combustion along the walls and in any crevices or small gaps such as formed by the piston and cylinder wall. In principle, if one could calculate the quench layer thickness, a prediction of the amount of unburned hydrocarbon that remains in the cylinder after combustion is possible.

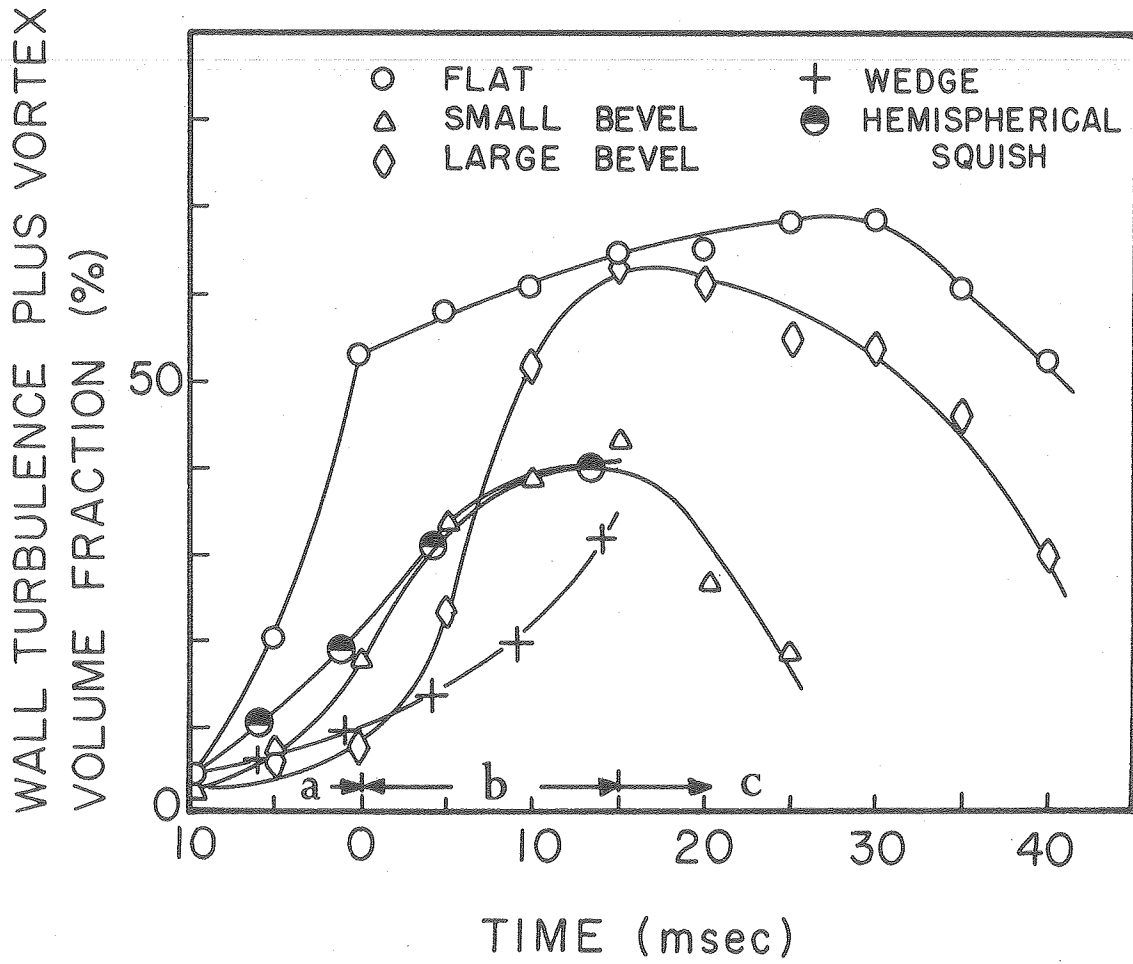
There is ample data for quenching processes in quiescent or laminar flows, and we have used such data to estimate the unburned methane fraction for the experiments reported above. A sample for the flat piston is shown in Figure 5.1. As can be seen, the measured methane exceeds the predicted amount by a large factor. The results for the other pistons are similar.

The conclusion we reach from these data is that a major cause of combustion inefficiency is turbulence enhanced quenching. This conclusion is supported by the data of Figure 5.2 in which the volume fraction of wall turbulence that the flame must propagate through is shown as a function of ignition timing for all five pistons. The trend toward lower efficiency as timing is delayed may thus be explained by the fact that the wall regions are more turbulent later in the cycle.



XBL 784-8143

Figure 5.1 Contribution of a) wall flame quenching, b) crevice flame quenching, and c) other effects to the observed unburned methane concentration



XBL 784-8142

Figure 5.2 Wall turbulence plus vortex volume fraction as a function of time; a) piston in compression, b) piston at rest at TDC, c) piston in expansion

For the piston withdrawal experiments one may observe directly the effect of turbulence on the quenching process. As can be seen from Figure 4.1, the flame along one side of the test section becomes turbulent at a point some 15 msec after ignition. At this time the flame propagation velocity in laboratory coordinates is about 915 cm/sec and the Reynolds number based on the length of the test section and the unburned gas properties is about 87,000. The maximum Reynolds number in a real engine is of the order of 10^5 so that it may be expected that even in a power stroke wall turbulence is introduced along the cylinder wall. This wall turbulence must play an important role in the quenching process and thus in determining hydrocarbon emissions.

To our knowledge, the problem of flame quenching on flat walls in the presence of turbulence has not been adequately studied. However, Ballal and Lefebvre⁽⁸³⁾, as discussed in section 2.3, have studied flame ignition and quenching in flowing mixtures, which should be similar qualitatively, and have shown that quench distances increase with turbulent intensity.

Although Figure 4.18 shows no effect of ignition timing on the unburned methane, this may be because the influence of wall turbulence is small for this case of piston withdrawal, or because the total amount of unburned methane is dominated by other effects. In particular, Figure 4.18 shows that about 50% of the initial methane is not burned. This high concentration of unburned fuel cannot be explained by quenching arguments alone, and thus, must be related in some way to bulk quenching phenomena^(16,17) at these low pressures.

The effect of the intake process will be to introduce additional complexity into the flow field. It is clear from work with hot wire

anemometers that a residual bulk turbulence remains after compression due to the intake process. Our own work indicates this as well (see Figure 4.4).

Whether the intake induced turbulence will strongly affect the formation of wall turbulence during compression can only be answered by additional experiments. However, it seems safe to assume that it can only increase the amount of wall turbulence the flame will encounter.

The nature of the exhaust process is critical in determining the quantity of unburned hydrocarbons that exit an engine. We have only measured the total remaining hydrocarbons in the cylinder after combustion, not the distribution within the cylinder or what fraction is exhausted. Tabaczynski, Heywood and Keck⁽³⁷⁾ have studied the exhaust process and have pointed out that not all the unburned hydrocarbons will exit through the exhaust valve. Thus, it is anticipated that were we able to add an exhaust stroke to our simulation, the measured methane concentrations would be less. However, the nature of the exhaust process has no influence on the original combustion process, and in fact, measurements of exhausted hydrocarbons in a real engine give a poor indication of the real quenching processes.

Upon interpreting the results presented in this work, some aspects of the model engine that differ from a real engine have to be kept in mind. First, the model engine walls are at room temperature so that water vapor contained in the combustion products is condensed. Combined effects of this cold wall and water vapor condensation may influence the wall flame quenching mechanisms which presumably increase the quench layer thicknesses. Secondly, as shown in Table 3.1, the

model engine has a large stroke to bore ratio compared to that of regular engines. The size of the rolled-up vortex then may be smaller to some extent in a real engine. Lastly, the gas mixture in the model engine is not subject to the intake induced turbulence. The flame is laminar until it encounters the wall turbulence while it may be turbulent in a real engine. The effect of combined turbulence, i.e., rolled-up vortex caused wall turbulence and intake induced bulk turbulence, has not been clarified yet in this work.

CHAPTER 6

Summary and Conclusions

A study of unburned hydrocarbons has been conducted in which the compression and expansion stroke of a spark ignition engine was simulated by a pneumatically operated compression-expansion machine. Schlieren observations of the combustion process were made from the side, and total remaining unburned fuel measured with a gas chromatograph.

The wall flame quenching processes were photographed and comparison with the observed thermal boundary layer thickness and calculated quenching distance was made. It has been found that quench layer thickness is of the same order of magnitude as that of thermal boundary layer.

The schlieren observations have shown a significant effect of piston shape and cycle timing on the flow field through which the flame must propagate. Even without the bulk turbulence that an intake process might introduce, wall turbulence can be generated during the compression stroke, both because of the roll-up vortex, and because of the unsteady boundary layers along the side walls. For complex piston shapes, large scale bulk motions are also induced.

The hydrocarbon measurements reveal a general trend of decreased combustion efficiency with retarded timing, and with total unburned fuel percentages much higher than that predicted by laminar quenching correlations.

The main conclusion we reach is that wall turbulence can significantly

increase the effective quenching layer thickness, and that observed trends in hydrocarbon emission can be explained only by detailed examination of the flow patterns in an individual engine.

An appropriate extension of the present work would be to reduce the stroke to bore ratio to that of a real engine and operate the piston with three consecutive strokes so as to allow observation of the effect of an intake stroke or the nature of the exhaust stroke.

REFERENCES

1. I. Glassman, Combustion, Academic Press, 1977.
2. Environmental Quality, Seventh Annual Report of Council on Environmental Quality, pp. 241-242, 1976.
3. J.T. Wentworth and W.A. Daniel, "Flame Photographs of Light-Load Combustion Point the Way to Reduction of HCs in Exhaust Gas," SAE Paper No. 425, 1955.
4. W.A. Daniel, "Flame Quenching at the Walls of an Internal Combustion Engine," Sixth Symposium (International) on Combustion, New York, Reinhold Publishing Corporation, 1957.
5. J.N. Shinn, D.R. Olsen, "Some Factors Affecting Unburned Hydrocarbons in Engine Combustion Products," SAE Paper No. 570146, 1957.
6. W.A. Daniel and J.T. Wentworth, "Exhaust Gas Hydrocarbons - Genesis and Exodus," Paper No. 486B, SAE Technical Progress Series, No. 6, 1962.
7. W.G. Gottenberg, D.R. Olsen and H.W. Best, "Flame Quenching During High Pressure, High Turbulence Combustion," Combustion and Flame, 7, 1963.
8. J.T. Wentworth, "Piston and Ring Variables Affect Exhaust Hydrocarbon Emissions," SAE Trans. 77, Paper 680109, 1968.
9. J.T. Wentworth, "The Piston Crevice Volume Effect on Exhaust Hydrocarbon Emissions," Combustion Science and Technology 4, 2, 1971.
10. J.G. Hansel, "Lean Automotive Engine Operation--Hydrocarbon Exhaust Emissions and Combustion Characteristics," SAE Paper No. 710164, 1971.
11. A.A. Quader, "Lean Combustion and the Misfire Limit in Spark-Ignition Engines," SAE Paper No. 741055, 1974.
12. T.W. Ryan III, S.S. Lestz, and W.E. Meyer, "Extension of the Lean Misfire Limit and Reduction of Exhaust Emissions of an S.I. Engine by Modifications of the Ignition and Intake System," SAE Paper No. 740105, 1974.
13. J.A. Harington, "A Study of Carburetic Effects on Power, Emission, Lean Misfire Limit, and EGR Tolerance of a Single-Cylinder Engine," SAE Paper No. 760754, 1976.
14. G.H. Shiomoto, R.F. Sawyer, B.D. Kelly, "Characterization of the Lean Misfire Limit," SAE Paper No. 780235, 1978.

15. A.A. Quader, "What Limits Lean Operation in Spark Ignition Engines-- Flame Initiation or Propagation?" SAE Paper No. 760760, 1976.
16. H.C. Barnett, R.R. Hibbard, "Basic Consideration in the Combustion of Hydrocarbon Fuels with Air," Report No. 1300, Lewis Flight Propulsion Laboratory, 1959.
17. O.I. Smith, "Lean Limit Combustion in an Expanding Chamber," Ph.D. Thesis, University of California, Berkeley, 1977.
18. H.H. Dietrich, "Automotive Exhaust Hydrocarbon Reduction During Deceleration by Induction System Devices," SAE Paper No. 170, 1957.
19. G.C. Hass, "California Motor Vehicle Emission Standards," SAE Paper No. 210A, 1960.
20. D.F. Hagen and G.W. Holiday, "The Effects of Engine Operating and Design Variables on Exhaust Emissions," SAE Paper No. 486C, 1962.
21. M.W. Jackson, W.M. Wiese, and J.T. Wentworth, "The Influence of Air-Fuel Ratio, Spark Timing, and Combustion Chamber Deposits on Exhaust Hydrocarbon Emissions," SAE Paper No. 486A, 1962.
22. J.A. Mega, J.R. Kinosion, "Motor Vehicle Emission Standards-- Present and Future," SAE Paper No. 66104, 1966.
23. M.P. Sweeny, M.L. Brubacher, "Exhaust Hydrocarbon Measurement for Tuneup Diagnosis?" SAE Paper No. 660105, 1966.
24. C.E. Scheffler, "Combustion Chamber Surface Area, A Key to Exhaust Hydrocarbons," Paper 660111 presented at SAE Annual Meeting, Detroit, 1966.
25. W.A. Daniel, "Engine Variables Effects on Exhaust HC Composition: A Single-Cylinder Engine Study with Propane as a Fuel," SAE Paper No. 670124, 1967.
26. L.J. Papa, "Gas Chromatography - Measuring Exhaust Hydrocarbons Down to Parts Per Billion," SAE Paper No. 670494, 1967.
27. T.A. Huls, P.S. Myers and O.A. Uyehara, "Spark Ignition Engine Operation and Design for Minimum Exhaust Emission," SAE Trans. 75, 1976.
28. G.D. Ebersole, L.A. McReynolds, "An Evaluation of Automobile Total Hydrocarbon Emissions," SAE Trans. 75, 1967.
29. J.S. Ninomiya, A. Golovoy, "Effects of A/F on Composition of HC Exhaust from Isooctane, Diisobutylene, Toluene and Toluene-n Heptane Mixture," SAE Paper No. 690504, 1969.
30. C.M. Heinen, "We've Done the Job--What's Next?" SAE Paper No. 690536, 1969.

31. W.A. Daniel, "Why Engine Variables Affect Exhaust Hydrocarbon Emissions," Automotive Engineering Congress, Detroit, Michigan, January 12-16, 1970.
32. P.S. Myers, "Automobile Emissions - A Study in Environmental Benefits versus Technological Costs," SAE Paper No. 700182, 1970.
33. J.T. Wentworth, "Effect of Combustion Chamber Surface Temperature on Exhaust Hydrocarbon Concentration," SAE Trans. 80, SAE Paper No. 710587, 1971.
34. T. Tamura, K. Sasaki, T. Kaneko, H. Kawasaki, "Ignition, Combustion, and Exhaust Emissions of Lean Mixtures in Automobile Spark Ignition Engines," SAE Paper No. 710159, 1971.
35. J.G. Hansel, "Lean Automotive Engine Operation--Hydrocarbon Exhaust Emissions and Combustion Characteristics," SAE Paper No. 710164, 1971.
36. J.T. Wentworth, "More on Origins of Exhaust Hydrocarbons-- Effects of Zero Oil Consumption, Deposit Location, and Surface Roughness," SAE Trans. 81, SAE Paper No. 720939, 1972.
37. R.J. Tabaczynski, J.B. Heywood, and J.C. Keck, "Time-Resolved Measurements of Hydrocarbon Mass Flowrate in the Exhaust of a Spark-Ignition Engine," SAE Paper No. 720112, 1972.
38. H. Daneshyar, D.E. Fuller, and B.E.L. Dekker, "Vortex Motion Induced by the Piston of an Internal Combustion Engine," Int. J. Mech. Sci. 15, 1973.
39. J.B. Heywood, J.C. Keck, "Formation of Hydrocarbons and Oxides of Nitrogen in Automobile Engines," Environmental Science and Technology 7, 3, March 1973.
40. J.B. Heywood, "Pollutant Formation and Control in Spark Ignition Engines," Fifteenth Symposium (International) on Combustion, p. 1191, 1974.
41. R.E. Hicks, R.F. Probst, J.C. Keck, "A Model of Quench Layer Entrainment During Blowdown and Exhaust of the Cylinder of an Internal Combustion Engine," SAE Paper No. 750009, 1975.
42. A.K. Oppenheim, R.K. Cheng, K. Teichman, O.I. Smith, R.F. Sawyer, K. Hom, H.E. Stewart, "A Cinematographic Study of Combustion in an Enclosure Fitted with a Reciprocating Piston," Conference on Stratified Charge Engines, London, England, 1976.
43. N. Ishikawa and J.W. Daily, "Flame Wall Quenching in a Single Compression Engine," Western States Section, The Combustion Institute Paper No. 77-12, Spring 1977.

44. R.J. Tabaczynski, D.P. Hoult and J.C. Keck, "High Reynolds Number Flow in a Moving Corner," J. Fluid Mech. 42, 1970.
45. D.A. Willis, W.E. Meyer, C. Birnie, Jr., "Mapping of Airflow Patterns in Engines with Induction Swirl," SAE Paper No. 660093, 1966.
46. K.H. Heubner, A.T. McDonald, "Experimental Determination of Airflow Patterns in Piston Engines with Induction Swirl," SAE Paper No. 720026, 1972.
47. M.J. Tindal, T.J. Williams, and A.H.A. El Kafaji, "Gas Flow Measurements in Engine Cylinders," SAE Paper No. 740719, 1974.
48. J.C. Dent and N.S. Salama, "The Measurement of the Turbulence Characteristics in an Internal Combustion Engine Cylinder," SAE Paper No. 750886, 1975.
49. M. Tsuge, H. Kido, Y. Nomiyama, "Decay of Turbulence in a Closed Vessel," Bull. J. S. M. E. 16, 1973.
50. D.R. Lancaster, "Effects of Engine Variables on Turbulence in a Spark-Ignition Engine," SAE Paper No. 760159, 1976.
51. R.K. Barton, S.S. Lestz, W.E. Meyer, "An Empirical Model for Correlating Cycle-by-Cycle Cylinder Gas Motion and Combustion Variations of a Spark Ignition Engine," SAE Paper No. 710163, 1971.
52. S. Matsuoka, T. Yamaguchi, Y. Uemura, "Factors Influencing the Cyclic Variation of Combustion of Spark Ignition Engines," SAE Paper No. 710586, 1971.
53. R.E. Winson, D.J. Patterson, "Mixture Turbulence--A Key to Cyclic Combustion Variation," SAE Paper No. 730086, 1973.
54. N. Ishikawa, M.C. Branch, "An Experimental Determination of the Quenching Distance of Methanol and Iso-Octane/Methanol Blends," Combustion and Flame 27, 65-72, 1976.
55. M.V. Blanc, P.G. Guest, G. Von Elbe, B. Lewis, "Ignition of Explosive Gas Mixtures by Electric Sparks. I. Minimum Ignition Energies and Quenching Distances of Mixtures of Methane, Oxygen and Inert Gases," Jour. of Chem. Phys. 15, 11, 1947.
56. R. Friedman, Johnston, "The Wall-Quenching of Laminar Propane Flames as a Function of Pressure, Temperature, and Air-Fuel Ratio," J. Appl. Phys. 21, 791, 1950.
57. A.E. Potter, A.L. Berlad, "The Effect of Fuel Type and Pressure on Flame Quenching," Sixth Symposium (International) on Combustion, Reinhold, New York, 27, 1951.

58. K.A. Green, J.T. Agnew, "Quenching Distance of Propane-Air Flames in a Constant-Volume Bomb," Combustion and Flame 15, 189-191, 1970.
59. J.M. Ellenberger, D.A. Bowlus, "Single Wall Quench Distance Measurements," 1971 Technical Session, Central States Section, The Combustion Institute, 1971.
60. V. Panduranga, "Correct Turbulence--A Way to Reduce the Concentration of Unburnt Hydrocarbons from Automotive Engines," Combustion and Flame 18, 461-467, 1972.
61. M.R.S. Nair, M.C. Gupta, "Measurement of Flame Quenching Distances in Constant-Volume Combustion Vessels," Combustion and Flame 21, 321-324, 1973.
62. D.R. Ballal, A.H. Lefebvre, "The Influence of Flow Parameters on Minimum Ignition Energy and Quenching Distance," Fifteenth Symposium (International) on Combustion, The Combustion Institute, Pittsburg, 1473-1481, 1974.
63. D.R. Ballal, A.H. Lefebvre, "Flame Quenching in Turbulent Flowing Gaseous Mixtures," Sixteenth Symposium (International) on Combustion, MIT, Cambridge, Massachusetts, 1976.
64. D.R. Ballal, A.H. Lefebvre, "Ignition and Flame Quenching in Flowing Gaseous Mixtures," Proc. R. Soc. London A 357, 163-181, 1977.
65. A.D. Goolsby, W.W. Haskel, "Flame Quench Distance Measurements in a CFR Engine," Combustion and Flame 26, 105-114, 1976.
66. J. Ducarme, M. Gerstein, A.M. Lefebvre, Progress in Combustion Science and Technology, 1, 145-183, 1960.
67. C.R. Ferguson, J.C. Keck, "On Laminar Flame Quenching and Its Application to Spark Ignition Engines," Combustion and Flame 28, 197-205 (1977).
68. R. Friedman, "The Quenching of Laminar Oxyhydrogen Flames by Solid Surfaces," Third Symposium (International) on Combustion, Williams and Wilkins, Baltimore, 1949.
69. K. Wohl, "Quenching, Flash-back, Blow-off--Theory and Experiment," Fourth Symposium (International) on Combustion, MIT, Cambridge, Massachusetts, 1952.
70. D.M. Simon, F.E. Belles, A.E. Spakowski, "Investigation and Interpretation of the Flammability Region for Some Lean Hydrocarbon-Air Mixtures," Fifth Symposium (International) on Combustion, Baltimore, Williams & Wilkins, 1953.
71. D.B. Spalding, "A Theory of Inflammability Limits and Flame Quenching," Proc. Roy. Soc. A 240, 83, 1957.

72. E. Mayer, "A Theory of Flame Propagation Limits Due to Heat Loss," Combustion and Flame 1, 438, 1957.
73. A.E. Potter, Jr., A.L. Berlad, "A Thermal Equation for Flame Quenching," N.A.C.A. TN 3398, 1955.
74. T. Von Karman, G. Millan, "Thermal Theory of a Laminar Flame Front Near a Cold Wall," Fourth Symposium (International) on Combustion, MIT, Cambridge, Massachusetts, 1952.
75. A.P. Kurkov, W. Mirsky, "An Analysis of the Mechanism of Flame Extinction by a Cold Wall," Twelfth Symposium (International) on Combustion, 615-624, 1969.
76. G.P. Tewari, F.J. Weinberg, "Structure of Flame Quenched by Cold Surfaces," Proc. Roy. Soc. A 296, 546-565, 1966.
77. J. Buckmaster, "The Quenching of Deflagration Waves," Combustion and Flame 26, 151-162, 1976.
78. M. Gerstein, W.B. Stine, "Analytical Criteria for Flammability Limits," Fourteenth Symposium (International) on Combustion, The Combustion Institute, Pittsburgh, 1973.
79. V. Christensen, B. Qvale, "Maximum Heat Transfer Rate in a S.I. Engine," Laboratory for Energetics, Technical University of Denmark, April 1, 1973.
80. N. Ishikawa, M.C. Branch, "A Simple Model of Transient Thermal Flame Quenching," SAE Trans. 8, Paper No. 770648, 1978.
81. J.N. Bradley, "Flame and Combustion Phenomena," Chapman and Hall Ltd. and Science Paperbacks, 1969.
82. G.A. Lavoie, "Correlations of Combustion Data for S.I. Engine Calculations - Laminar Flame Speed, Quench Distance and Global Reaction Rates," SAE Paper No. 780229, 1978.
83. D.R. Ballal, A.H. Lefebvre, "Ignition and Flame Quenching in Flowing Gaseous Mixtures," Proc. R. Soc. Lond. A 357, 163-181, 1977.
84. M.K. Gajendra Babu, B.S. Murthy, "Simulation and Evaluation of a 4-Stroke Single-Cylinder Spark Ignition Engine," SAE Paper No. 750689, 1975.
85. Karlovitz, Denniston and Wells, Journal of Chemical Physics 19, 1951.
86. F.A. Matekunas, "Ignition and Flame Propagation in a Rapid Compression Machine Simulating the Spark Ignition Engine," GMR-2681, General Motors Research Laboratories, Warren Michigan, 1978.

87. M.M. Kamel, E. Lundstrom, and A.K. Oppenheim, J. Sci. Inst. 1, p. 459, 1968.
88. E.R.G. Eckert, R.J. Goldstein, Measurements in Heat Transfer, 2nd Edition, Hemisphere Publishing Corporation, 1976.
89. J.P. Holman, Experimental Methods for Engineers, 2nd Edition, McGraw Hill Inc., 1971.
90. R.W. Landenberg, B. Lewis, R.N. Pease, H.S. Taylor, Physical Measurement in Gas Dynamics and Combustion, Princeton, New Jersey, Princeton University Press, 1954.
91. F.J. Weinberg, Optics of Flames, Butterworth & Co., Ltd., Belfast, Northern Ireland, 1963.
92. J.W. Hosch, J.P. Walters, "High Spatial Resolution Schlieren Photography," J. Applied Optics, 16, 2, 1977.
93. N. Ishikawa, J.W. Daily, "Observation of Flow Characteristics in a Model I.C. Engine Cylinder," SAE Paper No. 780230, 1978.
94. R.M. Fristrom and A.A. Westenberg, Flame Structure, 22-23, New York, McGraw Hill, 1965.

APPENDIX A

Transient Flame Quenching at One Wall

The analysis will be made for a one-dimensional system in which a laminar flame approaches an end wall. The governing equations will be given as follows:

(a) Conduction in wall,

$$\rho_w c_w \frac{\partial T}{\partial t} = \frac{\partial}{\partial x} \left(k_w \frac{\partial T}{\partial x} \right) \quad (A1)$$

(b) Flame,

overall mass

$$\frac{\partial \rho}{\partial t} + \frac{\partial(\rho u)}{\partial x} = 0 \quad (A2)$$

momentum

$$P = \text{const.} \quad (A3)$$

energy

$$\rho \frac{\partial h}{\partial t} + \rho u \frac{\partial h}{\partial x} = \frac{\partial}{\partial x} \left(\frac{k}{c_p} \frac{\partial h}{\partial x} \right) + Q_w \quad (A4)$$

The species equations will not involve the solution method since they are coupled only with reaction rate ω in the energy equation (A4) which will turn out to be immaterial in the region of interest. Flame quenching at a wall is caused by the excessive heat loss to the wall which results in failure to maintain the chemical reaction in the reaction zone. For a very short time the solid may be assumed to be semi-infinite. It will also be assumed that there is no contact resistance. Since the time constant for flame quenching is small

compared to that for local change in enthalpy of the gaseous region of interest, and in a very short period of time, it may be assumed that the flame maintains its initial quasi-steady laminar flame temperature profile, the $\partial/\partial t$ in the energy equation for flame propagation may be neglected. This has been shown to be a reasonable assumption⁽⁷⁵⁾.

Then one may apply the following two solutions: (a) heat conduction in a semi-infinite slab with a step change in temperature at the surface; and (b) thermal propagation of the flame, with matching conditions $-k_w \frac{\partial T}{\partial x} (0^-) = -k \frac{\partial T}{\partial x} (0^+)$ and $T_w(0^-) = T(0^+) = T_c$.

The mass conservation equation (A2) and constant pressure condition (A3) will not be directly involved with the solution of the energy equation. However, as will be discussed later, these fundamental restrictions for a gas flow play an important role in diffusive motions of radical species in the reaction zone near the wall.

(a) The governing equation for heat conduction in a semi-infinite slab with constant properties is

$$\frac{\partial^2 T}{\partial x^2} = \frac{1}{\alpha_w} \frac{\partial T}{\partial t} \quad (A5)$$

with boundary conditions $T(0,t) = T_c$, $T(-\infty,t) = T_w$ and initial condition $T(x,0) = T_w$. The solution is readily obtained by application of Laplace transform, i.e.

$$T(x,t) = T_w + (T_c - T_w) \operatorname{erfc} \frac{1}{2\sqrt{\alpha_w t}} \quad (A6)$$

This solution is valid only for $T_c = \text{constant}$. However, T_c increases very little during the process. The time constant for flame quenching is of the order of 10^{-3} sec while that for thermal diffusion is of

the order of 10^{-2} sec. In addition, thermal diffusivity in the vicinity of the wall is about one-fifth that at the reaction zone. Therefore, solution (A6) may be used. The corresponding heat flux at $x=0$ is given by differentiation of Eq. (A6) and letting $x=0$

$$q_w'' = - \left[k \frac{\partial T}{\partial x} \right]_{x=0} = -k_w(T_c - T_w) \frac{2}{\pi} \left(- \frac{1}{2\sqrt{\alpha_w t}} \exp\left(-\frac{x^2}{4\alpha_w t}\right) \right)_{x=0}$$

Then

$$q_w'' = - \sqrt{\frac{k_w \rho_w C_w}{\pi t}} (T_c - T_w) \quad (A7)$$

(b) The equation for the temperature profile in the preheating zone of a one-dimensional, laminar, premixed flame, might be written as

$$\frac{d}{dx} \left(k \frac{dT}{dx} \right) - \rho u C_p \frac{dT}{dx} + Q\omega = 0 \quad (A8)$$

where k is thermal conductivity, C_p is specific heat, Q is heat of reaction, ω is rate of reaction and u is velocity of unburned gas relative to the flame. In the preheating zone, Eq. (A8) reduces to

$$\frac{d}{dx} \left(k \frac{dT}{dx} \right) - \rho u C_p \frac{dT}{dx} = 0 \quad (A9)$$

since no significant chemical reactions take place in this region. With boundary conditions $T=T_i$ at $x=0$ and $dT/dx = 0$, $T=T_c$ at $x=-\infty$, the solution to Eq. (A9) will be

$$T = T_c + (T_i - T_c) \exp\left(\frac{u}{\alpha} x\right) \quad (A10)$$

where $\alpha = k/\rho C_p$. If we fix x in space and shift the origin of this coordinate system by the thickness of the preheating zone, $\delta^{(81)}$, and

allow the flame preheat zone to move toward the wall

$$T = T_c + (T_i - T_c) \exp \left[\frac{S_u}{\alpha} (x + \xi - \delta) \right] \quad (A11)$$

where $\xi = \xi(t)$ is the distance travelled by the reaction zone from its initial position (Figure 2.2) to its position at time t . In Eq. (A11) the velocity u has been replaced by the laminar burning velocity since we assume that the temperature profile is that of a laminar flame. Time $t=0$ corresponds to the moment when the reaction zone reaches a distance δ from the wall.

The heat flux at $x=0$ corresponding to the solid wall will be

$$q_g'' = -[k \frac{\partial T}{\partial x}]_{x=0} = -\frac{kS_u}{\alpha} (T_i - T_c) \exp \left[\frac{S_u}{\alpha} (\xi - \delta) \right] \quad (A12)$$

Now, at the interface or at $x=0$, the two heat fluxes must be equal, or

$$q_w'' = q_g'' \quad (A13)$$

therefore

$$-\sqrt{\frac{k_w \rho_w C_w}{\pi t}} (T_c - T_w) = -\frac{kS_u}{\alpha} (T_i - T_c) \exp \left[\frac{S_u}{\alpha} (\xi - \delta) \right] \quad (A14)$$

which yields

$$\frac{T_i - T_c}{T_c - T_w} = \sqrt{\frac{k_w \rho_w C_w}{\pi t}} \frac{\alpha}{kS_u} \exp \left[\frac{S_u}{\alpha} (\delta - \xi) \right] \quad (A15)$$

Solving for T_c

$$T_c = \frac{T_i + \theta T_w}{1 + \theta} \quad (A16)$$

where

$$\theta = \sqrt{\frac{k_w \rho_w C_w}{\pi t} \frac{\alpha}{k S_u}} \exp\left[\frac{S_u}{\alpha} (\delta - \xi)\right] \quad (A17)$$

One can calculate the heat flux due to conduction at x as follows:

$$q_g''|_x = \left[k \frac{\partial T}{\partial x} \right]_x = k(T_i - T_c) \frac{S_u}{\alpha} \exp\left[\frac{S_u}{\alpha} (x + \xi - \delta)\right] \quad (A18)$$

Substituting Eq. (A16) into Eq. (A18)

$$q_g''|_x = \frac{k(T_i - T_w)}{1 + 1/\theta} \frac{S_u}{\alpha} \exp\left[\frac{S_u}{\alpha} (x + \xi - \delta)\right]$$

The heat generation rate in the reaction zone per unit area must be

$$q_s'' = Q\omega\delta_r \quad (A19)$$

where δ_r is the thickness of the reaction zone. Finally, the flame is supposed to quench under the condition

$$q_g''|_{x=D_1} > q_s'' \quad (A20)$$

Substituting Eq. (A14) and Eq. (A15) into Eq. (A16) under the quenching conditions gives

$$\frac{k(T_i - T_w)}{1 + 1/\theta} \frac{S_u}{\alpha} \exp\left[\frac{S_u}{\alpha} (D_1 + \xi - \delta)\right] = Q\omega\delta_r \quad (A21)$$

The quenching distance is obtained by solving Eq. (A21) for D_1 . Since the reaction is modelled as a laminar flame approaching the wall the value of ξ away from the wall is $S_u t$. During the quenching process, however, the value of ξ will be very small. As the density of the fluid near the wall increases the resulting expansion away from the wall will oppose motion of the flame toward the wall, which stems from the two constraints, that is, the mass conservation Eq. (A2) and the constant pressure Eq. (A3). This retarding of the flame at the wall during

quenching has been observed in color schlieren cinematography by Ishikawa and Daily⁽⁴³⁾. The effect of this flame retarding is that the quenching condition is given to a first approximation by $\xi=0$.

$$k(T_i - T_w) \frac{S_u}{\alpha} \exp\left[\frac{S_u}{\alpha} (D_1 - \delta)\right] = Q\omega\delta_r \quad (A22)$$

which yields

$$D_1 = \delta + \frac{\alpha}{S_u} \ln\left[\frac{\alpha Q\omega\delta_r}{kS_u(T_i - T_w)}\right] \quad (A23)$$

Defining the thickness of the preheating zone δ ⁽⁸¹⁾ as the distance between two positions corresponding to temperatures T_i and $(T - T_c)/ (T_i - T_c) = 1/100$, one will get

$$\delta = 4.6 \frac{\alpha}{S_u} \quad (A24)$$

Eq. (A23) and Eq. (A24) yield a quenching Peclet number

$$\frac{D_1 S_u}{\alpha} = 4.6 + \ln\left[\frac{\alpha Q\omega\delta_r}{kS_u(T_i - T_w)}\right] \quad (A25)$$

From Eq. (A25), one can estimate the quenching distance if δ_r , ω , T_i , and S_u can be evaluated. In order to determine these quantities, one may use the following expression for heat loss from a quasi steady laminar flame which is obtained by an energy balance on a laminar flame without a wall⁽⁶⁶⁾.

$$q'' = \rho C_p S_u (T_f^a - T_f) = \frac{kS_u}{\alpha} (T_f^a - T_f) \quad (A26)$$

In this expression T_f^a is adiabatic flame temperature and T_f is actual flame temperature. Substituting Eq. (A26) into Eq. (A25) to replace $Q\omega\delta_r$, one gets

$$\frac{D_1 S_u}{\alpha} = 4.6 + \ln\left[\frac{T_f^a - T_f}{T_i - T_w}\right] \quad (A27)$$

Assuming $T_i \approx T_f$, which appears reasonable ⁽⁷⁵⁾, under quenching conditions gives

$$\frac{D_1 S_u}{\alpha} = 4.6 + \ln \left(\frac{T_f^a - T_f}{T_f - T_w} \right) \quad (\text{A28})$$

APPENDIX B

Wall Quench Volume, Crevice Quench Volume
and Turbulence Volume Fractions

(a) Wall Quench Volume Fraction

The wall quench volume is estimated by using the quenching distance predicted by Eq. (1) as

$$D_1 = FD_{11_0} \left(\frac{P_0}{P} \right)^\alpha \left(\frac{T_0}{T} \right)^\beta$$

Approximating the expansion process with combustion as isentropic, one may use the relation

$$\frac{T_0}{T} = \left(\frac{P_0}{P} \right)^{\frac{\gamma-1}{\gamma}} \quad (B1)$$

Substituting Equation (B1) into Equation (1) with average specific heat ratio 1.36 for the mixtures, Equation (1) reduces to

$$D_1 = 0.09 P^{-0.65} \quad (\phi = 1.0) \quad (B2)$$

$$D_1 = 0.16 P^{-0.65} \quad (\phi = 0.6) \quad (B3)$$

where the value of D_{11_0} in Ref. (54) has been used. Although the quench layer thicknesses are not uniform along the cylinder walls, the wall quench volume \bar{V} may be roughly estimated by

$$\bar{V} = 2D_1 a^2 + 4D_1 aL \quad (B4)$$

where L is the distance between the piston head and cylinder head and a is the side length of the square cross section. Since the instantaneous

total cylinder volume \bar{V}_T is given by

$$\bar{V}_T = La^2 \quad (B5)$$

the quench volume fraction F_Q is calculated by

$$F_Q = \bar{V}_Q / \bar{V}_T = 2D_1(1/L + 2/a) \times 100 \quad (\%) \quad (B6)$$

The values of L and D_1 (or P) can be determined from the pressure and the piston displacement records. An example is shown in Figure B1. The first deflection point in the decreasing pressure curve is assumed to correspond to the moment that a flame covers the entire cylinder surface, from which the piston location L is determined with the displacement fraction read out. The characteristic pressure is determined by the average value that yields equal area under the pressure trace curve between the ignition point and the first deflection point.

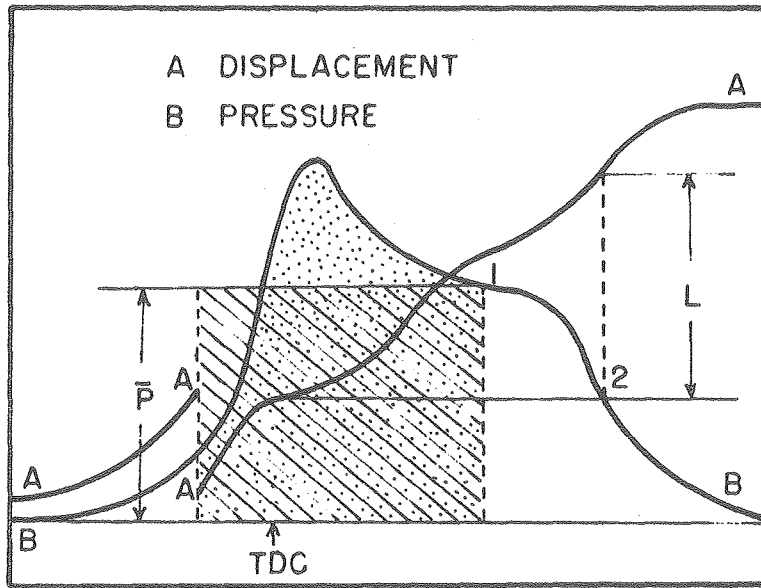
(b) Crevice Volume Fraction

It is assumed that there is no viscous effect for the gas mixture to get in and out of the crevice, and that the pressure in the crevices is the same as in the cylinder chamber. Assuming ideal gas and constant temperature process, the gas volume that comes out of the crevice may be approximated by

$$V - V_C = V_C \left(\frac{P_{\max}}{P} - 1 \right) \quad (B7)$$

where V_C corresponds to the gas volume in the crevices at the maximum chamber pressure P_{\max} , in other words, the crevice volume. The crevice volume fraction will then be given by

$$F_C = \frac{V - V_C}{V_T} \quad (B8)$$



XBL 787-9677

Figure B1 Pressure and piston displacement records

For this model engine, $V_c = 0.743 \text{ cm}^3$ and $V_T = 203.2 \text{ cm}^3$ so that Equation B7 reduces to

$$F_c = 0.366 (P_{\max} - 1) \quad (\text{B9})$$

where P_{\max} is read from the pressure records.

(c) Turbulence Volume Fraction

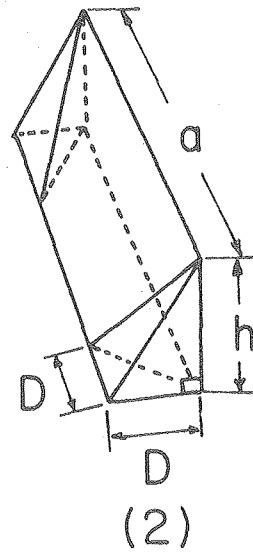
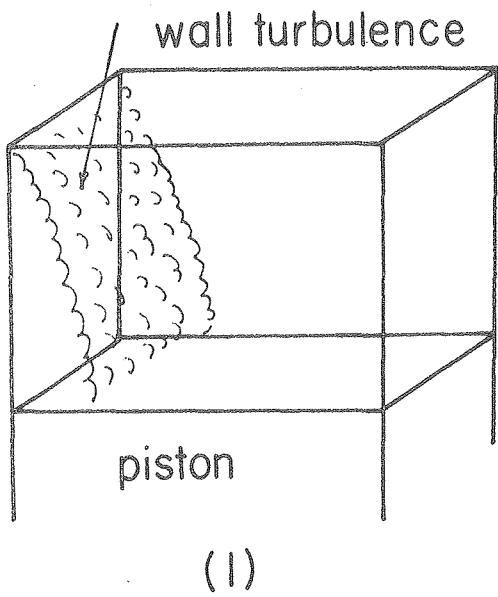
Figure B2 shows the sketch of (1) the wall turbulence and (2) its simplified model for a flat piston. The total turbulence volume V_T may be estimated by

$$V_T = Dh(2a - 4D/3) \quad (\text{B10})$$

The turbulence volume fraction F_T may be given by

$$F_T = (V_t/V_T) \times 100 \quad (\%) \quad (\text{B11})$$

The values in Equation (B10) are measured by the schlieren photographs. For the other types of piston, similar evaluation methods are used. They simply add complexity in geometry.



XBL 787-9678

Figure B2 Wall turbulence

This report was done with support from the Department of Energy. Any conclusions or opinions expressed in this report represent solely those of the author(s) and not necessarily those of The Regents of the University of California, the Lawrence Berkeley Laboratory or the Department of Energy.

Reference to a company or product name does not imply approval or recommendation of the product by the University of California or the U.S. Department of Energy to the exclusion of others that may be suitable.

TECHNICAL INFORMATION DEPARTMENT
LAWRENCE BERKELEY LABORATORY
UNIVERSITY OF CALIFORNIA
BERKELEY, CALIFORNIA 94720